MODELING OF DYNAMIC HYDROLOGIC CONNECTIVITY: HOW DO DEPRESSIONS AFFECT THE MODELING OF HYDROLOGIC PROCESSES?

A Dissertation
Submitted to the Graduate Faculty
of the
North Dakota State University
of Agriculture and Applied Science

By

Kendall Morgan Grimm

In Partial Fulfillment of the Requirements
for the Degree of
DOCTOR OF PHILOSOPHY

Major Department:
Civil and Environmental Engineering

November 2018

Fargo, North Dakota

North Dakota State University
Graduate School

Title

MODELING OF DYNAMIC HYDROLOGIC CONNECTIVITY: HOW DO DEPRESSIONS AFFECT THE MODELING OF HYDROLOGIC PROCESSES?

By

Kendall Morgan Grimm

The Supervisory Committee certifies that this ***disquisition*** complies with North Dakota State University's regulations and meets the accepted standards for the degree of

DOCTOR OF PHILOSOPHY

SUPERVISORY COMMITTEE:

Dr. Xuefeng Chu
Chair

Dr. Eakalak Khan

Dr. Wei Lin

Dr. Marinus Otte

Approved:

November 7, 2018
Date

Dr. David R. Steward
Department Chair

ABSTRACT

Traditional delineation and modeling methods do not consider the spatial arrangement and dynamic threshold control of surface depressions. Instead, full structural hydrologic connectivity, uniform well-connected drainage networks, and an invariant contributing area are often assumed. In reality, depressions play an important role in quantifying hydrologic connectivity and outlet discharge. Current literature lacks a preferred foundation and tools to identify and quantify hydrologic connectivity on depression-dominated landscapes. Therefore, the objectives of this dissertation research are to (1) develop a new procedure to analyze functional hydrologic connectivity related to surface topography, specifically in depression-dominated areas; (2) evaluate the impacts of the puddle-to-puddle (P2P) filling-spilling-merging processes and dynamic hydrologic connectivity on watershed outlet discharge; and (3) address the combined effect of topographic depressions and wetland functions on hydrologic connectivity and watershed outlet discharge. To accomplish these objectives, three studies are conducted where (1) a new procedure was developed for identifying and analyzing hydrologic connectivity in depression-dominated areas; (2) an improved HEC-HMS modeling framework was developed by incorporating a depression threshold control proxy; and (3) a new hydrologic categorization of wetlands was adapted for watershed-scale hydrologic modeling. The major findings from these studies include: (1) traditional delineation methods may fail to represent the realistic contributing area (CA), especially for depression-dominated surfaces; (2) the consideration of the P2P processes and dynamic contributing area is essential for hydrologic modeling of depression-dominated areas; and (3) different wetland types have unique characteristics of contributing area and depression storage that are not simulated in detail in most traditional models. The conclusions from this research also provides useful information for

future studies relating to sediment and pollutant transport in depression-dominated regions, ecological interactions in wetlands, and anthropogenic effects on hydrologic processes.

ACKNOWLEDGEMENTS

First, I would like to thank Dr. Xuefeng Chu for giving me the opportunity to be his graduate student. His patience and reassurance encouraged me to never give up and reach for the stars, or should I say a PhD. I never imagined, starting out as a master's student, that I would have gained the academic expertise and worldly experiences if it wasn't for his guidance, professional support, and kindness. Dr. Chu prepared me for a future where my opportunities are endless, and for that I am extremely grateful. I would also like to acknowledge the financial support from the National Science Foundation Established Program to Stimulate Competitive Research (NSF EPSCoR, Grant No. IIA-1355466), North Dakota Water Resources Research Institute (NDWRRI), and the Department of Civil and Environmental Engineering, without which this research would not have been possible.

Second, I would like to extend my gratitude to my other committee members: Dr. Eakalak Khan, Dr. Wei Lin, and Dr. Marinus Otte for their time, willingness to serve, and professional input and counseling. Third, my time at North Dakota State University would not have been so much fun and enjoyable without my graduate school colleagues and friends. Thank you Mohsen Tahmasebi Nasab for your endless positivity and love for all things water (i.e., Fun with Hydrology). You are truly going to make a difference in this world because you made a difference in mine. I would also like to thank Ning Wang, Hadi Bazrkar, and Lan Zeng for their contribution to the group research and making our research group a family.

Finally, thanks are due to my beloved parents, my dad, Michael Grimm and my mom, Lynda Grimm, and my fiancé, Kevin Himelright, for their endless love, support, and encouragement. Without their motivation and confidence in me I would probably still be writing this. I would also like to thank Darren Mueller and the NDSU softball team for initially opening

the door for me to become a Bison and Kassiann Landin for encouraging me pursue a PhD. My time at NDSU and travels around the country with you are memories I will never forget!

TABLE OF CONTENTS

LIST OF TABLES

LIST OF FIGURES

LIST OF ABBREVIATIONS

PPR .....Prairie Pothole Region.

PD .....Puddle Delineation.

P2P .....Puddle-to-puddle.

C2C .....Cell-to-cell.

MDS .....Maximum Depression Storage.

MPA .....Maximum Ponding Area.

PBU .....Puddle-based Unit, contributing area to highest-level puddles.

CBU .....Channel-based Unit, contributing area to an identified channel reach.

CA .....Contributing Area.

AC .....Connected Area.

NACf .....Normalized Connected Area Function.

RSCf .....Relative Surface Connection Function.

HEC-HMS .....Hydrologic Engineering Center- Hydrologic Modeling System

DTCP .....Depression threshold control proxy

MDS_j^{Sub} .....Maximum Depression Storage in Subbasin 'j'.

$MDS_{i,j}^{PBU}$ .....Maximum Depression Storage in PBU 'i' located in Subbasin 'j'.

$A_{i,j}^{PBU}$ .....Area of PBU 'i' located in Subbasin 'j'.

$A_{i,j}^{CBU}$ .....Area of CBU 'i' located in Subbasin 'j'.

$Q_{j,k}^{Sub}$ .....Discharge from Subbasin 'j' at time step 'k'.

$I_{j,k}^{Sub}$ .....Inflow to depressions in Subbasin 'j' at time step 'k'.

ΔS_j^{Sub} ..... Change in depression storage in Subbasin ‘j’ during Δt.

Δt ..... Change in time, ‘k-1’ to ‘k’.

$S_{i,j,k}^{PBU}$ ..... Depression storage in PBU ‘i’ located in Subbasin ‘j’ at time step ‘k’.

$I_{i,j,k}^{PBU}$ ..... Inflow to depressions in PBU ‘i’ located in Subbasin ‘j’ at time step ‘k’.

$Fill_{\Delta t}$ ..... Filling depth during Δt.

$S_{j,k}^{Sub}$ ..... Depression storage in Subbasin ‘j’ at time step ‘k’.

DA ..... Depressional Area.

NDA ..... Non-depressional Area.

$Q_{j,k}^{NDA}$ ..... Discharge from the NDA of Subbasin ‘j’ at time step ‘k’.

SWAT ..... Soil and Water Assessment Tool

A1 ..... Approach 1, Pothole only approach

A2 ..... Approach 2, Wetland only approach

FWA ..... Functional wetland approach

NSE ..... Nash-Sutcliffe Efficiency

PBIAS ..... Percent Bias

RSR ..... Ratio of the root mean square error to the standard deviation of measured data

1. GENERAL INTRODUCTION

Over the last three decades hydrologic studies and research focused on the advancement of computer technologies to analyze surface topography, delineate a surface, and model hydrologic processes. Specifically, the use of Digital Elevation Models (DEMs) to characterize surface elevations has led to the development of many computer-based tools and methodologies (Chen 2004). However, not all analysis, delineation, and modeling programs can be treated equally. The assumptions and methodologies behind each computer-based tool may elevate one tool over another based on the user's purpose. For example, in North Dakota, the abundance of prairie pothole depressions leads to the generation of a complex DEM in which topographic analysis, delineation, and hydrologic modeling can be problematic. This study analyzed and developed new hydrologic toolsets to improve the understanding and modeling of hydrologic processes in depression-dominated landscapes.

1.1. Problem Statement

Various properties of terrain, such as slope and aspect, can be determined by topographic analyses of a DEM. These topographic and geometric parameters can then be used in the basin delineation process. Traditional delineation methods (e.g., Marks *et al.*, 1984; O'Callaghan & Mark, 1984; Jenson & Domingue, 1988; Tarboron, 1997; Gabrecht & Martz, 1999), however, implement simplified delineation approaches for depressions. For instance, Marks *et al*. (1984) developed a recursive procedure for DEM-based delineation, in which all areas of a basin were assumed to be hydrologically connected to the outlet. O'Callaghan & Mark (1984) extracted major drainage networks from DEMs, assuming a dendritic drainage pattern. Jenson & Domingue (1988) developed a procedure to delineate watershed boundaries and determine drainage networks. The procedure was implemented in TOPAZ, an automated topographic

analysis program using DEMs (Gabrecht & Martz, 1999), in which all depressions are first filled, and then flow directions and accumulations are determined based on the depressionless DEMs. The first step for TOPAZ creates a depressionless surface to ensure a well-connected drainage system across the landscape. This guarantees that the surface delineated by using this traditional method has full structural hydrologic connectivity and an invariant contributing area, so the entire surface will contribute runoff to the basin outlet. Similarly, pit removal or filling depressions is implemented in TauDEM (Terrain Analysis Using Digital Elevation Models) (Tarboron, 1997), which is based on the D-infinity flow method. In the traditional methods, artificial slopes and flow directions are often introduced across the depressional areas. A new advance in DEM-based delineation, fuzzy logic has been used to handle errors in delineation and account for probability distribution of cells having multiple flow directions (Schwanghart & Heckmann, 2012). This can be important when studying flat landscapes with uncertain flow directions; however, not all cells on a surface should have a flow direction (i.e. depressions). Turcotte *et al.* (2001) proposed a method to identify flow directions in the presence of depressions and compared it against the D8 method. However, their method still worked best on dendritic watersheds.

Traditional delineation methods create a depressionless surface to conduct modeling because it is difficult to route overland flow across the surface unless all cells are hydrologically connected (Gabrecht and Martz 2000; USACE-HEC 2013). In reality, depressions are critical to determining the timing of runoff generation and the quantification of overland flow (Chu et al. 2010). The timing of runoff generation is not just a factor of rainfall intensity surpassing infiltration capacity; it is also affected by puddle-to-puddle (P2P) filling-spilling-merging-splitting processes, which are controlled by threshold behaviors of depressions (Chu et al. 2013).

A depression threshold controls the timing and quantity of water to be released to a downstream channel or depression.

Threshold behaviors and the P2P process can also impact hydrologic connectivity and contributing area to an outlet. Understanding hydrologic connectivity in a study area is critical to determining variable source areas and identifying areas within a watershed which will have a quick rainfall-runoff response. Progress has been made in a number of studies (Antoine *et al.*, 2009; Bracken *et al.*, 2013; Yang & Chu, 2013; Peñuela *et al.*, 2016; Rinderer *et al.*, 2017; Wu & Lane, 2017) to address the variability of hydrologically connected areas and contributing area across multiple landscapes. A thorough knowledge of the areas that contribute to runoff can also improve modeling of peak flow rates for event-based modeling, fate and transport of sediments, chemicals, and bacteria in surface water, especially for depression-dominated areas.

Currently, there is a need to better understand how depressions impact hydrologic processes. Once this understanding is achieved further research needs to be devoted to incorporating the dynamic hydrologic processes of depressions into popular and widely-used hydrologic models in order to enhance hydrologic computations for users studying depression-dominated landscapes.

1.2. Rationale

This research, related to depression-dominated landscapes, is applicable to hydrologic, ecologic, and climate studies in present-day highly stressed areas of the world, such as the Prairie Pothole Region (PPR) and the Arctic tundra. The PPR covers five U.S. states (North Dakota, South Dakota, Minnesota, Montana, and Iowa) and three Canadian provinces (Manitoba, Saskatchewan, and Alberta). This area is of particular interest because it is a unique region of the United States which provides valuable ecosystem services such as sediment/nutrient retention,

habitat for numerous species particularly waterfowl, and natural flood protection. The USGS Northern Prairie Wildlife Research Center (USGS NPWRC) has a particular interest in the ecology and hydrology of the PPR for which they founded the Cottonwood Lake Study Area (CLSA), a research site in central North Dakota. The CLSA has hosted long term ecologic studies since 1967 and began detailed hydrologic studies in 1979 (Euliss *et al.*, 2014). A majority of their studies focus on how the climate and hydrology impact specific species and the wetland ecosystem as a whole. Although the CLSA is relatively undisturbed, the rest of the PPR is severely impacted by the conversion of grassland to cultivated cropland and/or pastureland. This land conversion is impacting the hydrologic cycle within the disturbed areas which in turn effects native species and ecosystems.

Similarly, the arctic and subarctic tundra has been impacted by anthropogenic induced climate change. The depressional peat bogs in this ecosystem provide CO2 storage; however, mostly all wetlands are methane emitters (Lafleur, 2009). Complex hydrologic processes, biochemistry, and transport mechanisms within a single wetland and across a many wetlands make it difficult to quantify greenhouse gas fluctuations in these ecosystems (Lafleur, 2009). Therefore, an improved understanding of the complete hydrologic processes in these areas is necessary to predict future levels of greenhouse gasses in the atmosphere and to support developing a plan to control greenhouse gas release.

1.3. Scope of Research

This research investigated the impact of many depressions/wetlands on hydrologic processes at a local scale (i.e., single depression) and meso-scale (i.e., multiple depressions). When compiling the hydrologic impacts of many individual depressions, it is best to look at how they interact and impact an area of interest. This is where the term hydrologic connectivity

comes in to play. Different definitions have been used to describe hydrologic connectivity based on different approaches to understand flow parameters, soil-moisture patterns, and surface topography (Bracken *et al.*, 2013). The development of models to handle the identification of functional hydrologic connectivity and the development of connectivity indices lack a preferred foundation (Bracken *et al.*, 2013; Rinderer *et al.*, 2017). In this dissertation, the focus is strictly on hydrologic connectivity created by spatial flow patterns affected by topographic features. Hydrologic connectivity refers to the spatio-temporal conveyance of water and the related mass over a land surface (Pringle, 2003; Bracken & Croke, 2007). Across space, surface topography influences hydrologic connectivity. Surface depressions are one of the major topographic elements that create spatially-varying, hydrologically-connected units across the surface (Yang & Chu, 2013). Rainfall, a spatio-temporal variable, fills depressions, which leads to dynamic changes in hydrologically-connected areas controlled by rainfall characteristics, soil properties, surface topography, and other factors. Generation of overland flow, a spatio-temporal variable, also affects hydrologic connectivity.

To make the concept of connectivity more understandable, two types of hydrologic connectivity are commonly used. The first is structural hydrologic connectivity, derived directly from surface topography, terrain parameters, and other static spatial features. The second is functional hydrologic connectivity, derived from hydrologic quantity modeling of a surface with varying rainfall events (Antoine *et al.*, 2009; Bracken *et al.*, 2013). These terms have been developed to determine connectivity because it is easier to simulate spatial patterns in flow, rather than directly observe them (Güntner *et al*., 2004). Antoine et al. (2009) investigated functional connectivity for three types of surface microtopography: river fields, random fields, and crater fields. River fields reached a steady state runoff rate faster than the two other

microtopography types. Crater fields took the longest to reach a steady state runoff rate because the surface depression storage must be fully filled to reach a steady state (Antoine *et al.*, 2009). Although surface storage must be fully filled to reach a steady state runoff rate, that doesn't mean that surface depression storage must be fully filled to produce any runoff (Singh, 1995; Antoine *et al*., 2009).

Studies have been conducted to characterize overland flow behaviors based on hydrologic connectivity and surface topography. Darboux *et al*. (2002) considered runoff initiation and depression storage as key features affecting the size and distribution of individual hydrologically connected areas. In their study a depression filling model was used to analyze overland flow generation and hydrologic connectivity (Darboux *et al*., 2002). Appels *et al*. (2011) designed a study using synthetic elevation fields to simulate connectivity behavior and found that varying the spatial distribution of microtopography and infiltration properties in catchment modeling can determine connectivity on the surface across time. Although these studies made important findings for defining hydrologic connectivity, connections to basin outlets have been difficult to define because they depend on time and the threshold control of depressions.

An outlet hydrograph is affected by flow connectivity which is related to surface microtopography and surface roughness (Peñuela *et al.*, 2016). Antoine *et al*. (2011) found that functional connectivity was influenced by surface microtopography and depression storage dynamics simulated by different rainfall rates; however, surface detention during flow routing also delayed runoff. To account for surface detention, cumulative inflow was split into two parts: (1) filling depressions and (2) contributing to surface runoff (Antoine *et al*., 2011). Although, this corrective procedure more accurately modeled outlet discharge and contributing area to the

outlet based on functional connectivity, the application of dividing the water input of the entire landscape into two parts might not reflect the reality. The timing of runoff propagation is unique to each surface depression, so surface connectivity should be influenced by depression properties first, before connecting to downstream depressions or channels.

Contributing area can be defined as an area that contributes runoff from rainfall excess to a specific point. In this dissertation, contributing area will define the area connected to the outlet. Contributing area to the outlet is hydrologically connected area, however, not all hydrologically connected areas are contributing area to the outlet. It is difficult to determine the contributing area to an outlet because depression storage has a major influence on the timing of runoff contribution and evolution of the dynamic contributing area. Size and distribution of upstream depressions and their corresponding connected areas affect the timing of dynamic contributing area to the outlet. Although dynamic contributing area has been studied on a conceptual level, most modeling systems oversimplify or do not consider the effects of different microtopographic characteristics on contributing area to the outlet.

Quantifying dynamic contributing area has been simplified in traditional hydrologic modeling because most landscapes direct runoff to channels; therefore, it is assumed in most modeling methods that the entire landscape contributes to the outlet via channel flow (Singh, 1995). However, a landscape dominated by depressions (e.g., PPR) makes determining stream flow across the surface difficult because depressions should depict no stream flow, so connecting the entire landscape to the outlet becomes very difficult. Also, surface runoff and connections between potholes in the PPR vary spatially and temporally depending on the condition of the surface in the depression filling, spilling, merging, and splitting process. For this reason, a thorough study of how these factors affect contributing area to the outlet and outlet discharge is

needed to highlight the importance of quantifying dynamic contributing area in hydrologic modeling methods.

Areas like the PPR, are described as being topographically isolated from a stream network; i.e., under normal conditions there is no direct surface water connection (Richards & Brenner, 2004). Except under extreme rainfall events will some areas within a basin ever contribute surface runoff to the outlet. Following the generation of overland flow there are a number of terms proposed to identify how and why only a small proportion of a basin contributes surface runoff to the outlet. Hewlett & Hibbert (1967) first termed variable source area (VSA) to identify areas in a watershed where runoff occurs. Factors such as slope, soil infiltration, and proximity to a stream are typical VSAs where surface and subsurface flows begin (Richards & Brenner, 2004). Other relevant terms included partially contributing area (PCA) (Betson, 1964), saturated source area (SSA) (Ogden & Watts, 2000), hydrologically sensitive area (HSA) (Walter *et al*., 2000), and potentially contributing source area (PCSA) (Richards & Brenner, 2004). These terms arose from comprehensive research of one another in search of a more accurate way to define contributing area of surface flow.

In addition to defining the term of contributing area to the outlet, studies have also been conducted to quantify and locate contributing area to the outlet. Quantifying contributing area to the outlet can assist in evaluating runoff and its hydrologic consequences. Locating contributing area to the outlet can assist in understanding quick response runoff areas and their hydrologic consequences. This research topic is also of particular importance to pollutant and sediment transport modeling and the related water quality management. Studies done by Hewlett & Hibbert (1967), Dunne & Black (1970), and Engman & Rogowski (1974) provide the foundation of watershed runoff production, while studies following (e.g., Beven & Kirkby, 1978; Heerdegen

& Beran, 1982; Bernier, 1985; Walter *et al*., 2000; Richards & Brenner, 2004) focused on developing methods to model contributing area for different study areas. Hydrologic connectivity studies have also investigated groundwater interactions between depressions to evaluate water-balance and water quality in a wetland system (Hayashi et al, 2016; Neff and Rosenberry, 2018). The importance of understanding hydrologic responses to rainfall events and their effects on water quantity and quality are stressed in these studies.

1.4. Objectives

Hydrologic processes, especially overland flow, cannot be simulated by using traditional hydrologic models, in which a typical dendritic drainage system is assumed. Complex surfaces made up of permanent and semi-permanent potholes and the associated wetlands influence the timing and quantification of overland flow due to depressions and their impact on dynamic hydrologic connectivity. Thus, a new technique is needed to assess dynamic hydrologic connectivity associated with depression dominated landscapes and a new methodology/modified hydrologic model is needed for simulating the unique hydrologic processes associated with complex depressional areas like the PPR in North Dakota. Therefore, the objectives of this research are to:

- Develop a new procedure to analyze functional hydrologic connectivity related to topography, specifically in depression-dominated areas.
- Evaluate the impacts of the P2P processes and dynamic hydrologic connectivity on watershed outlet discharge.
- Address the combined effect of topographic depressions and wetland functions on hydrologic connectivity and watershed outlet discharge.

1.5. Organization of the Dissertation

Following this general introduction, Chapter 2 assesses the topographic similarities and differences of various land surfaces (i.e., depression-dominated surfaces and dendritic surfaces). These different surfaces are used to further define, quantify, and locate hydrologic connectivity and contributing area. The hydrologic processes governing the dynamic changes in hydrologic connectivity and contributing area are analyzed using the relative surface connectivity function (RSCf) (Antoine et al., 2009) and a new normalized connected area function (NACf) (Grimm and Chu 2018). The new analysis procedure developed in this chapter is also compared to a traditional delineation procedure (i.e., TauDEM) to highlight the improvements to identifying and quantifying dynamic hydrologic connectivity in a depression-dominated surface.

Chapter 3 takes a real application approach to identifying and quantifying hydrologic connectivity, specifically contributing area, and depression storage. In doing so, the impacts of the P2P processes and dynamic contributing area on outlet discharge are highlighted. Due to limitations in modeling hydrologic processes relating to depressions, an improved HEC-HMS model is developed in order to carry out the analysis. The improved modeling methodology introduces a depression threshold control proxy and an initial subdivision of contributing area to the outlet and contributing area to depression storage [i.e., non-depressional area (NDA) and depressional area (DA)]. The depression threshold control proxy specifies unique storage-discharge functions for each subbasin which reflects dynamic contributing area to the outlet. The improved model is compared to the basic HEC-HMS model to highlight the improved model accuracy and supplementary storage data provided by the improved model. The additional storage data can provide details relating to varying water availability and water levels within a subbasin which may help predict water shortages and ecological stresses on wetland habitats.

Lastly, chapter 4 takes another real application approach to analyze the impact of wetland type/function on hydrologic connectivity. An improved SWAT modeling approach is developed to simulate two different wetland functions and their impact on hydrologic connectivity. Classified wetlands from the cluster analysis in Rover et al. (2011) and Rover and Mushet (2015) were used to initially divide contributing areas and depression storage. The new modeling approach then utilizes two water routing functions in SWAT. The new modeling approach creates a more realistic representation of hydrologic processes within a depression-dominated region and provides more detailed water storage results based on wetland function. These storage results have the ability to indicate how land use change or climate may impact wetland areas and water availability.

1.6. References

Antoine M, Javaux M, and Bielders C. 2009. "What indicators can capture runoff-relevant connectivity properties of the micro-topography at the plot scale?" *Advances in Water Resources*, 32(8), 1297–1310.

Antoine M, Javaux M, Bielders CL. 2011. Integrating subgrid connectivity properties of the micro-topography in distributed runoff models, at the interrill scale. *Journal of Hydrology* 403: 213–223. DOI: 10.1016/j.jhydrol.2011.03.027

Appels WM, Bogaart PW, van der Zee SEATM. 2011. Influence of spatial variations of microtopography and infiltration on surface runoff and field scale hydrological connectivity. *Advances in Water Resources* 34: 303–313. DOI: 10.1016/j.advwatres.2010.12.003

Bernier PY. 1985. Variable source areas and storm-flow generation: An update of the concept and a simulation effort. *Journal of Hydrology* 79: 195–213. DOI: 10.1016/0022-1694(85)90055-1

Betson R. 1964. What is watershed runoff? *Journal of Geophysical research* 69: 1541–1552. DOI: 10.1029/JZ069i008p01541

Beven KJ, Kirkby MJ. 1979. A physically based, variable contributing area model of basin hydrology. *Hydrological Sciences Bulletin* 24: 43–69. DOI: 10.1080/02626667909491834

Bracken LJ, Croke J. 2007. The concept of hydrological connectivity and its contribution to understanding runoff-dominated geomorphic systems. *Hydrological Processes* 21: 1749–1763. DOI: 10.1002/hyp.6313

Bracken LJ, Wainwright J, Ali GA, Tetzlaff D, Smith MW, Reaney SM, and Roy AG. 2013. "Concepts of hydrological connectivity: Research approaches, pathways and future agendas." *Earth-Science Reviews*, 119, 17–34.

Chen YD. 2004. "Watershed Modeling : Where Are We Heading ?" *Information Sciences*, 2, 132–139.

Chu X, Yang J, Chi Y, and Zhang J. 2013. "Dynamic puddle delineation and modeling of puddle-to-puddle filling-spilling-merging-splitting overland flow processes." *Water Resources Research*, 49(6), 3825–3829.

Chu X, Zhang J, Chi Y, and Yang J. 2010. "An improved method for watershed delineation and computation of surface depression storage." *Watershed Management Conference 2010: Innovations in Watershed Management under Land Use and Climate Change*, 1113–1122.

Darboux F, Davy P, Gascuel-Odoux C, Huang C. 2002. Evolution of soil surface roughness and flowpath connectivity in overland flow experiments. *Catena* 46: 125–139. DOI: 10.1016/S0341-8162(01)00162-X

Dunne T, Black RD. 1970. An Experimental Investigation of Runoff Production in Permeable Soils. *Water Resources Research* 6: 478–490. DOI: 10.1029/WR006i002p00478

Engman ET, Rogowski AS. 1974. A partial area model for storm flow synthesis. *Water Resources Research* 10: 464–472. DOI: 10.1029/WR010i003p00464

Euliss NH, Mushet DM, Newton WE, Otto CR V, Nelson RD, LaBaugh JW, Scherff EJ, Rosenberry DO. 2014. Placing prairie pothole wetlands along spatial and temporal continua to improve integration of wetland function in ecological investigations. Journal of Hydrology 513: 490–503. DOI: 10.1016/j.jhydrol.2014.04.006

Gabrecht J, Martz LW. 2000. "TOPAZ: An Automated Digital Landscape Analysis Tool for Topographic Evaluation, Drainage Identification, Watershed Segmentation and Subcatchment Parameterization: TOPAZ User Manual." USDA Forest Service, Grazinglands Research Laboratory, USDA Agricultural Research Services, El Reno, OK.

Grimm K, and Chu X. 2018. "Modeling of spatiotemporal variations in runoff contribution areas and analysis of hydrologic connectivity." *Land Degradation & Development*, 29(8), 2629-2643. DOI: 10.1002/ldr.3076

Güntner A, Seibert J, Uhlenbrook S. 2004. Modeling spatial patterns of saturated areas: An evaluation of different terrain indices. *Water Resources Research* 40: W05114. DOI: 10.1029/2003WR002864

Hayashi M, van der Kamp G, Rosenberry DO. 2016. “Hydrology of prairie wetlands: Understanding the integrated surface-water and groundwater processes.” *Wetlands,* 36, 237-234. DOI: 10.1007/s13157-016-0797-9

Heerdegen RG, Beran MA. 1982. Quantifying source areas through land surface curvature and shape. *Journal of Hydrology* 57: 359–373. DOI: 10.1016/0022-1694(82)90155-X

Hewlett JD, Hibbert AR. 1967. Factors affecting the response of small watersheds to precipitation in humid areas. *Forest hydrology*, New York, Pergamon Press, 275–279

Jenson SK., Domingue JO. 1988. “Extracting topographic structure from digital elevation data for geographic information system analysis.” *Photogrammetric Engineering and Remote Sensing*, 54(11), 1593–1600.

Lafleur PM. 2009. Connecting Atmosphere and Wetland: Trace Gas Exchange. *Geography Compass* 3: 560–585. DOI: 10.1111/j.1749-8198.2008.00212.x

Marks D, Dozier J, and Frew J. 1984. “Automated Basin Delineation From Digital Elevation Data.” *Geo-Processing*, 2(3), 299–311.

Neff BP, Rosenberry DO. 2018. “Groundwater connectivity of upland-embedded wetlands in the prairie pothole region.” *Wetlands* 38, 51-63. DOI: 10.1007/s13157-017-0956-7

O ’Callaghan JF, Mark DM. 1984. “The Extraction of Drainage Networks from Digital Elevation Data.” *Computer Vision, Graphics, and Image Processing*, 28(2), 323–344.

Ogden FL, Watts BA. 2000. Saturated area formation on nonconvergent hillslope topography with shallow soils: A numerical investigation. *Water Resources Research* 36: 1795-1804. DOI: 10.1029/2000WR900091

Peñuela A, Darboux F, Javaux M, Bielders CL. 2016. “Evolution of overland flow connectivity in bare agricultural plots.” *Earth Surface Processes and Landforms*, 41(11), 1595–1613.

Pringle C. 2003. What is hydrologic connectivity and why is it ecologically important? *Hydrological Processes* 17: 2685–2689. DOI: 10.1002/hyp.5145

Richards PL, Brenner AJ. 2004. *Delineating Source Areas for Runoff in Depressional Landscapes: Implications for Hydrologic Modeling*. *Journal of Great Lakes Research* 30: 9-21. DOI: 10.1016/S0380-1330(04)70325-1

Rinderer M, Ali G, Larsen L. 2017. "Quantifying hydrologic connectivity with measures from the brain neurosciences – a feasibility study." *Geophysical Research Abstracts EGU General Assembly*, 19, 2017–8656.

Rover J, Mushet DM. 2015. "Mapping Wetlands and Surface Water in the Prairie Pothole Region." *R. Tiner, M. Lang and V. Klemas (eds) Remote Sensing of Wetlands: Applications and Advances*, CRC Press, Boca Raton, FL, 347–367.

Rover J, Wright CK, Euliss NH, Mushet DM, Wylie BK. 2011. "Classifying the hydrologic function of prairie potholes with remote sensing and GIS." *Wetlands*, Springer Netherlands, 31(2), 319–327.

Schwanghart W, Heckmann T. 2012. "Fuzzy delineation of drainage basins through probabilistic interpretation of diverging flow algorithms." *Environmental Modelling and Software*, 33, 106–113.

Singh VP. 1995. *Computer models of watershed hydrology*. Water Resources Publications, Highlands Ranch, CO.

Tarboron DG. 1997. "A new method for the determination of flow directions and upslope areas in grid digital elevation models." *Water Resources Research*, 33(2), 309–319.

Turcotte R, Fortin JP, Rousseau A, Massicotte S, Villeneuve JP. 2001. Determination of the drainage structure of a watershed using a digital elevation model and a digital river and

lake network. *Journal of Hydrology* 240: 225–242. DOI: 10.1016/S0022-1694(00)00342-5

USACE-HEC. (2013). "Hydrologic Modeling System HEC-HMS - User â€™ s Manual." (December), 442.

Walter MT, Walter MF, Brooks ES, Steenhuis TS, Boll J, Weiler K. 2000. Hydrologically Sensitive Areas: Variable Source Area Hydrology Implications for Water Quality Risk Assessment. *Journal of Soil and Water Conservation* 3: 277–284

Wu Q, Lane CR. 2017. Delineating wetland catchments and modeling hydrologic connectivity using LiDAR data and aerial imagery. Hydrology and Earth System Sciences 21: 3579–3595. DOI: 10.5194/hess-21-3579-2017

Yang J, Chu X. 2013. "Quantification of the spatio-temporal variations in hydrologic connectivity of small-scale topographic surfaces under various rainfall conditions." *Journal of Hydrology*, 505, 65–77.

2. MODELING OF SPATIO-TEMPORAL VARIATIONS IN RUNOFF CONTRIBUTION AREAS AND ANALYSIS OF HYDROLOGIC CONNECTIVITY[1]

2.1. Abstract

Traditional delineation and modeling methods do not consider the spatial arrangement and dynamic threshold control of surface depressions. Instead, full structural hydrologic connectivity, uniform well-connected drainage networks, and an invariant contributing area are often assumed. In reality, depressions play an important role in quantifying functional connected areas (ACs) and contributing area. This study is aimed to develop a new procedure to analyze functional hydrologic connectivity related to topography at a meso-scale, specifically in depression-dominated areas by: (1) characterizing surface topography, (2) quantifying and locating dynamic hydrologic connectivity, and (3) analyzing hydrologic connectivity and threshold-controlled dynamics of contributing area using a set of dimensionless indicators and a new normalized connected area function (NACf). Thorough analyses for different topographic surfaces provided improved understanding of the intrinsic relationship and interaction between structural and functional hydrologic connectivity patterns. In addition, the new procedure was compared against a traditional delineation method, TauDEM, to determine structural and functional connectivity. It was found that spatial arrangement and scale of depressions had a direct effect on hydrologic connectivity. A stepwise trend, unique to depression-dominated areas, highlighted the effect of threshold behaviors on contributing area and ACs. Conversely, dendritic

[1] The material in this chapter was co-authored by Kendall Grimm and Dr. Xuefeng Chu. Kendall Grimm had primary responsibility for developing the new analysis procedure and modeling of the system. Kendall Grimm was the primary developer of the conclusions that are advanced here. Kendall Grimm also drafted and revised all versions of this chapter. Dr. Xuefeng Chu served as proofreader and checked analysis conducted by Kendall Grimm.

surfaces showed an expedited surface connectivity due to the assumption of depressionless topography. Thus, precisely locating and quantifying ACs and contributing area via the new analysis procedure improve our understanding of the mechanisms of topography-controlled overland flow and sediment transport dynamics, and hence the findings are valuable in making informed decisions about water quantity and quality across varying topographic surfaces.

2.2. Introduction

Fundamental hydrologic processes, such as overland flow generation and sediment transport, are affected by surface topography. Generally, a land surface is not smooth, and some places can be greatly affected by the sizes and spatial distributions of depressions. Depressions on a landscape act as storage space for ponded water, and since all depressions on a landscape have different sizes, topographic characteristics, and hydrologic features, surface runoff often exhibits threshold behaviors depending on these variables (Chu, 2015). Characterization of surface topography and depressions is of importance in basin delineation, which further affects modeling and analyses of dynamic hydrologic connectivity.

Most basin delineation procedures have been based on a digital elevation model (DEM). Various properties of terrain, such as slope and aspect, can be determined by topographic analyses of the DEM. These topographic and geometric parameters can then be used in the basin delineation process. Traditional delineation methods (e.g., Marks et al., 1984; O'Callaghan & Mark, 1984; Jenson & Domingue, 1988; Tarboron, 1997; Gabrecht & Martz, 1999), however, implement simplified delineation approaches for depressions. For instance, in TOPAZ, a DEM-based automated topographic analysis program (Gabrecht & Martz, 1999), all depressions are first filled, and then flow directions and accumulations are determined based on the depressionless DEMs. Similarly, pit removal or depression filling is implemented in TauDEM

(Terrain Analysis Using Digital Elevation Models) (Tarboron, 1997), which is based on the D-infinity flow direction method. In the traditional methods, artificial slopes and flow directions are often introduced across the depressional areas of a surface, which guarantees that the surface will have full structural hydrologic connectivity and an invariant contributing area.

In reality, however, hydrologic connectivity and contributing area are dynamic features, and surface topography, specifically depressions, play important roles in quantifying these dynamic features. The spatial distribution and scale of depressions control the timing of overland flow initiation, and thus have an impact on dynamic contributing area. For this reason, traditional delineation approaches may not be appropriate to use when investigating dynamic hydrologic connectivity for depression-dominated surfaces. The Prairie Pothole Region (PPR) in North America, featuring numerous pothole depressions across scales, is of interest for many hydrologic and ecological studies (Euliss et al., 2004, 2014; Euliss & Mushet, 1996; Goldhaber et al., 2014; Mushet et al., 2015a, 2015b; Rover et al., 2011). Over the last century, the associated ecosystems have been degraded due to the conversion of wetlands/grasslands to cultivated croplands. And it is also of particular interest to quantify the impact of such conversion on water quality and quantity in the wetland areas that are not hydrologically connected to an outlet, but still experience dynamic connectivity between surrounding wetlands and pothole lakes (Euliss & Mushet, 1996). Progress has been made in recent studies (Antoine et al., 2009; Bracken et al., 2013; Yang & Chu, 2013; Peñuela et al., 2015, 2016; Rinderer et al., 2017; Wu & Lane, 2017) to address the variability of hydrologically connected areas and contributing area across multiple landscapes and scales. A thorough knowledge of the areas that contribute to runoff can improve modeling of water quantity, fate and transport of sediments, chemicals, and bacteria in surface water, especially for depression-dominated areas (e.g., PPR).

Different definitions have been used for hydrologic connectivity to understand flow parameters, soil moisture patterns, and surface topography (Bracken et al., 2013). Various terms such as variable source area (Hewlett & Hibbert, 1967), partially contributing area (Betson, 1964), saturated source area (Ogden & Watts, 2000), hydrologically sensitive area (Walter et al., 2000), and potentially contributing source area (Richards & Brenner, 2004) have been proposed to identify how and why only a small proportion of a basin contributes surface runoff to the outlet. Even with all of these terms, the development of models to handle the identification of functional hydrologic connectivity and the development of connectivity indices lack a preferred foundation (Bracken et al., 2013; Rinderer et al., 2017). Two types of hydrologic connectivity are commonly used. The first is structural hydrologic connectivity, derived directly from surface topography, terrain parameters, and other static spatial features (Borselli et al., 2008; Cavalli et al. 2013). The second is functional hydrologic connectivity, derived from hydrologic quantity modeling for a surface with varying rainfall events (Antoine et al., 2009; Bracken et al., 2013). These terms have been developed to determine connectivity because it is easier to simulate spatial patterns in flow, rather than directly observe them (Güntner et al., 2004).

It has been even more difficult to simulate hydrologic connectivity of depression-dominated surfaces. For instance, depression filling models have been used to analyze overland flow generation and hydrologic connectivity (e.g., Darboux et al. 2002; Appels et al. 2011; Antoine et al. 2011) and runoff initiation, depression storage, and spatial distribution of microtopography have been identified as key features affecting the size and distribution of individual hydrologically connected areas. Similarly, Antoine et al. (2009) investigated functional connectivity for three types of surface microtopography and found that river fields reached a steady state runoff faster than two other microtopography types (random and crater

fields). Although surface storage must be fully filled to reach a steady state runoff rate, this does not mean that surface depression storage must be fully filled to produce any runoff (Singh, 1995; Antoine et al., 2009). Other studies on evaluating the impacts of depressions on water quality and quantity modeling have shown that traditional delineation methods may not work for depressional areas (Shaw et al., 2012). For example, Temme et al. (2006) developed an algorithm to determine soil erosion and sediment transport in depressions that are commonly considered as extraneous in many erosion models. Lane et al. (2016) investigated connectivity and sediment transport on glacial slopes under the influence of depressions and found that pre-filling led to considering disconnected contributing areas. These studies, however, did not consider the influence of threshold behaviors of surface depressions on dynamic hydrologic connectivity. These threshold dynamics are controlled by time variant depression filling, spilling, and merging processes (Chu et al., 2013).

The overall goal of this study is to improve the understanding of functional hydrologic connectivity for varying topographic landscapes using a new analysis procedure that features characterization of surface topography, identification of spatial distribution of depressions, and modeling of discontinuous overland flow processes and the associated threshold behavior. Although land use and land cover, vegetation, rainfall event properties, and many other factors may affect some aspects of hydrologic connectivity, the purpose of this study is to analyze hydrologic connectivity created by spatial flow patterns mainly affected by topographic features. The specific objectives are to: (1) assess the topographic similarities and differences of land surfaces, (2) quantify and locate dynamic changes in hydrologic connectivity and contributing area to the basin outlets for different surfaces, (3) analyze hydrologic connectivity using a new normalized connected area function (NACf), and threshold-controlled dynamics of contributing

area using the relative surface connectivity function (RSCf) (Antoine et al., 2009) and other dimensionless indicators, and (4) compare TauDEM to the new analysis procedure and surface delineation/topography characterization methods for determining hydrologic connectivity for depression-dominated surfaces.

2.3. Methodology

Figures 2.1 and 2.2 provide the foundation of the new procedure proposed in this study for analyzing and identifying hydrologically connected areas (ACs) and contributing area to the outlet (CA) for depressional surfaces. Figure 2.1 shows the process in which a surface is characterized, spatial distribution of depressions is determined, and functional hydrologic connectivity is simulated to show possible surface connections relating to surface topography and precipitation. Figure 2.2 schematically depicts the relationships of typical topographic characteristics of surfaces (spatial distributions of depressions) with their outlet hydrographs (hydrologic response), and progressive evolution of hydrologic connectivity, ACs, and CA.

2.3.1. Characterization of Surface Topography

To characterize a surface, it is important to first identify depressions on the surface because their arrangement and spatial distribution on the surface can affect flow directions and accumulations (Figure 2.1). To identify depressions, a new depression-dominated delineation (D-cubed) algorithm (Tahmasebi Nasab et al., 2017a) was utilized. Topographic depressions or puddles in the algorithm can range in size depending on the scale. In this study, 10-m DEMs were utilized for delineation. By using the D-cubed algorithm, surface topography can be characterized into depressional and non-depressional units [i.e., puddle-based units (PBUs) and channel-based units (CBUs), respectively], and the puddle relationships throughout the puddle-to-puddle (P2P) process can be defined (Chu et al., 2010, 2013; Chu, 2015; Habtezion et al.,

2016; Tahmasebi Nasab et al., 2016; Tahmasebi Nasab et al., 2017b). To identify puddle cells, the algorithm implements a moving-window searching process. This process is continued until a threshold cell is found, through which a puddle spills when it is fully filled. Based on the topography, different types of puddles can be identified which are defined by the arrangement and the numbers of puddle centers and thresholds. In turn, the characteristics of these puddles will affect hydrologic processes (e.g., depression storage and connectivity), which consequently affect surface runoff. Once the components of first-level puddles (including puddle centers, puddle thresholds, and puddle cells) are defined, additional puddle levels can be determined. If two or more puddles share a threshold cell, they will merge to form a larger higher-level puddle as part of the P2P process. As this process continues, eventually the highest-level puddles are formed. In the D-cubed algorithm, cell-to-cell (C2C) flow directions are determined by the D8 method (O'Callaghan & Mark, 1984). All first-level puddle cells have flow directions toward their centers, and the puddle centers have a "zero" flow direction. Any higher-level puddles have multiple centers or flats (the ponding areas of their embedded lower-level puddles) with a "zero" flow direction, except for their threshold cells where water flows to an outside downstream cell. Thus, the flow directions of the same puddle cells can be different at different puddle levels, depending on their filling conditions. Flow accumulations are determined by flow directions. Note that when a puddle is fully filled, all puddle cells will have the same flow accumulation value because a fully-filled puddle has a "zero" flow direction and all puddle cells share a uniform water level. Finally, these topographic characteristics computed for all puddle levels are used in hydrologic modeling. For example, Tahmasebi Nasab et al. (2017c) utilized the D-cubed algorithm as a tool to obtain topographic details and incorporated them into the Soil and Water Assessment Tools (SWAT) to improve hydrologic modeling in depression-dominated areas. For

this study, surface topographic characteristics obtained from the delineation process are used to analyze dynamic connectivity and CA.

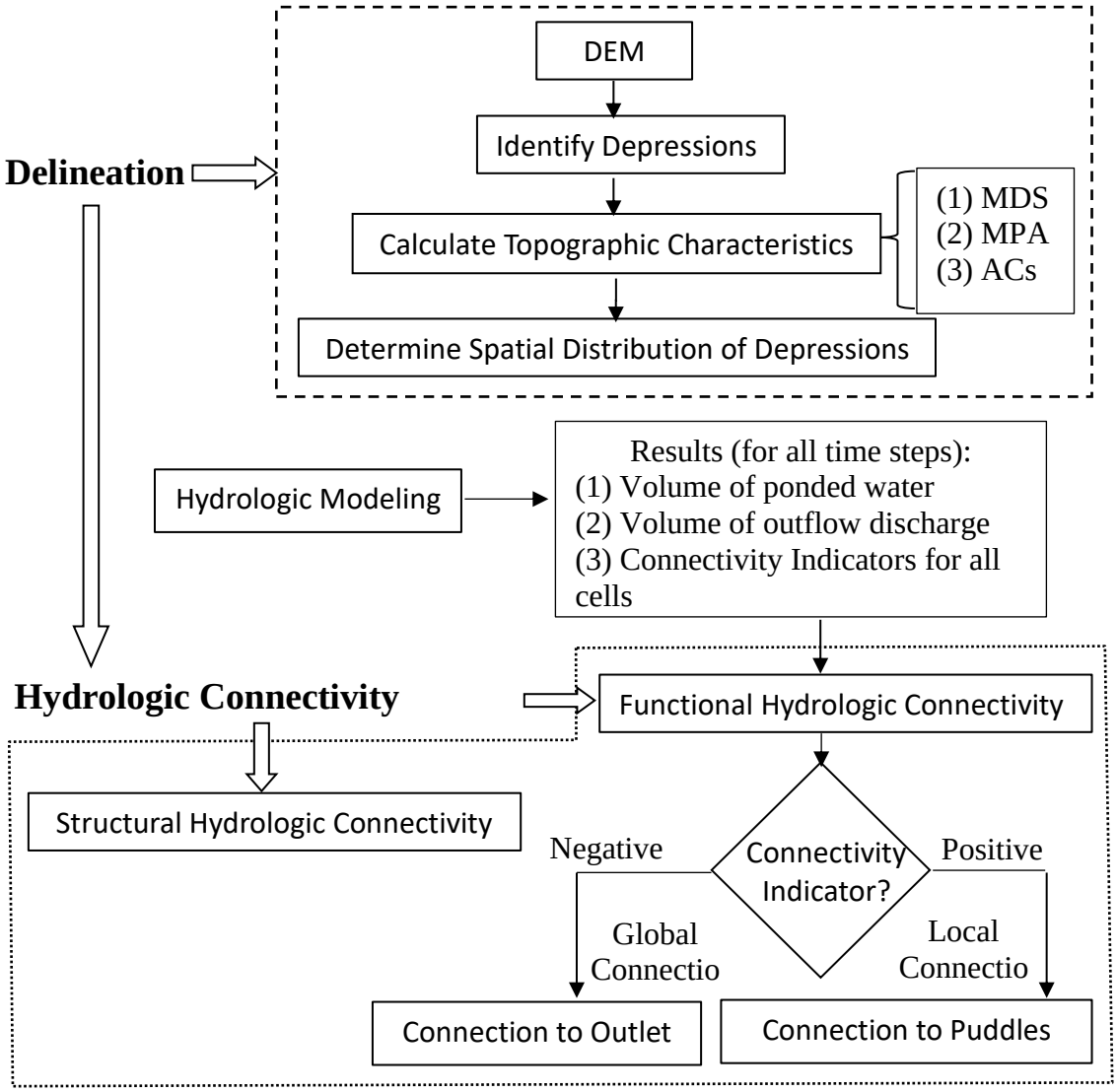

Figure 2.1. Flowchart of the methodology for analyzing hydrologic connectivity. Structural connectivity is determined based on surface delineation and the calculated surface topographic characteristics (maximum depression storage, MDS; maximum ponding area, MPA; and connected areas, ACs), and spatial distribution of depressions. Functional connectivity is determined by performing hydrologic modeling based on delineation results, and the analyses quantify contributing area to the outlet and connected area to potholes.

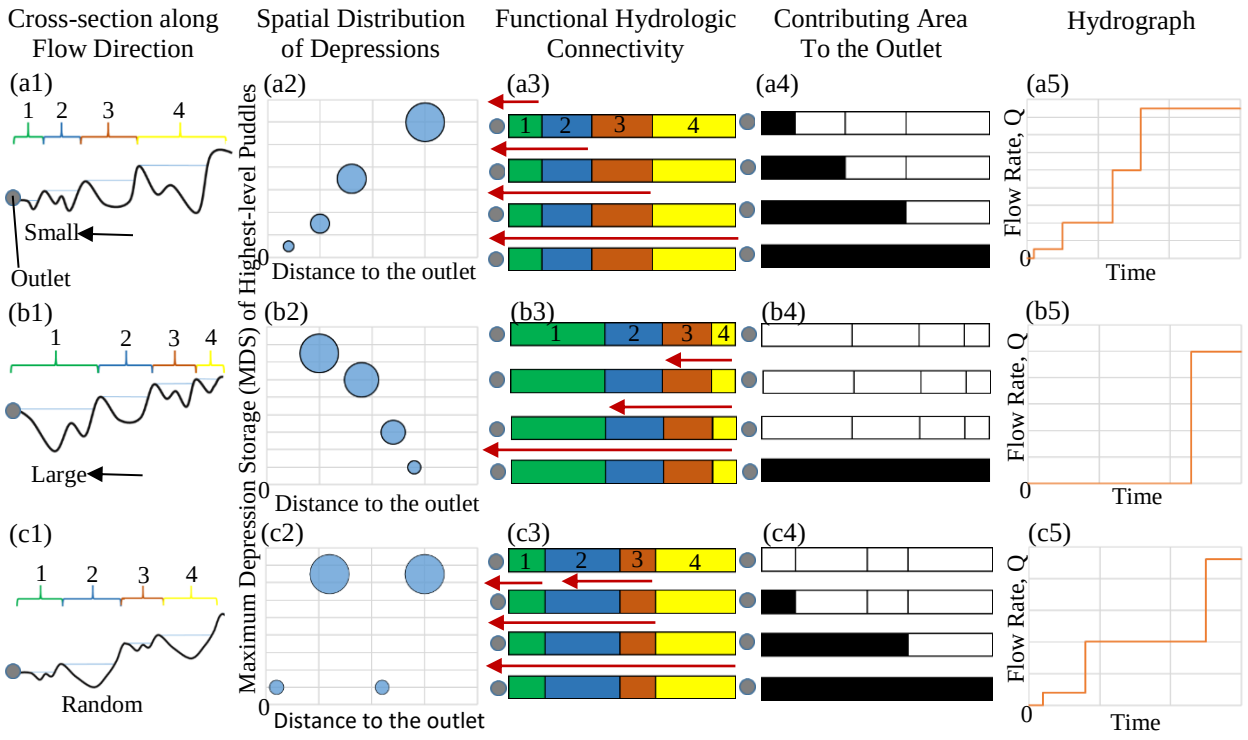

Figure 2.2. Illustration of cross sections of different types of spatial distributions of highest-level potholes (a1. small - large; b1. large - small; c1. example of random distribution) and a graphical representation of pothole maximum depression storage (MDS) vs. distance to the outlet (a2. small - large; b2. large - small; c2. example of random distribution). Corresponding to these typical spatial distributions, connected areas (ACs) are identified (a3-c3). The red arrows show the dynamic changes in connectivity and progressive connections of ACs (a3-c3). Dynamic hydrologic connectivity, in turn, affects the timing and evolution of contributing area to the outlet (a4-c4), and the timing and quantity of discharge through the outlet (a5-c5).

Once the hierarchical puddle levels are determined and the surface is delineated, topographic property parameters are computed (Figure 2.1). They include the surface area, maximum depression storage (MDS), maximum ponding area (MPA), mean contributing area, mean slope, mean maximum puddle depth, mean puddle depth, number of puddle levels, number of puddles, number of highest-level puddles, number of first-level puddles, and number of delineated basins. PBUs (i.e., areas contributing to the associated highest-level puddles) and CBUs are also identified. From the MDS parameters and the delineated surface, the spatial distribution of puddles along the dominant flow direction toward the outlet can be determined

(Figure 2.1 and Figures 2.2a1-2.2c1, 2.2a2-2.2c2). Additionally, ACs, which are the contributing areas to different associated puddle levels, are identified. These topographic characteristics provide the foundation for hydrologic connectivity analysis.

2.3.2. Modeling of Threshold-controlled Overland Flow and Hydrologic Connectivity

Hydrologic modeling is performed to determine functional hydrologic connectivity (Figures 2.1 and 2.2). In the current method, cell-to-cell (C2C) and dynamic P2P filling, spilling, merging, and splitting processes are simulated by using the P2P modeling system (Chu et al., 2013; Yang & Chu, 2015). Simultaneously, detailed dynamics of hydrologic connectivity are also simulated. In the modeling, the ACs control the flow of water over the surface, forming a cascading drainage network for all related contributing cells (C2C routing) and for all puddles (P2P routing) till flow is discharged through the basin outlet by a series of hydrologically connected areas. Runoff contribution from an upstream AC does not occur until the puddle threshold is breached. This implies that the entire basin will not contribute to the outlet until all ACs merge to form a connected unit and all highest-level puddles reach their MDS values (Figure 2.2).

Reaching full hydrologic connectivity highlights possible connections across the entire surface (Figure 2.1 and Figures 2.2a3-2.2c3), rather than just focusing on connections to the outlet (i.e., CA) (Figure 2.1 and Figures 2.2a4-2.2c4). Understanding dynamic connections over the entire surface provides valuable information that can be further used for sediment transport modeling and assessment of environmental impacts for areas of interest that may not be hydrologically connected to the outlet (i.e., ACs).

Figure 2.2 depicts the expected dynamic hydrologic connectivity, CAs, and hydrographs of some simplified, but typical depressional surfaces to highlight the methodology and the

fundamentals of the new analysis procedure. The surfaces in Figures 2.2a1- 2.2c1 show different spatial distributions of the highest-level puddles along the dominant flow direction of a basin. Figures 2.2a2-2.2c2 define the types of spatial distributions of puddles as the distance of the highest-level puddle from the outlet vs. its MDS. The conditions for hydrologic connectivity based on puddle levels are depicted as the first bars in Figures 2.2a3-2.2c3. Dynamic connectivity matures as all ACs are connected based on the spatial distributions and sizes of their puddles. A spatial distribution of puddles with a small-large pattern from the outlet has ACs expanding from AC1 to AC4 (Figure 2.2a3) because of the time required to fully fill the highest-level puddles. The highest-level puddle in AC1 is very small and will be first filled and connected to the outlet. Next, the slightly larger highest-level puddle in AC2 will be fully filled and connected to the outlet through AC1. This process continues until the entire surface is connected and all highest-level puddles are fully filled. In turn, the contributing area to the outlet will show the same pattern (Figure 2.2a4) and the hydrograph will show a gradual, stepwise change in discharge through the outlet as more ACs become connected to the outlet (Figure 2.2a5). A spatial distribution of puddles with a large-small pattern from the outlet has connected areas growing from AC4 to AC1 (Figure 2.2b3). There will be no contributing area to the outlet until the highest-level puddle in AC1 becomes fully filled (Figure 2.2b4). To become fully filled, the smaller upstream ACs must be fully filled and connected to the downstream to contribute runoff to AC1. Figures 2.2c1 and 2.2c2 show an example of a random distribution of puddles to depict dynamic connectivity possibilities. In this case, puddles fluctuate with a small-large-small-large pattern from the outlet. As shown in Figure 2.2c3, initially no highest-level puddles are fully filled. Therefore, the first bar in Figure 2.2c4 depicts no contributing area to the outlet. The highest-level puddles in AC1 and AC3 become fully filled at the same time, so AC1

connects to the outlet while AC3 connects to AC2 (Figure 2.2c3) The additional connected area from AC3 allows for the highest level puddle in AC2 to become fully filled faster than the highest-level puddle in AC4 which has the same MDS as AC2. When the highest level puddle AC2 becomes fully filled, it connects downstream to the outlet through AC1. At this time, AC1, AC2, and AC3 will contribute to the outlet (Figure 2.2c4). The large highest level puddle in AC4 will take the longest to be fully filled since it has no upstream ACs connecting to it. When the large puddle in AC4 becomes fully filled, the entire surface contributes to the outlet. Similarly, the hydrograph depicts large, and sometimes uneven steps in increasing flow through the outlet (Figure 2.2c5).

2.3.3. Hydrologic Connectivity Analysis and Quantification of Contributing Areas

In this study, functional hydrologic connectivity is determined based on modeling of the P2P dynamics. The results are analyzed and processed to quantify and locate the changes in ACs and CA over time. A hydrologic connectivity indicator is determined during modeling to denote whether a specific cell at a specific time step contributes runoff water to a puddle (positive value) or to the basin outlet (negative value) (Figure 2.1). That is, this indicator not only shows the connection status, but also the type of the connected elements (i.e., puddle or outlet). In this way, the contributing area to the final outlet(s) of the entire surface (negative indicator) and connected areas within a basin at all time steps (positive indicator) are quantified and located. This approach to quantify contributing area uses the topographic characterization results, threshold behavior of puddles, and dynamic P2P and C2C processes. This method considers dynamic changes in contributing area across depression-dominated landscapes, rather than a potentially fixed hydrologic connectivity and contributing area assumed in traditional delineation and modeling methods for dendritic basins.

First, based on the modeling results, ACs at different stages of puddle filling-spilling-merging (similar to Figure 2.2a3-2.2c3) were identified and quantified. Particularly, a new normalized connected area function (NACf) was proposed in this study to analyze dynamic ACs during the P2P process. The NACf is defined as the ratio of the number of delineated basins to the dynamic number of ACs. Thus, for NACf = 1, all basins are fully connected to their outlets. The relationship of normalized depression storage (ratio of water-filled depression storage to MDS) vs. NACf links topographic characteristics, or structural connectivity characteristics, to simulated functional hydrologic connectivity.

Second, several dimensionless indicators, such as the relative surface connection function (RSCf) (Antoine et al., 2009), were utilized to analyze functional hydrologic connectivity and dynamic variations of CA as a function of the calculated surface topographic characteristics, rather than a function of time. Peñuela et al. (2015, 2016) utilized similar normalized analyses to study CA for different surfaces based on microtopography. In this study, the RSCfs were computed to relate the normalized depression storage to the normalized contributing area (ratio of contributing area to the total surface area) and reveal the functional connectivity of the surface and the dynamic influence of surface depression storage. Normalized depression storage was analyzed based on the dynamic water storage from the P2P modeling and the calculated MDS. Studying the trend of RSCfs reveals the effect of different structural characteristics on functional CA.

Third, simplified hydrographs (Antoine et al., 2009; Darboux et al., 2002; Peñuela et al., 2016) were created to study the relationship between normalized outlet runoff (ratio of cumulative runoff to cumulative rainfall, i.e., ratio of outflow to inflow) and dimensionless

cumulative rainfall (ratio of cumulative rainfall to the total rainfall at the time of fully matured connectivity) or dimensionless time (ratio of time to the total simulation period).

Fourth, to gain insight into the intrinsic interrelations and interactions between hydrologic processes (e.g., surface runoff) and topographic characteristics (e.g., depression storage), the relationships between normalized runoff and normalized depression storage and MDS-normalized cumulative rainfall (ratio of cumulative rainfall to MDS) were examined. Such relationships are indicators of both surface topography and functional connectivity (Antoine et al., 2009). The MDS-normalized rainfall also accounts for the effect of surface topography on runoff initiation because MDS is a function of topography. These indicators reflect the relationships of connectivity and CA, and reveal the influence of surface topography on overland flow generation, runoff initiation, and discharge. Since these indices are dimensionless, different surfaces can be compared side by side.

2.3.4. Selection of Study Areas and Modeling Scenarios

Three different land surfaces with dissimilar topographic features (Figure 2.3) were selected in this study for analyzing hydrologic connectivity and quantifying contributing areas under dissimilar topographic conditions. The three surfaces are located in the Prairie Pothole Region (PPR) in North Dakota. This region in the Northern Great Plains is characterized by mid-tall grass prairies and numerous permanent and semi-permanent potholes and the associated wetlands (Euliss et al., 2014). The climate of this region is characterized by dry/wet cycles of drought and deluge, which consequently affect the volume and depths of the potholes and wetlands on the landscape (Mushet et al., 2015b). Average yearly precipitation for the most recent wet cycle from 1993 to 2014 was 505.4 mm and evapotranspiration accounts for the largest water loss (Mushet et al., 2015b). For the study surfaces, 10-m DEM data were

downloaded from the USGS Map Viewer (https://viewer.nationalmap.gov/launch/) and used for topographic delineation and hydrologic connectivity analysis based on the aforementioned new procedure (Figure 2.1).

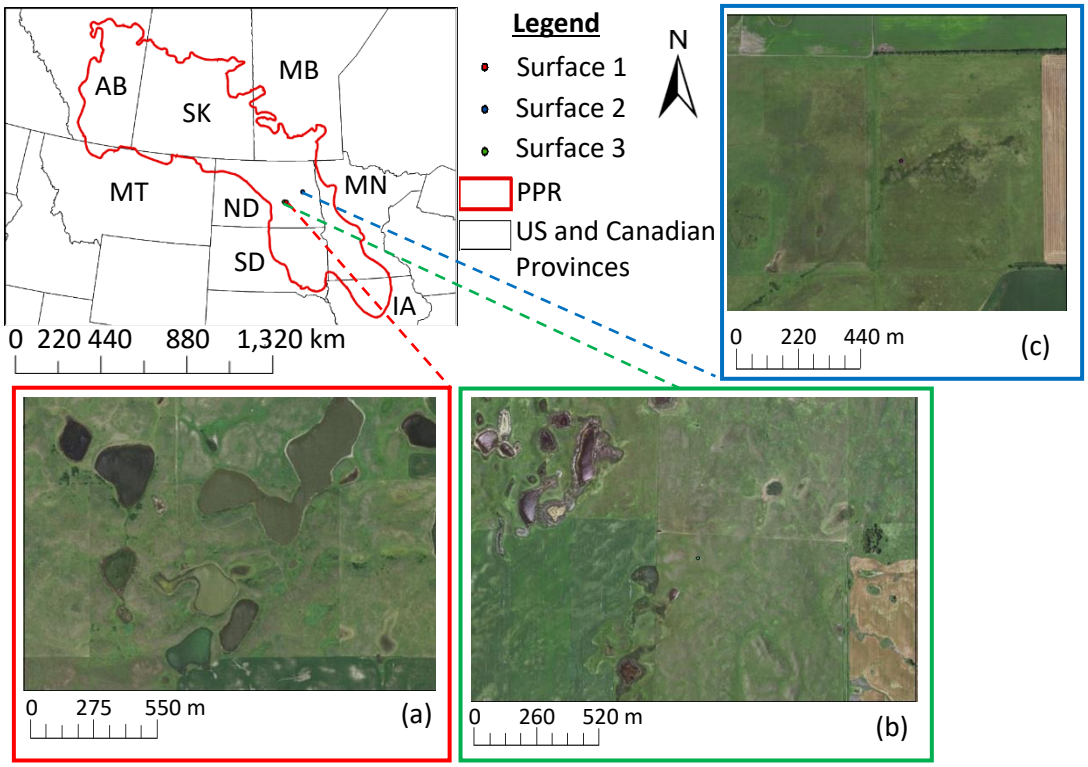

Figure 2.3. Locations of three selected surfaces in the Prairie Pothole Region of North Dakota and the corresponding satellite imageries for (a) Surface 1; (b) Surface 2; (3) Surface 3.

Surface 1 is located in the Cottonwood Lake Study Area (CLSA) and is featured by many large embedded, uniformly-distributed potholes across a landscape with an area of 2.5 km^2 and an average local slope of 7.6% (Figure 2.3a) (latitude = 47.0992 N, longitude = -99.0988 E). The CLSA, a research site of the USGS Northern Prairie Wildlife Research Center (NPWRC), is pristine prairie and has hosted long-term ecologic and hydrologic studies since 1967 (Winter, 2003). Surface 1 was selected for further analyses throughout this study to focus on the impact of meso-scale depression-dominated topography on hydrologic connectivity. Surface 2 is a herbaceous range land and has a group of well-connected potholes along with many very small

depressions (Figure 2.3b) (latitude = 47.1159 N, longitude = -99.2360 E) over an extent of 2.3 km2 with an average local slope of 3.2%; and Surface 3 is a mixture of herbaceous range land and farm land that is characterized by a well-defined, channelized drainage system and a relatively flat landscape without any major depressions (Figure 2.3c) (latitude = 47.5758 N, longitude = -97.9836 E) over an extent of 1.4 km2 with an average local slope of 0.6%. These surfaces were selected because they represent three different surface types, from which dynamic hydrologic connectivity and contributing area patterns assessed by using the new procedure developed in this study can be compared.

To analyze functional hydrologic connectivity and characterize contributing areas under the influence of surface topography using the new analysis procedure, a modeling scenario was considered for the three selected surfaces (Figure 2.3). Steady and uniform rainfall was used for modeling to analyze incremental changes in contributing area. The net rainfall quantity (both intensity and duration) was determined to ensure all depressions were fully filled, showing the complete coverage of the entire dynamic evolution of threshold-controlled contributing areas (Figure 2.1). Thus, the simulation for each surface did not represent real conditions, and each simulation stopped when the surface reached a fully-filled condition. The rainfall intensity for the modeling was 7.5 mm h-1, which represents a storm in central North Dakota with a 1-year recurrence interval lasting 3-6 hours (NOAA, 2017). The total simulation periods for the three surfaces were 116 hours with 1-h time steps, 24.5 hours with 15-min time steps, and 20 hours with 15-min time steps, respectively. Different simulation time intervals were used to ensure to capture any small changes in hydrologic connectivity for Surfaces 2 and 3 which have smaller depression storage than Surface 1.

2.3.5. Different Delineation Approaches for Hydrologic Connectivity Analysis and Quantification of Contributing Areas

To compare the applicability of the new procedure with the traditional methods, structural hydrologic connectivity was also determined and analyzed by using TauDEM (Tarboron, 1997) that has been incorporated in ArcGIS. Like other traditional methods, TauDEM also calculates flow directions, slopes, and flow accumulations based on a hydrologically conditioned DEM or a DEM with depressions removed by raising the elevations of depressional cells. In contrast, the method described in this study is able to gather topographic information such as depression storages, depressional areas, flow accumulations in both depressions and channels, as well as MDS values of puddles at different levels. To compare the new analysis procedure and TauDEM, Surface 1 (Figure 2.3a) was selected and delineated by using both methods. After delineation, the original DEM of Surface 1 was subtracted by the filled DEM created by the TauDEM method. The elevation differences of these two DEMs show the depressions and their distributions.

To determine structural hydrologic connectivity, delineation was performed by using the D-cubed algorithm for an unfilled condition (i.e., using the original DEM). The connectivity to all first-level puddle centers was identified and quantified. Similarly, using the TauDEM toolbox in ArcMap, flow directions and accumulations were determined, and contributing area was identified and quantified based on the filled DEM. Note that in TauDEM, contributing area is determined for any selected channel cell for a depressionless surface, while the new analysis procedure identifies contributing area for a landscape with depressions which can be a locally connected, closed flow system, depending on their filling-spilling conditions. Additionally, the contributing areas to the highest-level puddles were determined based on the threshold cells

identified in the new method. Comparing the results from these two methods highlights the fundamental differences in methodology, and demonstrates how the delineation and modeling methodology affects hydrologic connectivity analysis and identification of contributing areas especially for depression-dominated surfaces.

2.4. Results

2.4.1. Characterization of Surface Topography

The D-cubed algorithm identified puddles/depressions for the three study areas (Surfaces 1-3, Figure 2.3), and computed topographic parameters. Figures 2.4a1, 2.4b1, and 2.4c1 show all puddles and their corresponding centers and thresholds on the three surfaces. Table 2.1 lists the major topographic parameters such as number of puddles, number of puddle levels, mean puddle depth, number of basins, MDS, MPA, and mean slope. Over Surface 1 with an area of 2.5515 km^2, there are 126 puddles identified across 17 different puddle levels. In contrast, smaller Surfaces 2 and 3 had 247 and 335 puddles across 6 and 4 puddle levels, respectively. The sizes of the puddles and their spatial distributions differ for the three surfaces. Significant differences in MDS and MPA, as well as the numbers of PBUs and CBUs can be observed (Table 2.1). The delineation algorithm determined flow directions and accumulations, from which 17, 45, and 34 basins were identified for the three selected surfaces, respectively (Figures 2.4a2, 2.4b2, and 2.4c2).

Table 2.1. Major topographic property parameters of surfaces 1, 2, and 3.

Parameters	Surface 1	Surface 2	Surface 3
Surface area (km^2)	2.5515	2.3622	1.3734
Number of puddle levels	17	6	4
Number of puddles across all levels	126	247	335
Number of initial connected areas (ACs)	36	69	53
Number of puddle-based units (PBUs)	33	46	138
Number of channel-based units (CBUs)	72	143	121
Mean puddle depth (m)	0.358	0.031	0.013
Number of basins	17	45	34
Maximum depression storage (MDS) (m^3)	1,145,571	48,979	2,259
Maximum ponding area (MPA) (m^2)	548,600	200,200	74,600
Mean slope (%)	7.651	3.313	1.147

In traditional delineation methods, all surface depressions are assumed to be fully filled, creating a modified DEM so depressions and their slopes have no effect on flow directions and flow accumulations (Marks et al., 1984; O 'Callaghan & Mark, 1984; Jenson & Domingue, 1988; Gabrecht & Martz, 1999). In contrast, the new procedure employs an unmodified DEM to identify topographic characteristics which affect the quantification of structural and functional hydrologic connectivity, as shown in the following comparison of TauDEM and the new analysis procedure. The parameters in Table 2.1 highlight the topographic differences among the surfaces. Figure 2.5a shows the flow directions of Surface 1. As shown in Figure 2.5b, the flow directions determined by the delineation algorithm for depressions are different compared to the traditional methods. Unlike the traditional methods based on depressionless DEMs that introduce artificial slopes and flow directions across depressions, the algorithm utilized in this study assigned a "zero" flow direction to all inundated depressional cells (Figure 2.5b). Figure 2.5c displays the flow accumulations calculated by the algorithm for Surface 1. As expected, all cells within a puddle have the same flow accumulation value, which is determined based on the

number of cells on the surface that contribute runoff to the puddle. Overland flow is concentrated towards all major puddles/potholes from contributing areas and eventually discharges, subject to threshold control, through basin outlets. The spatial distribution and changing pattern of flow accumulations for Surface 3 differ from those of Surfaces 1 and 2. A channelized drainage system can be observed from the distribution of flow accumulations of Surface 3 in Figure 2.5d. The flow accumulations of Surface 2 display two groups of well-connected puddles/potholes and some channels – a mixed puddle-channel drainage pattern. A number of puddles are very small and shallow, while some clustered potholes are larger and potentially have threshold control on runoff from their contributing areas.

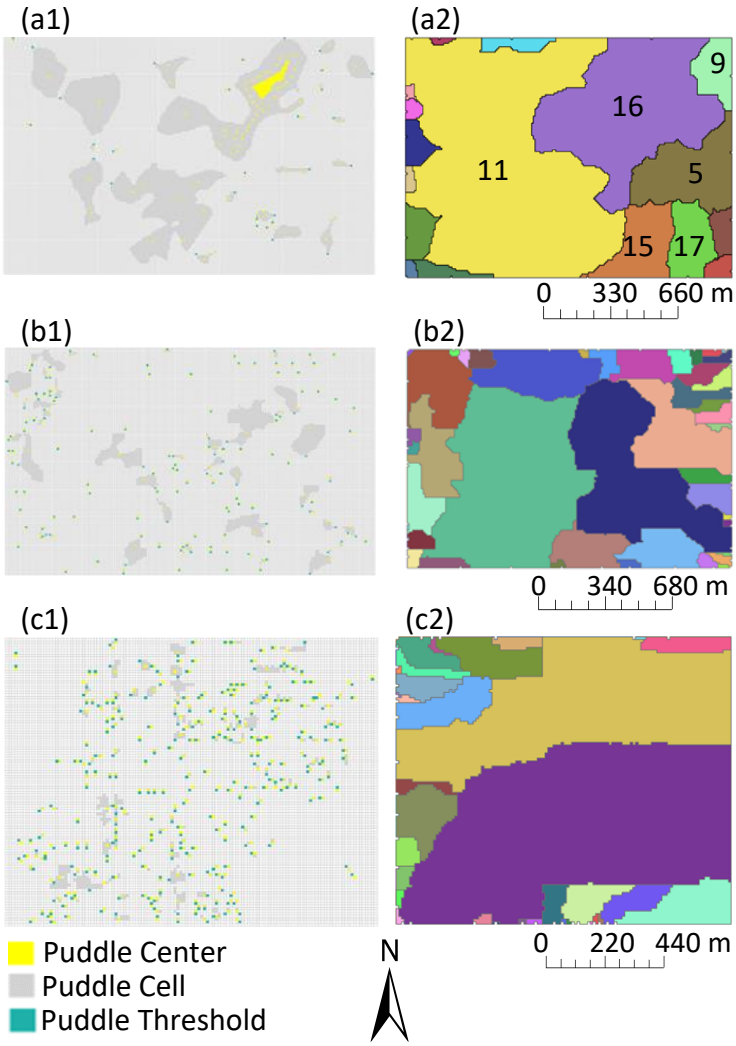

Figure 2.4. Puddles/potholes and basins delineated by the D-cubed algorithm for (a) Surface 1 (17 basins); (b) Surface 2 (45 basins); (c) Surface 3 (33 basins).

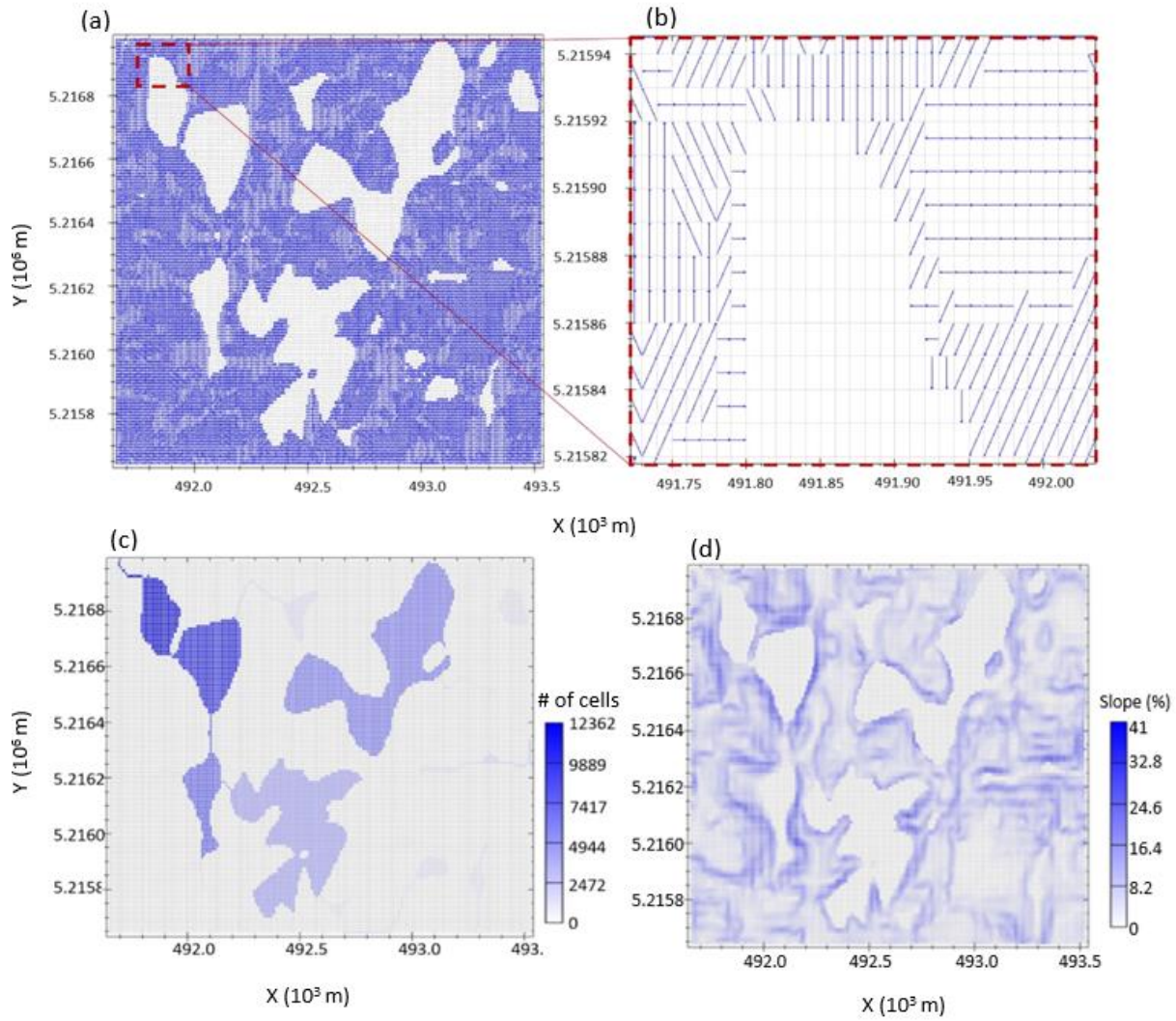

Figure 2.5. Delineation results from the D-cubed algorithm: (a) flow directions of Surface 1; (b) zoomed-in view of flow directions through a depression for Surface 1; (c) flow accumulations of Surface 1; (d) flow accumulations of Surface 3.

2.4.2. Relationships between Structural and Functional Hydrologic Connectivity and Contributing Area

Figure 2.6a shows relationships of the normalized depression storage vs. NACf for the 3 surfaces. This analysis highlights the impact of structural variables (S/MDS) on hydrologically connected areas that are not necessarily connected to the outlets. ACs gradually merge to create larger ACs as puddles fill, spill, and merge. When puddles become fully filled, the surface reaches full hydrologic connectivity and the entire surface contributes runoff to the outlets.

Figures 2.6b-2.6f depict the dynamic changes in hydrologic connectivity throughout the surface. Ponded areas show how ACs are dependent on puddle filling. As depression storage increases from the initial puddle level (Figure 2.6b) to the highest puddle level (Figure 2.6f), ponded areas increase, causing ACs to merge until NACf equals 1 or the number of ACs is same as the number of the delineated basins.

Surfaces 1 and 2 depict a gradual stepwise increase in NACf (Figure 2.6). Since depressions are large, the P2P process is more gradual. All surfaces reach the maximum NACf (i.e., NACf = 1) when the normalized depression storage equals 1; however, Surfaces 1 and 2 have ACs which merge incrementally due to the incremental filling of depression storage. Larger areas contribute to larger depressions, so the merging of ACs to equal the number of the delineated basins occurs more gradually than Surface 3. Surface 3 has more identified depressions than Surfaces 1 and 2; however, these depressions are small and are filled more quickly. For Surface 3, about 80% of the surface storage must be filled before its NACf is similar to those of Surfaces 1 and 2, and Surface 3 reaches 80% of its surface depression storage quickly because its overall MDS is small compared to those of Surfaces 1 and 2. That is, if NACf is based on a function of normalized time, the ACs of Surface 3 would merge more quickly than Surfaces 1 and 2. The shapes of these NACf curves and the contributing areas to puddles can be related to the PBUs of each surface denoted in Table 2.1. All surfaces are similar in size, but the number of PBUs for each surface varies greatly, especially for Surface 3. The threshold of a highest-level puddle is breached when the area contributing to that puddle (or its corresponding PBU) fully fills the puddle. Figures 2.6g and 2.6h show the NACf curves for Basin 11 and Basin 16 of Surface 1, respectively. The initial NACf of Basin 11 is smaller than that of Basin 16 because there are more ACs and more identified depressions. Basin 16 reaches full connectivity

near 60% of the storage capacity because of the spatial distribution of depressions along the flow paths to the outlet. At 60% of the storage, all depressions are fully filled except the largest depression closest to the outlet (circled in Figure 2.6e). All areas of Basin 16 except the outlet contribute to this depression until it is fully filled and only then does the entire surface contribute to the outlet.

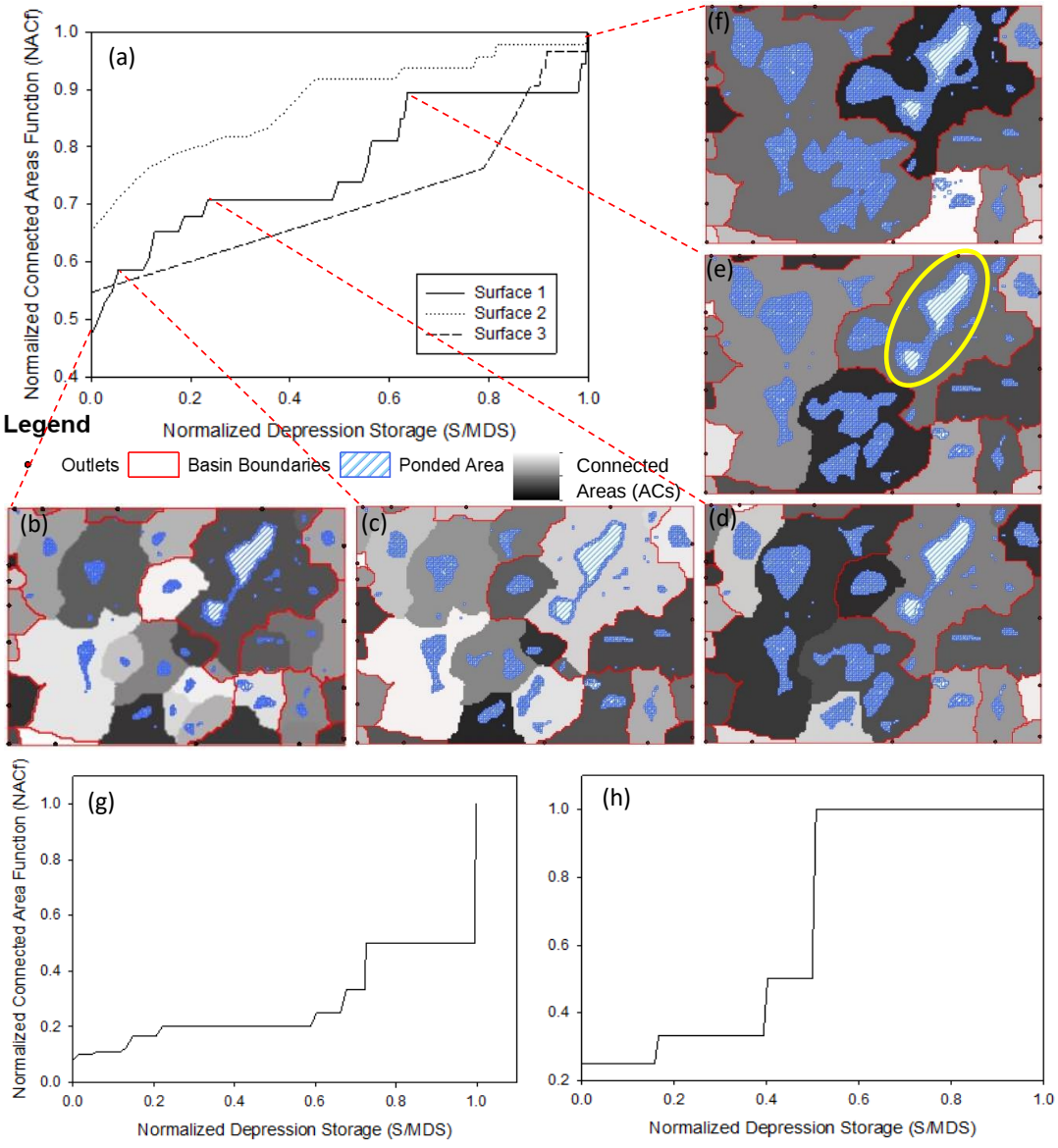

Figure 2.6. Normalized connected area function (NACf) and dynamic connected areas (ACs): (a) NACf curves for Surfaces 1-3; (b)-(f) major stepwise jumps which refer to merging of ACs for Surface 1; (g)-(h) NACf curves for Basins 11 and 16 of Surface 1.

2.4.3. Intrinsic Relationships between Topographic Characteristics and Contributing Area

Figure 2.7a shows the relative surface connection functions (RSCf) computed for the three surfaces, which relate the influence of topography to CA. As shown in Figure 2.7a, the relationship between normalized depression storage and RSCf reveals unique patterns for different surfaces. These results reflect how the method works for different topography types as demonstrated by Antoine et al. (2009). Surface 1 exhibits sudden and large stepwise increases in CA. As discussed previously, a full contributing area to the outlet (i.e., RSCf = 1) did not occur until all puddles were fully filled and the entire surface reached its MDS (i.e., normalized depression storage = 1). The large depressions on Surface 1 were made up of 17 hierarchical puddle levels; these highest-level puddles took a long time to be filled; and small puddles on this surface were generally not directly connected to the outlet, but instead connected to the associated large puddles. Therefore, a surface of topographic characteristics similar to Surface 1 will exhibit large jumps in CA, followed by a long puddle-filling period before the next large jump in CA. The dynamic distributions of CAs to the outlets, which are quantified in Figure 2.7a, are displayed in Figures 2.7b-2.7f. Callouts are used to visualize the dynamic CA to the outlet for specific jumps in the RSCf. The dynamic CA to the outlet of Basin 11 (Figures 2.7b-2.7f) is similar to the CA in Figure 2.2a4, while the dynamic CA of Basin 16 (Figures 2.7b-2.7f) is similar to the CA in Figure 2.2b4. Figures 2.7b-2.7f can also be compared to Figures 2.6b-2.6f. Similar dynamic connections to the outlets can be observed (e.g., ACs near the outlets in Figure 2.6b depict CAs in Figure 2.7b; Figure 2.6e is comparable to Figure 2.7d; and Figure 2.6f is comparable to Figure 2.7f).

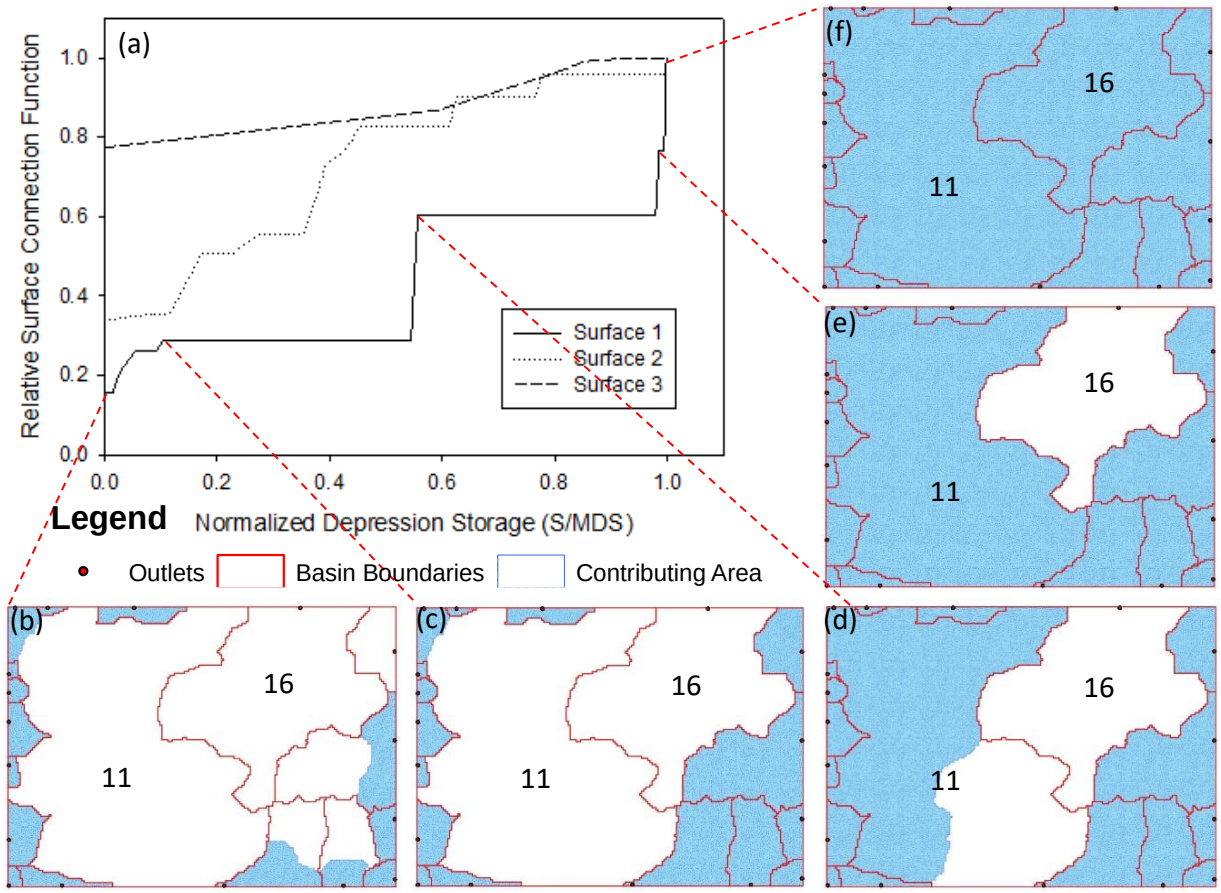

Figure 2.7. (a) Relative surface connection function (RSCf), normalized depression storage (ratio of water-filled depression storage S to maximum depression storage MDS, i.e., S/MDS) vs. normalized contributing area (ratio of contributing area CA to the total surface area A, i.e., CA/A); (b)-(f) associated changes in contributing area to the outlet for Surface 1.

Surface 2 also displays a stepwise increasing pattern in contributing area (Figure 2.7a). However, the normalized CA to the outlet was much larger than that of Surface 1 for most of the depression filling stages. This can be attributed to fewer puddle levels and puddles with smaller MDS values, as well as preferential flow paths for Surface 2. The smooth stepwise increases in contributing area relate to the patterns of the large and small puddles on the surface. Small puddles on Surface 2 are either connected to other small puddles which are connected to the outlet or, like Surface 1, connected to large puddles which are connected to the outlet or other small puddles. The first scenario creates a smooth, but rapid increase in CA to the outlets on

Surface 2. Small puddles are filled quickly and are well connected to the outlet. The second scenario is visually comparable to the stepwise increases on Surface 1 (Figure 2.7a). Sudden jumps in CA occur because large puddles and their corresponding ACs are fully filled and then are immediately connected to the outlet (threshold control, Figure 2.7a).

Surface 3 exhibits a slight stepwise increase in CA; however, the most noticeable feature about this surface is the high starting RSCf (Figure 2.7a). The small puddles on this surface are easily filled and therefore nearly 80% of the surface area contributes to the outlets. A similar trend can be observed in traditional modeling methods for dendritic basins. That is, the majority of a surface can be well connected via drainage channels, and sequentially contributes to the outlet. Of all the small depressions on Surface 3, most were gradually filled, and thus, exhibited a smooth, rather than sudden, stepwise increases in CA (Figure 2.7a). This finding is similar to those from the RSCf analyses by Antoine et al. (2009) and Peñuela et al. (2016).

2.4.4. Analysis of Hydrographs

To understand the effect of topography on outlet discharge, the simulated runoff was normalized and compared against normalized time or cumulative rainfall (Fig. 2.8a). As discussed previously, a surface reaches its MDS and full contributing area at the final time step (e.g., t/T equals 1). Surface 3 is the first to reach a steady state runoff rate. The steep slope in the first 20% of the simulation time is specifically related to the small puddles and the well-connected drainage system on Surface 3. Nearly 60% of depressions were fully filled and almost 80% of the surface was contributing runoff to the outlets after time step 1. The tail of the curve of Surface 3 (Figure 2.8a) was increasing slightly as the small, encapsulated puddles were filled to their MDS values and connected to the outlets. Also, nearly 100% of the cumulative effective

rainfall was available for surface runoff for Surface 3 (Figure 2.8a) since its MDS and MPA were very small.

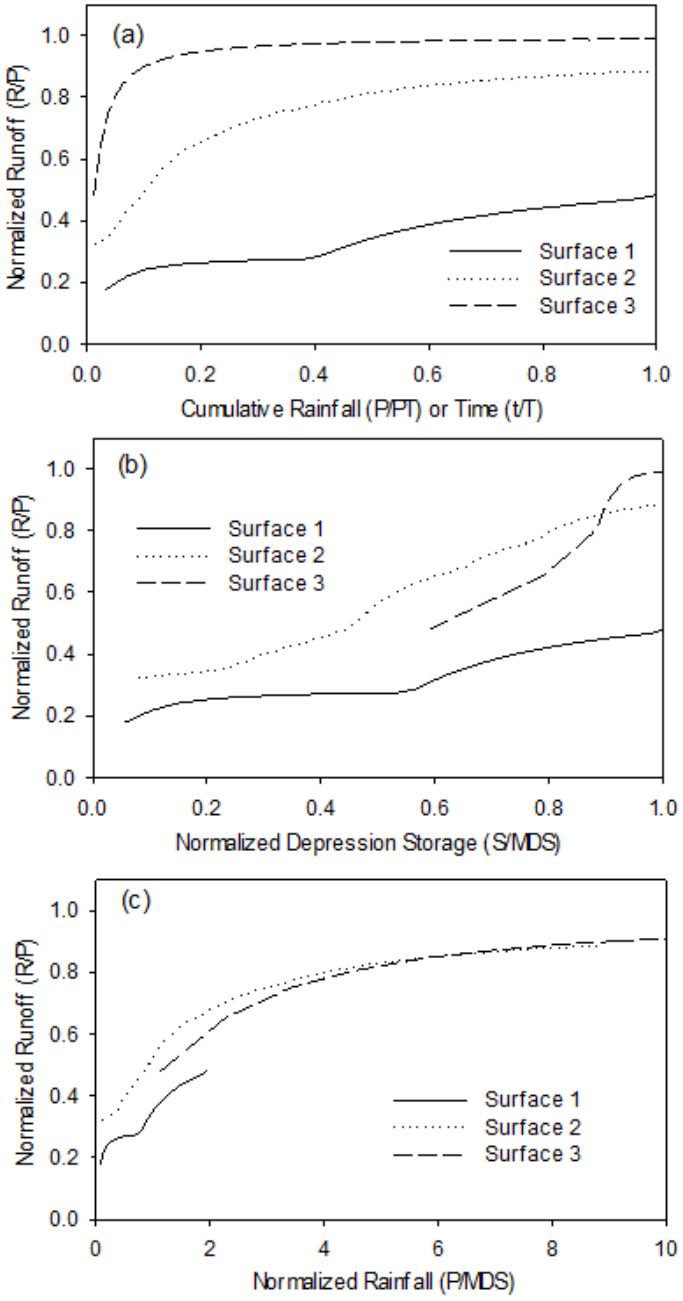

Figure 2.8. Comparisons of surface runoff for the three surfaces: (a) normalized runoff (ratio of cumulative runoff R to cumulative rainfall P, i.e., R/P) vs. dimensionless cumulative rainfall (ratio of cumulative rainfall P to the total rainfall at the time of fully matured connectivity PT, i.e., P/PT); (b) normalized runoff (R/P) vs. normalized depression storage (ratio of depression storage S to maximum depression storage MDS, i.e., S/MDS); (c) normalized runoff (R/P) vs. MDS-normalized cumulative rainfall (ratio of cumulative rainfall P to MDS, i.e., P/MDS).

Surface 2 contributed less available rainwater to surface runoff, only about 80% by the final time step (Figure 2.8a). Runoff initiated prior to all depressions being fully filled; however, it was delayed to reaching a steady state runoff rate due to puddle filling, spilling, and merging, as well as the threshold behavior of the highest-level puddles. This dynamic process was gradual due to the spatial arrangement and connection of different size puddles on the surface. The puddles with small MPA and MDS accumulated runoff very quickly for Surface 3, whereas the puddles with small and medium MPA and MDS on Surface 2 accumulated runoff quickly at first, and then began to slow down as large puddles needed to fulfill the P2P process.

Surface 1 exhibits a slight stepwise trend (Figure 2.8a) which is unique to the spatial arrangement of large puddles on this surface. Also, only 40% of cumulative rainfall was available for runoff by the final time step (Figure 2.8a). This is because large puddles stored a majority of the effective rainfall. At the beginning of the simulation, only about 20% of available runoff was flowing through the outlet (Figure 8a).

2.4.5. Intrinsic Relationships between Surface Runoff and Topography

A simplified hydrograph directly links hydrologic processes to topographic property parameters. Figure 2.8b shows the relationships between normalized runoff and normalized depression storage for the three surfaces. The large depressions on Surface 1 took the longest to fill and reach their MDS values. Again, as shown in Figure 2.8b, surface storage does not need to be completely filled before runoff is initiated. As water accumulated in depressions, depression storage and runoff rate increased gradually (Surfaces 1 and 2) or rapidly (Surface 3). Runoff increases gradually when a surface contains a large variety of puddle sizes. Over the course of the simulation, small puddles were first fully filled and contributed runoff, followed by medium and large puddles. Initially, runoff on Surface 2 was higher than that on Surface 1 because more

small puddles were present. Surface 1 still exhibited a stepwise increase in runoff because after all small highest-level puddles close to the outlet were filled, their corresponding ACs initiated runoff. It took a long time for enough rainwater to accumulate and completely fill large puddles. Runoff initiated on Surface 3 and immediately surface storage reached about 60% (Figure 2.8b). The small depressions and the channelized drainage network allowed the surface to be well connected and, therefore, contribute runoff at a high rate to all outlets. The small MDS also allowed a majority of the cumulative rainfall to contribute to runoff.

Excess rainfall, available for runoff, also exhibited differences based on surface topography (Fig. 2.8c). A majority of rainfall on Surface 1 went into filling depressions and a small amount, about 50%, was available for runoff. 80% of the cumulative effective rainfall was locked in depression storage. A stepwise trend can be observed for Surface 1 (Figure 2.8c) due to excess rainfall linking the connected areas to the outlet, only when large puddles became fully filled. Surfaces 2 and 3 had more excess rainwater available for runoff initiation because they had smaller puddles and smaller average slopes. Thus, less rainwater was used as storage; puddles were filled more quickly; and hydrologically connected areas contributed more runoff to the outlets. As shown in Figures 2.8b and 2.8c, Surface 2 initiated runoff at a faster rate than Surface 3. This can be attributed to the spatial arrangement of depressions on the surface. Small depressions or no depressions close to the outlet caused immediate runoff initiation while larger depressions were the last to fill and contribute to the outlets.

2.5. Discussion

2.5.1. Impacts of Topographic Characteristics on NACf, RSCf, and Simplified Hydrographs

The thorough analysis of the quantitative topographic information obtained from the delineation algorithm enables one to simulate hydrologic processes under the control of surface depressions and quantify functional hydrologic connectivity and evolution of contributing area. Antoine et al. (2009) investigated three different types of surface microtopography to understand functional connectivity. However, specific topographic characteristics of the surfaces (e.g., MDS, MPA, PBUs, and CBUs) were not calculated (Antoine et al. 2009). It can be difficult to compare how hydrologic connectivity will occur under different landscapes and to investigate the full extent of connectivity possibilities without a summary of specific topographic characteristics. Thus, the characterization of surface topography done in this study becomes a fundamental step for determining functional hydrologic connectivity across different types of topographic surfaces, especially depression-dominated surfaces.

From the D-cubed delineation and P2P simulation, the new NACf analysis was developed. Other studies have identified and quantified contributing area by dividing it into two parts, contributing to the outlet and non-contributing area (Antoine et al., 2009; Peñuela et al. 2015, 2016). In this study, a non-contributing area was further divided by identifying and quantifying connectivity of areas that were not connected to the outlet to investigate how these ACs changed spatially and temporally. In the study by Yang and Chu (2013), ACs were analyzed as structural characteristics; however, in this study, since ACs varied temporally based on the simulated puddle filling, ACs were a functional connectivity indicator which impacted CA. It was found that topographic properties (e.g., PBU area and CBU area) and geometric properties

of puddles (e.g., puddle MDS and puddle MPA) impacted the dynamic AC. The NACf analysis has potential to investigate the impacts of sediment transport and water quality/quantity on pothole lakes and wetlands that are typically hydrologically disconnected from a stream and an outlet. Further studies could expand upon this analysis by adding vegetation variables which impact runoff generation and hydraulics of overland flow. For instance, this study can be combined with the one by Puigdefabregas et al. (1999), in which water and sediment redistribution were analyzed at the patch and hillslope scales under the influence of vegetation, to investigate the impact of vegetation on dynamic ACs at a patch scale or an AC scale. In addition, the spatial heterogeneity of vegetation may impact soil erosion and the trapping of sediments, nutrients, and water within each AC. Sediments, nutrients, and water trapped within each initial AC may influence the pothole/wetland to which the AC contributes; and depending on the temporal distribution and intensity of rainfall, they may also impact water quantity and quality at the outlet or downstream ACs to which the depressions fill and spill (Kidron 2011). Since Surfaces 1 and 2, located in the Northern Great Plains, are dominated by prairie plants and grasses, the root systems are very dense, signifying a homogeneous spatial arrangement of vegetation. Therefore, the factors such as soil erosion and water quantity may be more likely to be affected by the vegetation in this area compared to an area with bare ground patches (Puigdefabregas and Sanchez, 1996).

In this study, the RSCf (Antoine et al. 2009; Peñuela et al. 2016) was analyzed and used to compare dynamic CA patterns of different types of surface topography. It was found that geometric properties of puddles (e.g., puddle MDS, puddle MPA, and number of puddle levels) and the spatial arrangement of these puddles had the most impact on the RSCf patterns of different surfaces. The RSCf curves can be used to identify the periods of puddle filling and

puddle spilling during an event simulation, which potentially can impact the water quality at the outlet, depending on the water quality of individual puddles that contribute runoff water (and hence pollutants) to the outlet when they are fully filled. The RSCf can also be used to quantify flow and locate contributing area when puddles are not filled (i.e., S/MDS equals zero in Figure 2.7). The relationships between ACs and CAs were also investigated in this analysis. In the modeling, surface runoff was controlled by the spilling thresholds and the merging of ACs to CAs. Note that detailed subsurface flows and the potential saturation excess overland flow (Dunne & Black 1970) were not simulated in this study. Under certain circumstances, such an overland flow generation mechanism could have a potential to affect CAs and ACs. The impact of vegetation on ACs, discussed previously, could also affect water quality and quantity at the outlet. Water quantity, a function of contributing area, at the outlets was further investigated in the analysis of hydrographs.

The dimensionless variables used in the hydrograph analyses showed that surface topographic characteristics were directly linked to the temporal patterns of discharge. Studies conducted by Darboux et al. (2002), Antoine et al. (2009), Antoine et al. (2011), Appels et al. (2011), and Peñuela et al. (2016) interpreted hydrographs with variables unique to each simulation time, cumulative rainfall, or rainfall rates, whereas the dimensionless variables used in this study allowed us to compare hydrographs of different surfaces and relate the results directly to the P2P processes rather than the unique rainfall inputs. It was found that discharge shown in the simplified hydrographs (Figures 8a-c) was impacted by the spatial arrangement of puddles, surface MDS, and the initiation of the P2P processes. Specifically, effective rainfall, available for outlet discharge, was determined by surface MDS while the timing of increased outlet discharge was impacted by the spatial arrangement of different size puddles and the

initiation of puddle spilling to the outlet. Puddle spilling led to puddle merging which was directly linked to merging of ACs. The ACs that were connected to the outlet became part of CA. The analyses conducted in this study showed the interrelations of topographic characteristics, spatial arrangement of puddles, dynamic ACs and CA, and surface runoff.

2.5.2. Comparison of Two Delineation Approaches to Determine Hydrologic Connectivity

Surface 1 (Figure 2.3a), with the largest and most embedded potholes, was selected to highlight the differences in methodology and the effects of the two methods (new algorithm and TauDEM) on terrain analysis and identification of hydrologic connectivity. According to the delineation results from the new method, Surface 1 had a MDS of 1,145,571 m^3 (Table 2.1). Based on TauDEM, the original DEM for Surface 1 underwent hydrologic conditioning or depression filling. As a result, a depressional volume of 1,145,569 m^3 was filled. Figure 2.9 shows the spatial distribution of the filled depths or the differences between the pre-filling and post-filling DEMs. While a similar MDS can be calculated by analyzing the depression-filling results from TauDEM (Zhang & Chu, 2015), this value does not influence identification of flow directions and flow accumulations in the TauDEM method. Rather, like other traditional methods, TauDEM connects the surface by creating synthetic channels, instead of considering the dynamic P2P process. Although some depressions on a surface can be spurious ones due to the errors in the DEM and should be removed (Wallis et al., 2009), the TauDEM method did not calculate the topographic characteristics at different puddle levels as the new algorithm did.

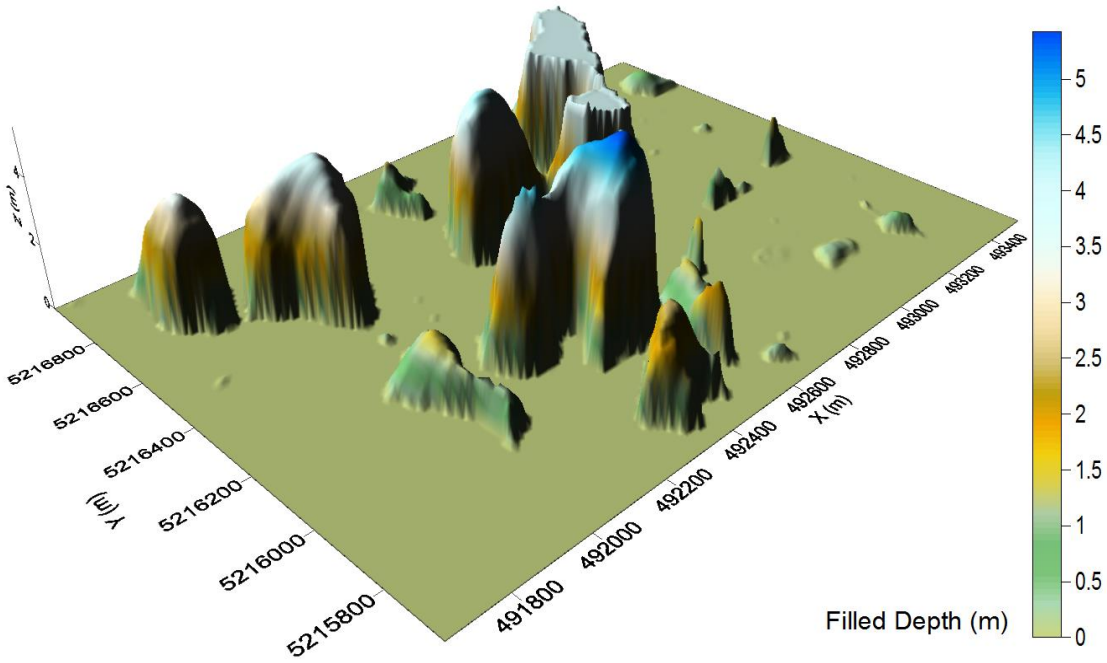

Figure 2.9. Spatial distribution of filled depression depths in TauDEM (i.e., elevation differences between the pre-filling and post-filling DEMs).

The contributing areas determined by the TauDEM method and the new method were compared to highlight the differences in the methodology. Structural connectivity was determined based on the first-level puddles for the new method and the corresponding channels for the TauDEM method. Figure 2.10 shows that the identified structural connectivity differs for the two methods. The TauDEM method determines contributing area to the channel cell upstream of the puddle based on the hydrologically conditioned DEM (Figure 2.10a1). Flow directions point toward channel cells (Figure 2.10a1). Figure 2.10a2 shows the flow paths of all cells calculated by TauDEM. In TauDEM, the outlet chosen for Puddle 26 is upstream of Puddle 26; however, because of the hydrologically conditioned DEM, only some of the cells within Puddle 26 contribute to this point (Figure 2.11a1). Other cells within Puddle 26 are connected along a flow path to channel cells further upstream. In reality, if some cells within a puddle contribute to a specific point, all other cells in the puddle also should contribute to the same point. In the new method, however, contributing area to the puddle center is determined based on

the flow directions of the original DEM. Under an unfilled condition, all cells in Puddle 26 contribute to the puddle center (Figure 2.10b1). All cells contributing to the cells of Puddle 26 also contribute to the center of Puddle 26 (Figure 2.10b1). In the unfilled puddle condition, puddle cells depicted by the new method point toward the center of the first-level puddle (Figure 2.10b2). This puddle center has a "zero" flow direction because it is the point of accumulation for Puddle 26 cells in the unfilled condition and all surrounding cells contribute to the cells of Puddle 26 (Figure 2.10b2). Thus, the underlying differences in the two methods resulted in dissimilar contributing areas and connectivity patterns.

Identifying connected areas at a fully-filled condition is interesting because the contributing area calculated by the TauDEM method is similar to that from the new method (Figures 2.11a1, 2.11b1, and 2.11b2). Although the identified areas are similar, the methods behind determining contributing area differ. To determine contributing area using the TauDEM method for the fully-filled condition, the threshold cell of Puddle 1 identified by the new algorithm is used because it is also on the main channel delineated by TauDEM that connects all upstream cells (Figure 2.11a1). TauDEM shows flow directions occurring within the highest-level Puddle 1 (Figure 2.11a2). In the new method, the fully-filled puddles have a "zero" flow direction; only the threshold cell has a flow direction towards its outside downstream cell (Figure 2.11b3). The puddle as a whole, however, including the threshold cell, has the same contributing area and flow accumulation.

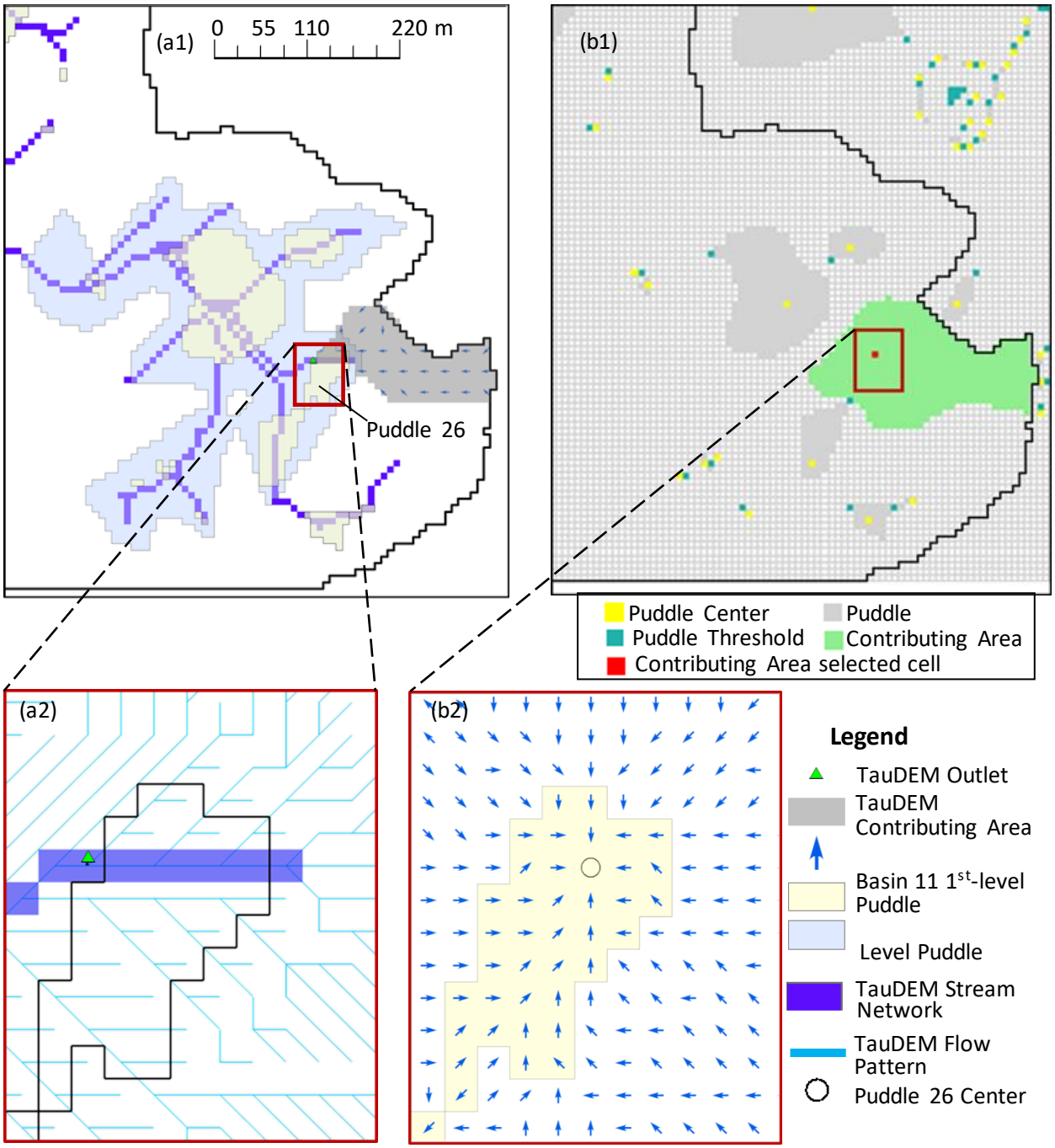

Figure 2.10. Comparison of contributing areas and the underlying methods of TauDEM and the new analysis procedure: (a1) contributing area for a point downstream of puddle 26 and flow directions pointing toward the channel; (a2) corresponding flow patterns determined by TauDEM; (b1) contributing area determined by the new algorithm for the puddle center; (b2) flow directions pointing toward the puddle center.

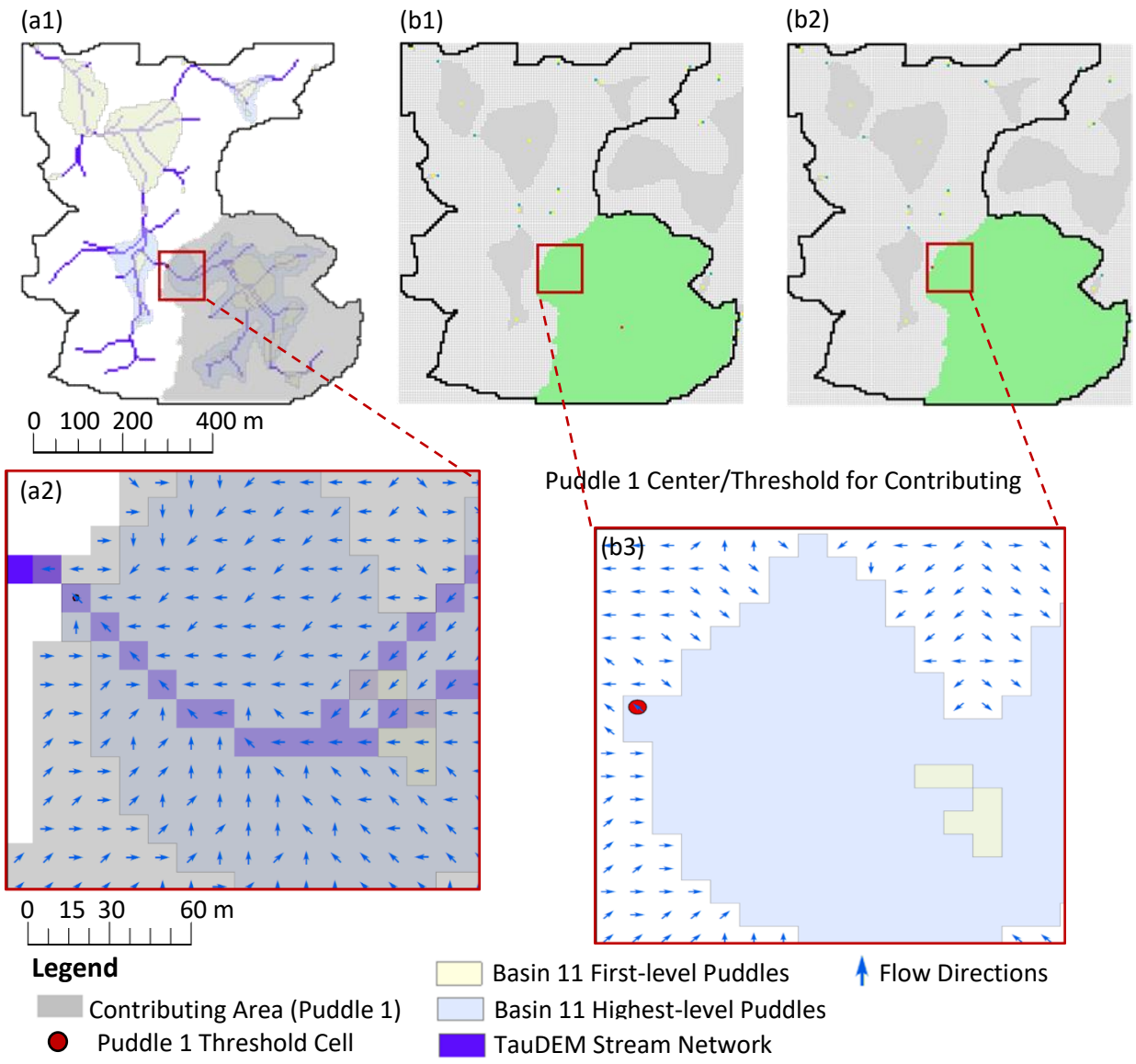

Figure 2.11. Comparison of contributing areas and the underlying methods of TauDEM and the new analysis procedure: (a1) contributing area determined by TauDEM; (a2) flow directions calculated by TauDEM (toward channel cells); (b1) contributing areas determined by the new algorithm for the center of highest-level puddle 1; (b2) contributing areas determined by the new algorithm for the threshold of highest-level puddle 1; (b3) flow directions calculated by the new algorithm (toward highest-level puddle 1).

2.6. Conclusions

This study introduced a new procedure for identifying and analyzing hydrologic connectivity. Based on the delineation results, hydrologic modeling was conducted and functional hydrologic connectivity was spatially and temporally analyzed for different surfaces.

The new NACf proposed in this study, and the established RSCf and simplified hydrographs were created to examine the intrinsic relationships and interactions between structural topographic characteristics and dynamic hydrologic processes. The major conclusions can be summarized as follows.

The traditional delineation methods (i.e., filling depressions prior to modeling) represent unrealistic CA, especially for depression-dominated surfaces. The new analysis procedure and the NACf proposed in this study can be effectively utilized to analyze dynamic hydrologic connectivity of areas, which are not necessarily connected to the outlet. It was found that NACf and RSCf were interrelated and they both identified stepwise trends unique to depression-dominated areas due to the threshold behaviors observed during the P2P process. For dendritic surfaces, a smoother increasing pattern of NACf and RSCf was observed. The analysis of structural characteristics vs. functional connectivity emphasized the dominant role of topography in meso-scale surface connectivity.

Simplified hydrographs highlighted the impacts of surface topography, mainly depression storage, on the timing and available water for runoff. This implies that caution should be taken when considering filling a DEM before identifying and quantifying ACs and CA throughout a surface. Lastly, the new method described in this study was compared against the existing TauDEM for terrain analysis and surface delineation. TauDEM did not provide all the topographic parameters calculated in the new procedure. Thus, it was difficult to determine the initial structural connectivity by using TauDEM, in which all depressions on a surface were already filled.

It should be noted that stable surface topography was assumed in the current modeling and analysis. In reality, however, surface topography may change due to soil erosion. In addition,

subsurface flows may influence the modeling results, depending upon the actual overland flow generation mechanisms. Spatially varied vegetation can further affect modeling of hydrologic processes and analyses of hydrologic connectivity, as highlighted in other studies (e.g., Puigdefabregas and Sanchez 1996; Puigdefabregas et al. 1999). Temporal distribution and intensities of rainfall may also impact temporal changes in connectivity (Kidron 2011). Thus, more studies are needed in the future to address these complex issues. The findings from this study improve our understanding of the mechanisms of overland flow generation and runoff processes, and provide a foundation for future studies dealing with hydrologic connectivity, modeling calibration, contaminant transport, soil erosion, and sediment transport dynamics under the influence of surface topography.

2.7. References

Antoine M, Javaux M, Bielders C. 2009. What indicators can capture runoff-relevant connectivity properties of the micro-topography at the plot scale? Advances in Water Resources 32: 1297–1310. DOI: 10.1016/j.advwatres.2009.05.006

Antoine M, Javaux M, Bielders CL. 2011. Integrating subgrid connectivity properties of the micro-topography in distributed runoff models, at the interrill scale. Journal of Hydrology 403: 213–223. DOI: 10.1016/j.jhydrol.2011.03.027

Appels WM, Bogaart PW, van der Zee SEATM. 2011. Influence of spatial variations of microtopography and infiltration on surface runoff and field scale hydrological connectivity. Advances in Water Resources 34: 303–313. DOI: 10.1016/j.advwatres.2010.12.003

Betson R. 1964. What is watershed runoff? Journal of Geophysical Research 69: 1541–1552. DOI: 10.1029/JZ069i008p01541

Borselli L, Cassi P, and Torri D. 2008. Prolegomena to sediment and flow connectivity in the landscape: A GIS and field numerical assessment. Catena 75: 268-277. DOI: 10.1016/jcatena.2008.07.006.

Bracken LJ, Wainwright J, Ali GA, Tetzlaff D, Smith MW, Reaney SM, Roy AG. 2013. Concepts of hydrological connectivity: Research approaches, pathways and future agendas. Earth-Science Reviews 119: 17–34. DOI: 10.1016/j.earscirev.2013.02.001

Cavalli M, Trevisani S, Comiti F, and Marchi L. 2013. Geomorphometric assessment of spatial sediment connectivity in small Alpine catchments. Geomorphology 188:31-41. DOI: 10.1016/j.geomorph.2012.05.007.

Chu X. 2015. Delineation of pothole-dominated wetlands and modeling of their threshold behaviors. Journal of Hydrologic Engineering 22: 431–438. DOI: 10.1061/(ASCE)HE.1943-5584.0001224

Chu X, Yang J, Chi Y, Zhang J. 2013. Dynamic puddle delineation and modeling of puddle-to-puddle filling-spilling-merging-splitting overland flow processes. Water Resources Research 49: 3825–3829. DOI: 10.1002/wrcr.20286

Chu X, Zhang J, Chi Y, Yang J. 2010. An improved method for watershed delineation and computation of surface depression storage. Watershed Management Conference 2010: Innovations in Watershed Management under Land Use and Climate Change, 1113–1122. DOI: 10.1061/41148(389)100

Darboux F, Davy P, Gascuel-Odoux C, Huang C. 2002. Evolution of soil surface roughness and flowpath connectivity in overland flow experiments. Catena 46: 125–139. DOI: 10.1016/S0341-8162(01)00162-X

Dunne T, Black R. 1970. Partial area contributions to storm runoff in a small New England watershed. Water Resources Research 6(5): 1296-1311.

Euliss NH, Labaugh JW, Fredrickson LH, Mushet DM, Laubhan MK, Swanson GA, Winter TC, Rosenberry DO, Nelson RD. 2004. The wetland continuum: A conceptual framework for interpreting biological studies. Wetlands 24: 448–458. DOI: 10.1672/0277-5212(2004)024[0448:TWCACF]2.0.CO;2

Euliss NH, Mushet DM. 1996. Water-level fluctuation in wetlands as a function of landscape condition in the prairie pothole region. Wetlands 16: 587–593. DOI: 10.1007/BF03161350

Euliss NH, Mushet DM, Newton WE, Otto CR V, Nelson RD, LaBaugh JW, Scherff EJ, Rosenberry DO. 2014. Placing prairie pothole wetlands along spatial and temporal continua to improve integration of wetland function in ecological investigations. Journal of Hydrology 513: 490–503. DOI: 10.1016/j.jhydrol.2014.04.006

Gabrecht J, Martz LW. 1999. TOPAZ: An Automated Digital Landscape Analysis Tool for Topographic Evaluation, Drainage Identification, Watershed Segmentation and Subcatchment Parameterization: TOPAZ User Manual. USDA Forest Service: Grazinglands Research Laboratory, USDA Agricultural Research Services, El Reno, OK.

Goldhaber MB, Mills CT, Morrison JM, Stricker CA, Mushet DM, LaBaugh JW. 2014. Hydrogeochemistry of prairie pothole region wetlands: Role of long-term critical zone processes. Chemical Geology 387: 170–183. DOI: 10.1016/j.chemgeo.2014.08.023

Güntner A, Seibert J, Uhlenbrook S. 2004. Modeling spatial patterns of saturated areas: An evaluation of different terrain indices. Water Resources Research 40(5): W05114. DOI: 10.1029/2003WR002864

Habtezion N, Tahmasebi Nasab M, Chu X. 2016. How does DEM resolution affect microtopographic characteristics, hydrologic connectivity, and modelling of hydrologic processes? Hydrological Processes 30: 4870-4892. DOI: 10.1002/hyp.10967

Hewlett JD, Hibbert AR. 1967. Factors affecting the response of small watersheds to precipitation in humid areas. In: Forest Hydrology, edited by W.E. Sopper and H.W. Lull, pp. 275–290, Elsevier, New York.

Jenson SK, Domingue JO. 1988. Extracting topographic structure from digital elevation data for geographic information system analysis. Photogrammetric Engineering and Remote Sensing 54: 1593–1600. DOI: 0099-1112/88/5411-1593$02.25/0

Kidron G. 2011. Runoff generation and sediment yield on homogeneous dune slopes: Scale effect and implications for analysis. Earth Surface Processes and Landforms 36(13): 1809–1824. DOI: 10.1002/esp.2203

Lane S, Bakker M, Gabbud C, Micheletti N, Saugy J. 2016. Sediment export, transient landscape response and catchment-scale connectivity following rapid climate warmin and Alpine glacier recession. Geomorphology 277: 210-227. DOI:10.1016/j.geomorph.2016.02.015

Marks D, Dozier J, Frew J. 1984. Automated basin delineation from digital elevation data. Geo-Processing 2: 299–311.

Mushet DM, Calhoun AJK, Alexander LC, Cohen MJ, DeKeyser ES, Fowler L, Lane CR, Lang MW, Rains MC, Walls SC. 2015a. Geographically isolated wetlands: Rethinking a misnomer. Wetlands 35: 423–431. DOI: 10.1007/s13157-015-0631-9

Mushet DM, Goldhaber MB, Mills CT, McLean KI, Aparicio VM, McCleskey RB, Holloway JM, Stockwell CA. 2015b. Chemical and biotic characteristics of prairie lakes and large

wetlands in south-central North Dakota—Effects of a changing climate. Scientific Investigations Report. DOI: 10.3133/SIR20155126

National Oceanic and Atmospheric Administration (NOAA). 2017. NOAA's National Weather Service Hydrometeorological Design Studies Center: Precipitation Frequency Data Server (PFDS). http://hdsc.nws.noaa.gov/hdsc/pfds/pfds_map_cont.html?bkmrk=nd (Aug. 12, 2017).

O'Callaghan JF, Mark DM. 1984. The extraction of drainage networks from digital elevation data. Computer Vision, Graphics, and Image Processing 28: 323–344. DOI: 10.1016/S0734-189X(84)80047-X

Ogden FL, Watts BA. 2000. Saturated area formation on nonconvergent hillslope topography with shallow soils: A numerical investigation. Water Resources Research 36: 1795-1804. DOI: 10.1029/2000WR900091

Peñuela A, Darboux F, Javaux M, Bielders CL. 2015. How do slope and surface roughness affect plot-scale overland flow connectivity. Journal of Hydrology 528: 192-205. DOI: 10.1016/j.jhydrol.2015.06.031

Peñuela A, Darboux F, Javaux M, Bielders CL. 2016. Evolution of overland flow connectivity in bare agricultural plots. Earth Surface Processes and Landforms 41: 1595–1613. DOI: 10.1002/esp.3938

Puigdefabregas J, Sanchez G. 1996. Geomorphological implications of vegetation patchiness on semi-arid slopes. In: Advances in Hillslope Processes, vol. 2. pp. 1027–1060, edited by M.G. Anderson and S.M. Brooks, Wiley, Chichester.

Puigdefabregas J, Sole A, Gutierrez L, Del Bario G, Boer M. 1999. Scales and processes of water and sediment redistribution in drylands: Results from the Rambla Honda field site

in Southeast Spain. Earth-Science Reviews 48: 1, 39-70. DOI: 10.1016/S0012-8252(99)00046-X.

Richards PL, Brenner AJ. 2004. Delineating source areas for runoff in depressional landscapes: Implications for hydrologic modeling. Journal of Great Lakes Research 30: 9-21. DOI: 10.1016/S0380-1330(04)70325-1

Rinderer M, Ali G, Larsen L. 2017. Quantifying hydrologic connectivity with measures from the brain neurosciences – a feasibility study. Geophysical Research Abstracts EGU General Assembly 19: 2017–8656

Rover J, Wright CK, Euliss NH, Mushet DM, Wylie BK. 2011. Classifying the hydrologic function of prairie potholes with remote sensing and GIS. Wetlands 31: 319–327. DOI: 10.1007/s13157-011-0146-y

Shaw DA, Vanderkamp G, Conly FM, Pietroniro A, Martz L. 2012. The fill-spill hydrology of prairie wetland complexes during drought and deluge. Hydrological Processes 26: 3147–3156. DOI: 10.1002/hyp.8390

Singh V. 1995, Computer Models of Watershed Hydrology. Water Resources Publications, LLC.

Tahmasebi Nasab M, Jia X, Chu X. 2016. Modeling of subsurface drainage under varying microtopographic, soil and rainfall conditions. Proceedings of the Tenth International Drainage Symposium pp. 1–6. American Society of Agricultural and Biological Engineers. DOI: 10.13031/IDS.20162499952

Tahmasebi Nasab M, Zhang J, and Chu X. 2017a. A new depression-dominated delineation (D-cubed) method for improved watershed modeling. Hydrologic Processes 31: 3364-3378. DOI: 10.1002/hyp.11261

Tahmasebi Nasab M, Grimm K, Wang N, Chu X. 2017b. Scale analysis for depression-dominated areas: How does threshold resolution represent a surface? Watershed Management, Irrigation and Drainage, and Water Resources Planning and Management, Proceedings of World Environmental and Water Resources Congress 2017, American Society of Civil Engineers, Reston, VA, pp. 164-174. DOI: 10.1061/9780784480601.016.

Tahmasebi Nasab M, Singh V, Chu X. 2017c. SWAT modeling for depression-dominated areas: How do depressions manipulate hydrologic modeling? Water 9: 1-14. DOI: 10.3390/w9010058

Tarboron DG. 1997. A new method for the determination of flow directions and upslope areas in grid digital elevation models. Water Resources Research 33: 309–319. DOI: 10.1029/96WR03137

Temme AJAM, Schoorl JM, Veldkamp A. 2006. Algorithm for dealing with depressions in dynamic landscape evolution models. Computers & Geosciences 32: 452–461. DOI: 10.1016/j.cageo.2005.08.001

Wallis C, Wallace R, Tarboton DG, Watson DW, Schreuders KAT, Tesfa TK. 2009. Hydrologic Terrain Processing Using Parallel Computing, pp. 2540-2545. In: Proceeedings of the 18th World IMACS Congress and MODSIM09 International Congress on Modelling and Simulation. Modelling and Simulation Society of Australia and New Zealand and International Association for Mathematics and Computers in Simulation, Cairns, Australia

Walter MT, Walter MF, Brooks ES, Steenhuis TS, Boll J, Weiler K. 2000. Hydrologically sensitive areas: Variable source area hydrology implications for water quality risk assessment. Journal of Soil and Water Conservation 3: 277–284.

Winter TC. 2003. Hydrological, Chemical, and Biological Characteristics of a Prairie Pothole Wetland Complex Under Highly Variable Climate Conditions - The Cottonwood Lake Area, East-Central North Dakota, pp109. U.S. Geological Survey Professional Paper 1675. Denver, CO.

Wu Q, Lane CR. 2017. Delineating wetland catchments and modeling hydrologic connectivity using LiDAR data and aerial imagery. Hydrology and Earth System Sciences 21: 3579–3595. DOI: 10.5194/hess-21-3579-2017

Yang J, Chu X. 2013. Quantification of the spatio-temporal variations in hydrologic connectivity of small-scale topographic surfaces under various rainfall conditions. Journal of Hydrology 505: 65–77. DOI: 10.1016/j.jhydrol.2013.09.013

Yang J, Chu X. 2015. A new modeling approach for simulating microtopography-dominated, discontinuous overland flow on infiltrating surfaces. Advances in Water Resources 78: 80–93. DOI: 10.1016/j.advwatres.2015.02.004

Zhang J, Chu X. 2015. Impact of DEM resolution on puddle characterization: Comparison of different surfaces and methods. Water 7: 2293–2313. DOI: 10.3390/w7052293

3. DEPRESSION THRESHOLD CONTROL PROXY TO IMPROVE HEC-HMS MODELING OF DEPRESSION-DOMINATED WATERSHEDS[2]

3.1. Abstract

Many hydrologic models (e.g., HEC-HMS) utilize delineation results from traditional methods, in which surface depressions are fully filled, creating a hydrologically connected drainage system. However, in depression-dominated areas, the topographic characteristics of depressions are vital to modeling unique hydrologic processes associated with the puddle-to-puddle (P2P) filling-spilling dynamics. The objective of this study is to evaluate the impacts of the P2P processes and dynamic changes in contributing area on outlet discharge. To address this objective, an improved HEC-HMS model is developed by incorporating a depression threshold control proxy (DTCP) and a new conceptual framework and is compared against the basic HEC-HMS model. The DTCP uses a storage-discharge function to simulate the unique P2P dynamics. The improved conceptual framework counteracts the effect of full hydrologic connectivity created by traditional delineation methods on modeling results by introducing a depressional area (DA) and a non-depressional area (NDA) to each subbasin, and routing the DA runoff through a DTCP, which thus introduces dynamic contributing area into the HEC-HMS model. Applications of the improved and basic HEC-HMS models to a watershed in North Dakota indicated that the latter (basic HEC-HMS) tended to be difficult to calibrate and validate depending on the storm event, whereas the improved HEC-HMS model accurately simulated outlet discharge and

[2] The material in this chapter was co-authored by Kendall Grimm and Dr. Xuefeng Chu. Kendall Grimm had primary responsibility for developing the new modeling methodology and analysis of the modeling results. Kendall Grimm was the primary developer of the conclusions that are advanced here. Kendall Grimm also drafted and revised all versions of this chapter. Dr. Xuefeng Chu served as proofreader and checked analysis conducted by Kendall Grimm.

provided surface connectivity and depression storage results. This study demonstrated the necessity of considering the P2P processes and dynamic variations in contributing area in hydrologic modeling for depression-dominated areas. The methodology proposed in this study can also be used to improve other traditional hydrologic models.

3.2. Introduction

Surface (micro)topography impacts overland flow generation and surface runoff (Darboux and Huang 2005). Specifically, depression-dominated surfaces often exhibit dynamic puddle-to-puddle (P2P) overland filling, spilling, merging, and splitting processes, which affect contributing area and outlet discharge (Chu et al. 2013; Chu 2015). Over the past three decades, the advancements in computer technologies have provided effective tools to analyze surface topography/depressions and more easily delineate surfaces based on high-resolution digital elevation models (DEMs) (Chen 2004; Chu et al. 2010; Gabrecht and Martz 1999; Jenson and Domingue 1988; Marks et al. 1984; Martz and Garbrecht 1993; Tahmasebi Nasab et al. 2017a; O'Callaghan and Mark 1984). Traditional DEM-based surface delineation involves filling/removing sinks, and identifying flow directions, flow accumulations, and basin boundaries; however, not all delineation methods produce the same results. Most traditional delineation methods are designed to be used for dendritic surfaces, but they have been incorporated into many popular modeling software packages, such as WMS (Watershed Modeling System) (WMS 2015), HEC-GeoHMS (Flemming and Doan 2009), and SWAT (Arnold et al. 1998). Therefore, users should apply various traditional delineation methods with caution, especially for depression-dominated areas.

The traditional delineation methods (O'Callaghan and Mark 1984; Marks et al. 1984; Jenson and Domingue 1988; Martz and Garbrecht 1993; Gabrecht and Martz 1999) implement

simplified delineation approaches to handle problematic depressions and create a well-connected channel network. For example, Jenson and Domingue (1988) specified a three-step procedure for DEM-based delineation, including (1) filling DEM sinks, (2) determining flow directions, and (3) calculating flow accumulations. These steps provide the data to further identify major drainage networks and delineate watershed boundaries; however, these delineation results are determined based on a "hydrologically-corrected" DEM (USACE-HEC 2016). Thus, all DEM cells are well connected, producing a defined channelized drainage system across the surface making overland flow routing easier (Gabrecht and Martz 2000; USACE-HEC 2016). This methodology has been implemented in many delineation programs, such as the widely used Topographic Parameterization (TOPAZ) (Gabrecht and Martz 1999), which has been incorporated into WMS (WMS 2015) for surface delineation.

In reality, depressions are critical to the initiation of surface runoff and the quantification of overland flow (Chu et al. 2010; Habtezion et al. 2016). The timing of runoff initiation is not only controlled by the overland flow generation mechanisms (i.e., infiltration excess or saturation excess), but also affected by the P2P processes. The P2P filling-spilling-merging-splitting dynamics are controlled by threshold behaviors of depressions (Chu et al. 2013). The threshold of a depression acts as a "gatekeeper" and controls the timing and quantity of water to be released to its downstream when the threshold water level within the depression is surpassed (Tahmasebi Nasab et al. 2017b). This dynamic threshold behavior is not simulated in the traditional hydrologic models, so incorporating this feature into widely-used hydrologic models could improve watershed modeling for depression-dominated areas.

In recent years, studies have been conducted on the impact of microtopography and depressions on surface delineation and modeling (e.g., Appels et al. 2011; Chu 2015; Chu et al.

2010, 2013; Darboux et al. 2002; Habtezion et al. 2016; Tahmasebi Nasab et al. 2016, 2017c; Peñuela et al. 2015; Yang and Chu 2015, 2012). Runoff initiation under the influence of microtopography was investigated by Darboux et al. (2002), in which a threshold roughness term was proposed to relate topography to storage capacity and runoff initiation. Chu et al. (2010) developed the puddle delineation (PD) algorithm, which identifies depressions and their hierarchical relationships, while also calculating topographic parameters [e.g., maximum depression storage (MDS)]. The PD algorithm was further incorporated into the P2P modeling system which simulates the puddle filling, spilling, merging, and splitting processes (Chu et al. 2013). Chu (2015) conducted further research on delineation and modeling of depression-dominated areas, quantified depression threshold behaviors, and demonstrated the impact of surface topography on the quantity and timing of discharge from depression-dominated surfaces. Yang and Chu (2012) and Grimm and Chu (2018) investigated hydrologic connectivity by utilizing the PD algorithm to quantify structural and functional hydrologic connectivity across varying topographic surfaces. Antoine et al. (2009) developed the relative surface connection function (RSCf) to analyze functional hydrologic connectivity. Appels et al. (2011) investigated the effect of field microtopography and infiltration properties on hydrologic connectivity and used the RSCf to determine the status of connectivity at specific times and under certain hydrologic conditions.

Unlike the PD and P2P, WMS (WMS 2015) and HEC-HMS (USACE-HEC 2016) have been widely used for watershed delineation and modeling, typically, for dendritic drainage systems (e.g., Chu and Steinman 2009; Paudel et al. 2009; Gyawali and Watkins 2013; Wałęga 2013). To the best of our knowledge, HEC-HMS has not been successfully applied to simulate hydrologic processes specifically in depression-dominated regions. Due to the intricacies of

depression-dominated topography, traditional delineation and modeling cannot accurately simulate the P2P processes and the depression-associated threshold behaviors. The objective of this study is to evaluate the impacts of the P2P processes and the dynamic changes in contributing area on outlet discharge using the HEC-HMS model. To do this, the specific tasks are to: (1) identify and analyze the topographic characteristics of a depression-dominated watershed, (2) develop an improved HEC-HMS conceptual framework and a depression threshold control proxy (DTCP), and (3) highlight the impacts of the improved HEC-HMS framework and DTCP on the simulation of the effects of the P2P processes and dynamic hydrologic connectivity on outlet discharge.

3.3. Methodology

3.3.1. Introduction to Puddle Delineation (PD) and Depression-dominated Delineation (D-cubed)

The applicability of the PD program to analyze depression-dominated surfaces [e.g., landscapes in the Prairie Pothole Region (PPR)] has been evaluated in several studies (Chu 2015; Chu et al. 2010, 2013; Habtezion et al. 2016; Tahmasebi Nasab et al. 2016, 2017a, 2017c; Zhang and Chu 2015). This delineation approach uses a DEM to identify puddle cells, puddle centers, puddle thresholds, puddle levels, and the hierarchical relationships of all puddles. In order to identify puddle cells, the PD algorithm first searches for puddle center cells. A puddle center may be one or many cells (a flat) determined by being the local minimum on the surface. All cells within the puddle have elevations higher than that of the puddle center and, therefore, will contribute runoff to the puddle center cell(s). A threshold cell is a point of overflow, where one puddle is fully filled and begins to spill or merge with a surrounding puddle. This threshold acts as a gatekeeper that controls the P2P overland flow processes (Tahmasebi Nasab et al. 2017a).

To be considered as a puddle, it should have at least one center and one threshold. If two or more puddles share a threshold cell, they will merge to form a larger higher-level puddle. As this process continues, eventually the highest-level puddles are formed. Once puddles are identified for all levels, the PD algorithm calculates the MDS and maximum ponding area (MPA) for each highest-level puddle on the entire surface. Each highest-level puddle, together with its contributing area, forms a puddle-based unit (PBU) (Chu 2015; Chu et al. 2013). In the depression-dominated delineation (D-cubed) method (Tahmasebi Nasab et al. 2017a), a channel and its contributing area are identified as a channel-based unit (CBU). Ultimately, specific topographic parameters [e.g., MDS of subbasin *j* (MDS_j^{Sub}), MDS of *PBU i* in subbasin *j* ($MDS_{i,j}^{PBU}$), area of *PBU i* in subbasin *j* ($A_{i,j}^{PBU}$), and area of *CBU i* in subbasin *j* ($A_{i,j}^{CBU}$)] are quantified and used to develop the improved HEC-HMS model.

3.3.2. Development of the Improved HEC-HMS Model for Depression-dominated Areas

Throughout the study, the improved HEC-HMS model is compared against a basic HEC-HMS counterpart. The basic HEC-HMS model has a channelized drainage system delineated by using TOPAZ, in which full hydrologic connectivity is assumed across a subbasin. In the basic HEC-HMS model, depressions are considered by using a lumped initial abstraction rather than simulating the P2P processes. The steps taken to create the improved HEC-HMS model are schematically shown in Figure 3.1. First, a selected watershed is delineated using the traditional methods to obtain subbasin boundaries (step 1, Figure 3.1). In this study, DEM-based watershed delineation is performed by using TOPAZ, in which stream network extraction is based on the D8 single flow direction method in WMS (Gabrecht and Martz 1999; WMS 2015) (Figure 3.1a). To extract the topographic information from each subbasin that is delineated in step 1, the original unfilled DEM is clipped to each subbasin and each subbasin DEM (i.e., Subbasin_j,

Figure 3.1b) is processed to identify depressions and depression relationships by using the D-cubed method (Tahmasebi Nasab et al. 2017a) (Figure 3.1b). The extracted topographic information (e.g., $A_{i,j}^{PBU}$, $A_{i,j}^{CBU}$, $MDS_{i,j}^{PBU}$, MDS_{j}^{Sub}) is used to create the improved conceptual framework (step 3, Figure 3.1) and DTCP (step 4, Figure 3.1).

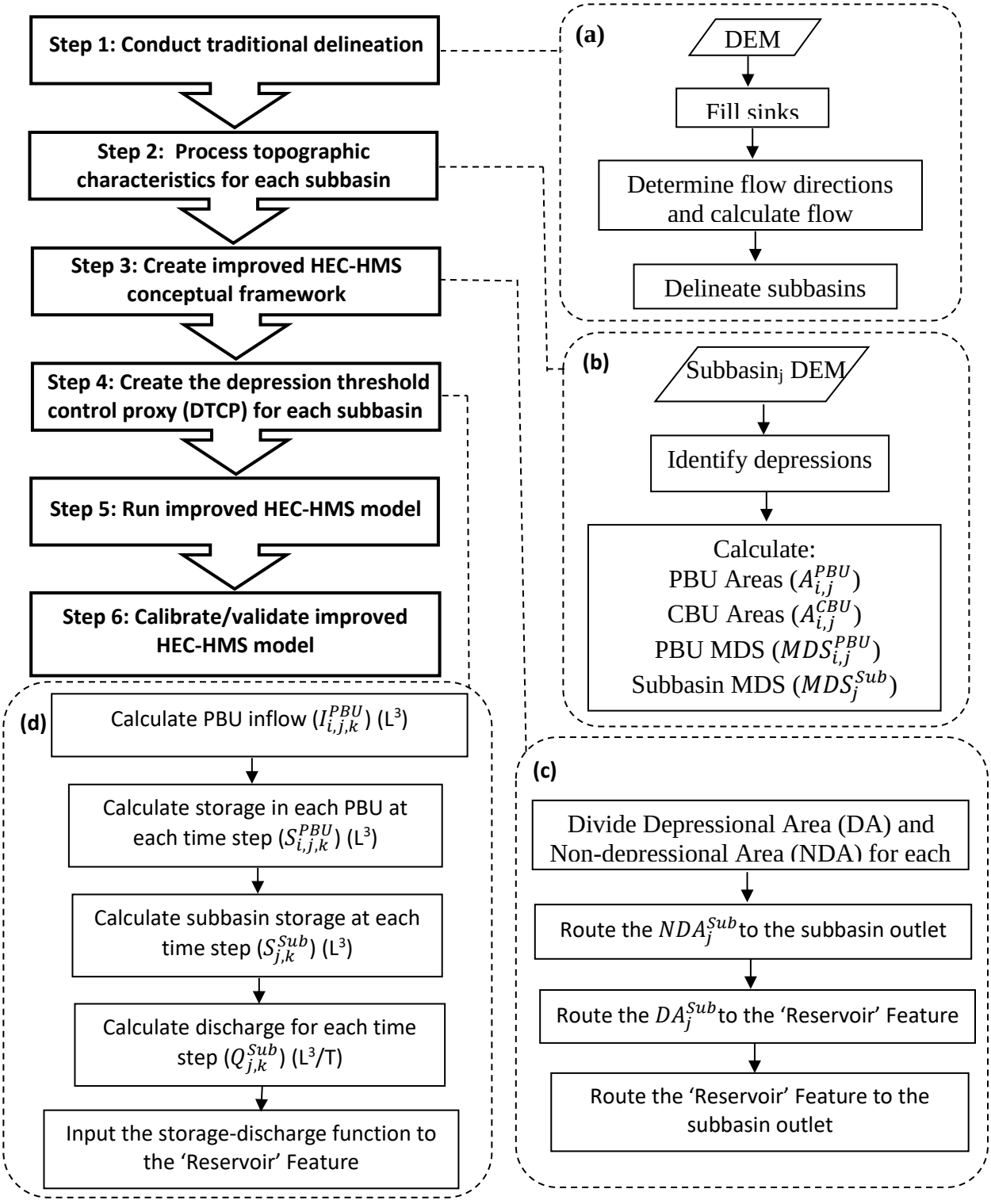

Figure 3.1. Flowchart of the improved HEC-HMS modeling: (a) how to delineate the surface, (b) how to process topographic characteristics, (c) how to create the improved conceptual framework, and (d) how to create the storage-discharge function.

The basic HEC-HMS conceptual framework is depicted in Figure 3.2a. This framework is altered to create the improved HEC-HMS conceptual framework (step 3, Figure 3.1). The topographic characteristics processed in Figure 3.1b indicate that each subbasin consists of many PBUs and CBUs. Since CBUs contain no depressions, surface runoff is not detained. Therefore, these areas are referred to as non-depressional areas (NDA) and they are assumed to directly contribute runoff water to the subbasin outlet (Figure 3.1c). A lumped NDA of a subbasin can be expressed as:

$$NDA_j^{Sub} = \sum_{i=1}^{n_i} A_{i,j}^{CBU} \tag{3.1}$$

where NDA_j^{Sub} is the NDA for subbasin *j* (L^2); $A_{i,j}^{CBU}$ is the area of *CBU i* in subbasin *j* (L^2); and n_j is the total number of CBUs in subbasin *j*. NDA_j^{Sub} is specified as a 'subbasin feature' in HEC-HMS (Figure 13b). PBUs contain depressions that store runoff water. Therefore, these areas are referred to as depressional areas (DA) and they are assumed to have a dynamic contribution to the subbasin outlet based on threshold behaviors of depressions (Figure 3.1c). A lumped DA of a subbasin can be given by:

$$DA_j^{Sub} = \sum_{i=1}^{m_i} A_{i,j}^{PBU} \tag{3.2}$$

where DA_j^{Sub} is the DA for subbasin *j* (L^2), $A_{i,j}^{PBU}$ is the area of *PBU i* in subbasin *j* (L^2), and m_j is the total number of PBUs in subbasin *j*. DA_j^{Sub} is specified as a 'subbasin feature' in HEC-HMS (Figure 3.2b). In the improved conceptual framework, DA_j^{Sub} is routed by the HEC-HMS 'reservoir' feature (Figure 3.1c), which stores and releases ponded water to mimic the fill and spill P2P dynamics controlled by depression thresholds (Figure 3.1d). To ensure that the spatial distributions of depression filling-spilling dynamics are accounted for, a DTCP is created and

allocated in the 'reservoir' feature for each subbasin. The HEC-HMS 'reservoir' feature is then connected to the subbasin outlet (Figure 3.1c and Figure 3.2b).

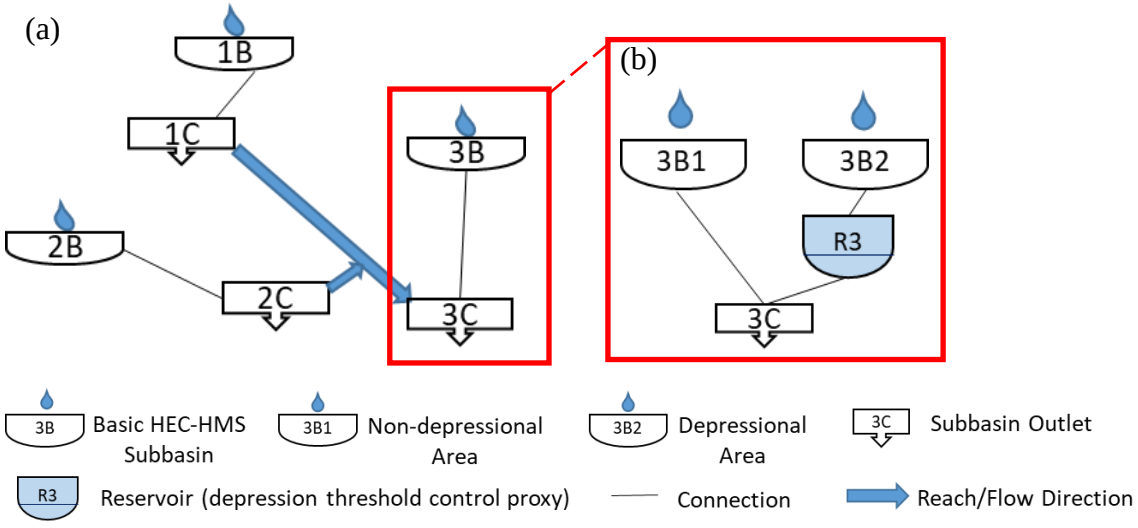

Figure 3.2. Conceptual frameworks for (a) basic HEC-HMS model and (b) improved HEC-HMS model.

Step 4 (Figure 3.1) involves the development of the DTCP, which is accomplished by utilizing the reservoir routing feature in HEC-HMS. The reservoir feature stores and releases ponded water, according to the Modified Puls Routing method and a specified storage-discharge function (USACE-HEC 2000). For HEC-HMS to solve the Modified Puls reservoir routing equation (Equation 3.3) for an event simulation, a storage-discharge function must be defined for each subbasin to solve for the unknowns on the left-hand side of Equation 3.3.

$$\left(2S_{j,k}^{Res}/\Delta t + Q_{j,k}^{Res}\right) = \left(I_{j,k-1}^{Res} + I_{j,k}^{Res}\right) + \left(2S_{j,k-1}^{Res}/\Delta t - Q_{j,k-1}^{Res}\right) \quad (3.3)$$

where $S_{j,k}^{Res}$ is the storage of the 'reservoir' of subbasin *j* at time step *k* (L^3), $Q_{j,k-1}^{Res}$ and $Q_{j,k}^{Res}$ are respectively the outflows or water releases from the 'reservoir' of subbasin *j* at time step *k-1* and *k* (L^3/T), $I_{j,k-1}^{Res}$ and $I_{j,k}^{Res}$ are respectively the inflows into the 'reservoir' of subbasin *j* at time step *k-1* and *k* (L^3/T), and Δt is the time interval between time steps *k* and *k-1* (T). The storage-

discharge relationship is commonly defined for a reservoir by using water-surface profile computations or historical observed flow and stage data (USACE-HEC 2000). In this study, the storage-discharge function for the DA of a subbasin DA_j^{Sub} is defined by (1) artificially filling the subbasin depression storage and (2) calculating the subbasin discharge. The subbasin depression storage is calculated by using a constant user-specified 'fill depth' to fully fill all depressions in the subbasin. This fill depth is distributed across each subbasin PBU and is identified as an inflow to the PBU (Figure 3.1d):

$$I_{i,j,k}^{PBU} = Fill_{\Delta t} \times A_{i,j}^{PBU} \tag{3.4}$$

where $Fill_{\Delta t}$ is a constant filling depth increment for time interval Δt (L); and $I_{i,j,k}^{PBU}$ is the water contributing to filling the depression storage of PBU *i* of subbasin *j* at time step *k* (L^3). Next, the storage is simulated for each PBU depression by (Figure 3.1d):

$$\text{If } S_{i,j,k}^{PBU} < MDS_{i,j}^{PBU}:$$

$$S_{i,j,k}^{PBU} = S_{i,j,k-1}^{PBU} + I_{i,j,k}^{PBU} \tag{3.5}$$

$$\text{If } S_{i,j,k}^{PBU} \geq MDS_{i,j}^{PBU}:$$

$$S_{i,j,k}^{PBU} = MDS_{i,j}^{PBU} \tag{3.6}$$

where $S_{i,j,k-1}^{PBU}$ and $S_{i,j,k}^{PBU}$ are respectively the depression storages of PBU *i* in subbasin *j* at time step *k-1* and *k* (L^3), and $MDS_{i,j}^{PBU}$ is the maximum depression storage of PBU *i* in subbasin *j* (L^3). In order to create one storage-discharge function for each subbasin, the subbasin storage at each time step ($S_{j,k}^{Sub}$) is calculated by (Figure 3.1d):

$$S_{j,k}^{Sub} = \sum_{i=1}^{m_i} S_{i,j,k}^{PBU} \tag{3.7}$$

When $S_{j,k}^{Sub} = MDS_j^{Sub}$, all highest-level puddles in subbasin *j* are fully filled and finally the subbasin discharge is given by (Figure 3.1d):

$$Q_{j,k}^{Sub} = \left(I_{j,k}^{Sub} - \left(S_{j,k}^{Sub} - S_{j,k-1}^{Sub}\right)\right)/\Delta t \tag{3.8}$$

where $Q_{j,k}^{Sub}$ is the discharge of subbasin *j* at time step *k* (L^3/T), $I_{j,k}^{Sub}$ is the inflow to subbasin *j* at time step *k* (L^3), and $S_{j,k-1}^{Sub}$ and $S_{j,k}^{Sub}$ are respectively the storages of subbasin *j* at time step *k-1* and *k* (L^3). The storage-discharge function is created by pairing $S_{j,k}^{Sub}$ with $Q_{j,k}^{Sub}$. Once the storage-discharge function is established, it is input to the HEC-HMS subbasin 'reservoir' feature (Figure 3.1d). With the improved HEC-HMS model (step 5, Figure 3.1), reservoir routing (i.e., depression threshold control) is simulated by using the storage-discharge function to recursively solve Equation 3.3 for $Q_{j,k}^{Res}$ using a trial and error procedure (USACE-HEC 2000).

3.3.3. Real Application of the Improved HEC-HMS Model

To test the improved HEC-HMS model, the Baldhill Creek watershed, a part of the Middle Sheyenne River basin (USGS HUC 8), is selected. This watershed is located in the PPR in central North Dakota (Figure 3.3a) and it is characterized by numerous potholes and wetland areas created by the last glaciation period (Winter 2003). Cropland and herbaceous prairie grassland are the dominant land covers in this watershed (Winter 2003). The climate in Central North Dakota is dominated by dynamic continental conditions where evapotranspiration is the main source of water loss and average yearly precipitation is only 44.68 cm (Mushet et al. 2015). A 30-m DEM was downloaded from the USGS National Map Viewer (https://viewer.nationalmap.gov/launch/) and the discharge at the final outlet of the Baldhill Creek watershed was obtained from the USGS (05057200 gauging station) (Figure 3.3b). A precipitation station

located at 47.39° N and -98.32° W (Figure 3.3b) was set up in this study, where a heated tipping bucket rain gauge was utilized to continuously collect precipitation data at a 5-minute interval. Figure 3.3c shows the hydrography of the selected watershed (https://viewer.nationalmap.gov/launch/). Most depressions and potholes are clustered along the western half of the watershed; therefore, the P2P processes are expected to have a major impact on hydrologic simulations in these areas.

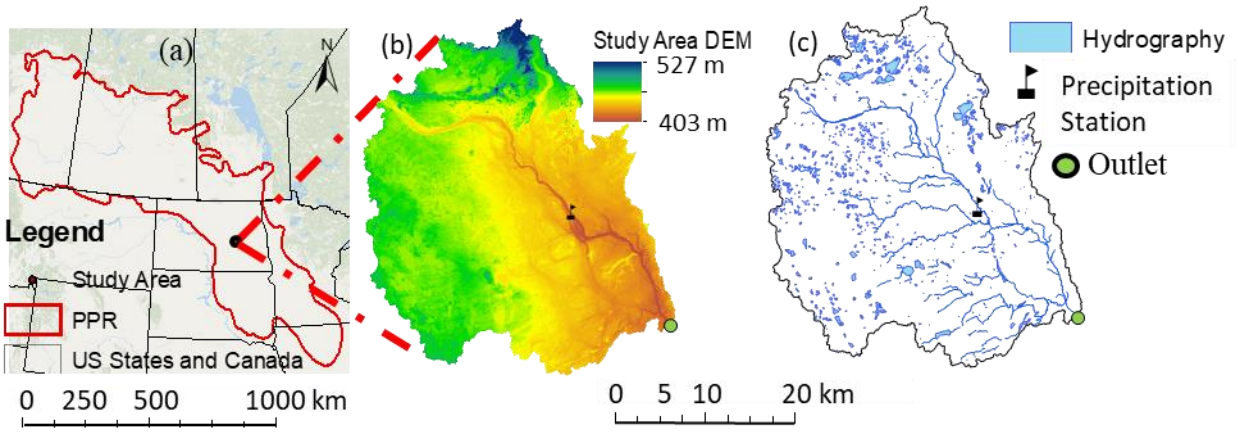

Figure 3.3. (a) Study area selected within the Prairie Pothole Region (PPR), (b) DEM of the Baldhill Creek watershed, and (c) hydrography of the watershed.

The WMS (WMS 2015) was used to delineate the selected watershed and the resulting data were used to calculate initial parameters for hydrologic modeling. In this study, the curve number (CN) method was selected for event modeling (USDA 1986) to take advantage of the available spatially-distributed GIS data in the Baldhill Creek watershed. The STATSGO soil data (NRCS 2016) and the 2011 NLCD land use data (Homer et al. 2011) were used to calculate CNs. To ensure that the basic and improved models are comparable, the CN for subbasin *j* in the basic model is the same as the corresponding subbasin DA_j^{Sub} and NDA_j^{Sub} in the improved model. The initial abstraction coefficient was selected and calibrated for both the improved and basic models. The SCS unit hydrograph method was selected for subbasin routing; the recession

method was selected for baseflow simulation; and the lag method was used for channel routing in both the improved and basic HEC-HMS models.

Two storm events were selected to calibrate and validate the improved and basic HEC-HMS models. The calibration event ranged from 6/13/2017, 04:45 to 6/15/2017, 03:00, and the validation event was from 8/18/2016, 05:00 to 8/25/2016, 06:15. The time interval for both events was 5 minutes. The peak discharge (Q_p), residual discharge volume, and graphical methods were used to compare the effectiveness of the basic vs. improved HEC-HMS models. Particularly, to evaluate the performances of the two models, three quantitative statistics, Nash-Sutcliffe efficiency (NSE) (Nash and Sutcliffe 1970), percent bias (PBIAS) (Guppta et al., 1999), and ratio of the root mean square error to the standard deviation of measured data (RSR) (Singh et al. 2004) were calculated:

$$NSE = 1 - \sum_{i=1}^{n}\left(Q_i^{obs} - Q_i^{sim}\right)^2 \Big/ \sum_{i=1}^{n}\left(Q_i^{obs} - \bar{Q}^{obs}\right)^2 \tag{3.9}$$

$$PBIAS = \sum_{i=1}^{n}\left(Q_i^{obs} - Q_i^{sim}\right)^2 \times 100 \Big/ \sum_{i=1}^{n} Q_i^{obs} \tag{3.10}$$

$$RSR = \sqrt{\sum_{i=1}^{n}\left(Q_i^{obs} - Q_i^{sim}\right)^2} \Big/ \sqrt{\sum_{i=1}^{n}\left(Q_i^{obs} - \bar{Q}^{obs}\right)^2} \tag{3.11}$$

where Q_i^{obs} is the *i*th observed outlet discharge (L^3/T); Q_i^{sim} is the *i*th simulated outlet discharge (L^3/T); $\bar{Q}^{obs}$ is the mean of the observed outlet discharges(L^3/T); and *n* is the total number of discharge data points. Following Moriasi et al. (2007, 2015), NSE > 0.50, PBIA= ± 15%, and RSR ≤ 0.70 are considered satisfactory for model performance.

3.4. Results and Discussions

3.4.1. Traditional Delineation and Topographic Processing Results

Traditional watershed delineation results are shown in Figure 3.4. The Baldhill Creek watershed was delineated into 20 subbasins (Figure 3.4a). During the delineation process, all sinks were filled and artificial slopes across the depressional areas were introduced to ensure full connectivity (Gabrecht and Martz 1999). Note that the artificial channels in Figure 3.4b differs from the actual streams/rivers depicted in the USGS hydrography in Figure 3.3c. The basic HEC-HMS model was calibrated, and Table 3.1 displays the subbasin and reach parameters for the basic model.

To create the improved HEC-HMS model, topographic characteristics, specifically $A_{i,j}^{PBU}$ and $MDS_{i,j}^{PBU}$, were processed for all subbasins. Figure 3.4c shows the identified PBUs and CBUs in subbasin 20 as an example of how $A_{i,j}^{PBU}$ and $MDS_{i,j}^{PBU}$ are paired. This information was extracted for all subbasins. Table 3.2 shows the DA and its corresponding MDS and the calibrated lag time, as well as the NDA and its calibrated lag time for the improved model. Note that the sum of the DA and NDA for each subbasin in Table 3.2 is the same as the corresponding subbasin area in Table 3.1 for the basic HEC-HMS model. Except subbasin 2, the DA is larger than the NDA for all other subbasins, and the NDAs are all smaller than 2% of the total corresponding subbasin areas (Table 3.2). Thus, the contributing areas to the subbasin outlets and the resulting discharges from the subbasins differ greatly between the basic and improved HEC-HMS models. Note that the same calibrated CNs for each subbasin in the basic model are used for the corresponding subbasins in the improved model. In order to make the basic and improved models comparable, the basic model accounts for depressions using a calibrated initial

abstraction coefficient of 0.28 for all subbasins while the improved model explicitly accounts for surface depressions and the dynamic P2P processes in the DTCP for all subbasins.

Table 3.1. Subbasin and reach characteristics and calibrated parameters for the basic HEC-HMS model.

Basin ID	Basin Area (km^2)	CN	SCS Lag Time (min)	Reach ID	Lag Time (min)
1B	139.63	64.19	1,984.20	1R	81.80
2B	84.43	68.09	558.44	2R	57.24
3B	38.36	61.36	1,830.40	3R	26.00
4B	21.40	74.96	545.14	4R	31.52
5B	32.42	78.96	208.94	5R	100.82
6B	82.71	74.62	1,152.00	6R	2,309.80
7B	99.37	63.57	2,869.90	7R	742.50
8B	55.78	64.68	1,388.20	8R	113.63
9B	81.22	67.25	2,001.90	9R	128.78
10B	224.50	64.21	2,062.20	10R	642.09
11B	96.02	74.87	649.96	11R	26.26
12B	90.09	66.9	1,046.40	12R	127.26
13B	183.38	69.69	1,275.70	13R	114.75
14B	32.62	69.66	1,640.50	14R	24.39
15B	93.88	70.03	2,644.90	15R	19.70
16B	19.75	70.38	567.02	16R	19.60
17B	50.33	65.77	2,138.30	17R	19.60
18B	190.70	62.69	694.45	18R	67.00
19B	92.38	67.38	1,978.30	19R	67.50
20B	11.82	76.96	87.08		

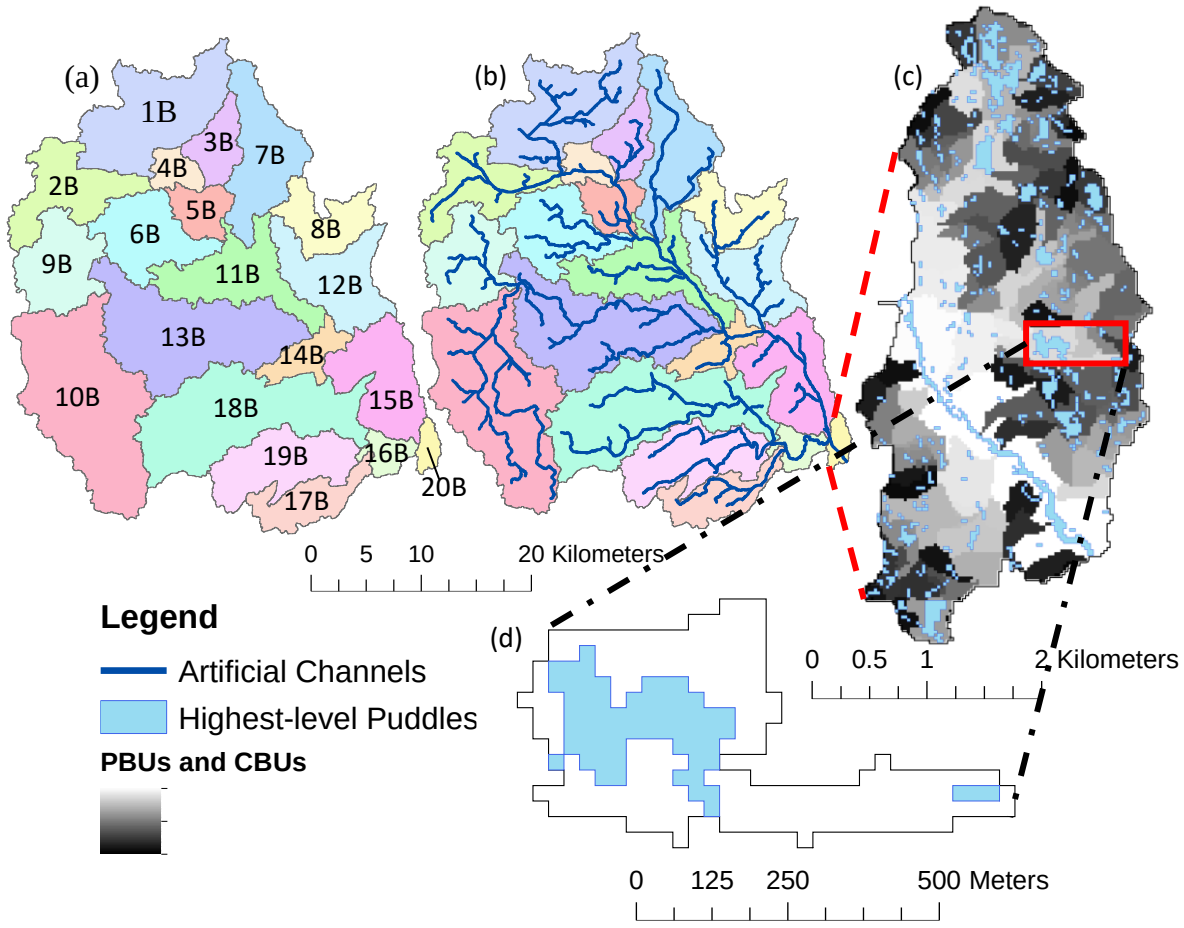

Figure 3.4. (a) Delineated subbasins, (b) artificial stream network, (c) puddle-based units (PBUs)/channel-based units (CBUs) and the highest-level puddles identified by the Puddle Delineation (PD) algorithm, and (d) a PBU with its corresponding highest-level puddles.

Figure 3.4d highlights a PBU of subbasin 20, in which $A_{i,j}^{PBU}$ and $MDS_{i,j}^{PBU}$ were paired to create the storage-discharge function. Figure 3.4d shows the corresponding $A_{i,j}^{PBU}$ and $MDS_{i,j}^{PBU}$ results for the PBU within subbasin 20. This particular PBU has a contributing area of 0.22 km^2 and an MDS of 11,419 m^3 (Figure 3.4d). Such paired values were used to create the storage-discharge function described in Figure 3.1d.

Table 3.2. Subbasin characteristics and calibrated parameters for the improved HEC-HMS model.

Basin ID	DA (km^2)	MDS ($x10^5$ m^3)	DA Lag Time (min)	NDA (km^2)	NDA Lag Time (min)	Total Area (km^2)
1B	127.14	638.29	1,723.80	12.48	260.44	139.63
2B	12.12	4.03	283.47	72.31	274.97	84.43
3B	30.57	32.34	1,605.60	7.78	224.83	38.36
4B	17.74	5.31	1,725.30	3.66	201.42	21.40
5B	27.36	8.85	629.15	5.05	186.65	32.42
6B	79.10	58.92	840.48	3.60	311.47	82.71
7B	83.59	90.62	1,675.80	15.77	1,194.10	99.37
8B	53.58	160.65	1,123.20	2.20	265.03	55.78
9B	76.82	170.94	1,726.20	4.39	275.67	81.22
10B	215.80	838.69	1,147.90	8.69	914.29	224.50
11B	88.34	60.08	1,547.30	7.67	199.36	96.02
12B	84.44	130.36	777.62	5.64	268.81	90.09
13B	172.22	131.30	1,111.70	11.16	163.98	183.38
14B	29.03	15.76	1,591.70	3.59	48.83	32.62
15B	81.47	173.60	2,380.80	12.40	264.15	93.88
16B	18.05	14.28	1,838.70	1.69	47.40	19.75
17B	47.00	44.02	1,734.20	3.32	404.06	50.33
18B	175.60	273.69	487.04	15.10	207.41	190.70
19B	83.04	46.43	1,707.90	9.33	270.37	92.38
20B	10.26	4.72	281.13	1.56	76.88	11.82

3.4.2. Impact of the Storage-discharge Function on Dynamic Contributing Area and P2P Processes

Figure 3.5 shows the normalized storage-discharge function for all 20 subbasins in the study area. For a fully-filled state (i.e., S/MDS = 1), the normalized discharge (Q/Q_p) equals one (Figure 3.5) (i.e., maximum discharge is reached). The overall shapes of these storage-discharge curves differ. For example, the subbasins which have smaller depression storage form a smoother curve and reach a peak discharge more quickly, while the depression-dominated subbasins exhibit a stepwise changing pattern.

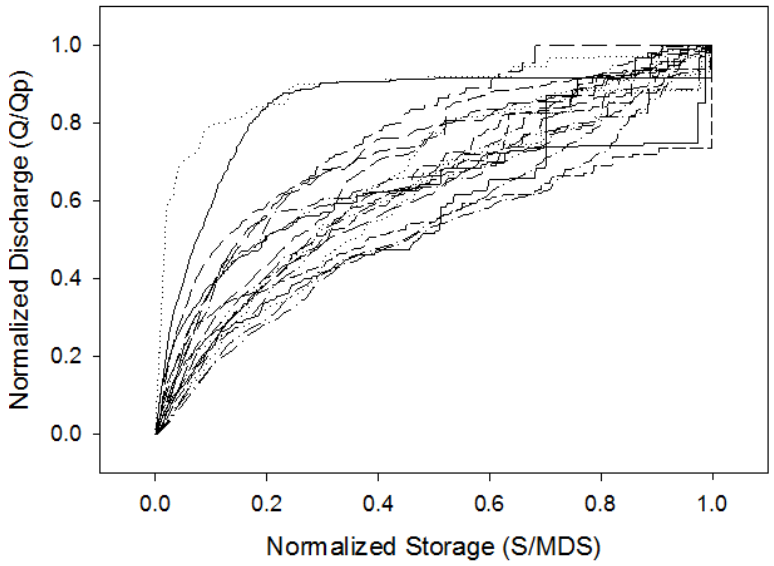

Figure 3.5. Normalized storage-discharge functions implemented into the depression threshold control proxy (DTCP) 'reservoir' features of all 20 subbasins in the improved HEC-HMS model (S = depression storage; MDS = maximum depression storage; Q = discharge; and Qp = peak discharge).

To further investigate this phenomenon, the storage-discharge function was converted to normalized storage vs. normalized contributing area [i.e., relative surface connection function (RSCf)] (Antoine et al. 2009; Grimm and Chu 2018) so that when the normalized contributing area of a subbasin equals 1, the total DA contributes runoff water to the subbasin outlet (i.e., depressions are fully filled and the entire subbasin is hydrologically connected). Figure 3.6 shows the RSCf of the DAs for two selected representative subbasins, subbasin 15 (Figure 3.6a) and subbasin 1 (Figure 3.6b). Subbasin 1 is depression-dominated while subbasin 15 has a main channel running through it and a smaller MDS. The shapes of these two RSCf curves in Figure 3.6 are in accordance with the findings by Grimm and Chu (2018) for depression-dominated (e.g., subbasin 1, Figure 3.6b) and less depression-dominated areas (e.g., subbasin 15, Figure 3.6a). The rates, at which the contributing areas increase, differ for the two selected subbasins. Subbasin 15 (Figure 3.6a) has nearly 90% of the DA contributing to the outlet at only 20% of its MDS. This implies that a majority of the surface is comprised of small depressions which

experience a short fill-spill process and contribute runoff to the outlet quickly (i.e., spilling period). The remaining 10% of the DA contributes to a few larger depressions with large storages. This is depicted in the RSCf graph (Figure 3.6a) in the highlighted section. The line, highlighted in Figure 3.6a, has a very low slope, which indicates that the remaining 10% of the DA is contributing to filling large depressions (i.e., filling period). Only at the very last time step does the surface reach its MDS and full hydrologic connectivity is achieved. Subbasin 1 (Figure 3.6b) transitions from filling periods to spilling and back again. This is an indicator of the size and distribution of the depressions and their contributing areas (i.e., $A_{i,j}^{PBU}$) on the surface. For example, the initial spilling period takes place until the storage of the subbasin reaches 35% of its MDS (i.e., S/MDS = 0.35) (Figure 3.6b). This part of the curve for subbasin 1 increases relatively gradually compared to the corresponding part for subbasin 15 in Figure 3.6a. Three distinct filling periods can be identified, as highlighted in Figure 3.6b. These three filling periods are followed by a stepwise increase in contributing area (i.e., spilling period), so it can be concluded that the filling periods (with a low slope, Figure 3.6b) are directly related to the filling and spilling of specific depressions on the surface of subbasin 1. The multiple steps with varying increases in connectivity is an indicator of the more complex depression-dominated surface, subbasin 1. The dynamic contributing area controlled by the storage-discharge function and the separation of DA and NDA in the improved modeling framework restrict the amount of discharge from each subbasin outlet, which results in different simulations from the basic HEC-HMS model.

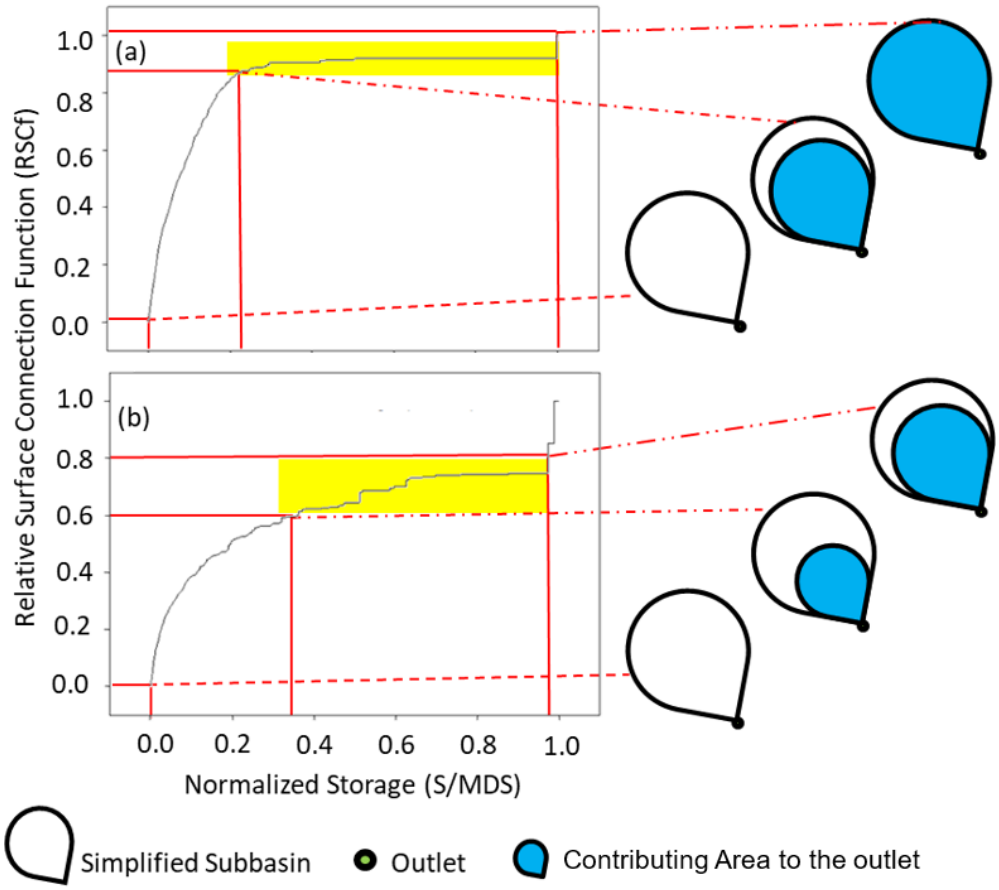

Figure 3.6. Relative surface connection function (RSCf) of depressional area (DA) and the corresponding depiction of their simplified dynamic contributing areas to the outlet for (a) subbasin 1 (depression-dominated, large MDS) and (b) subbasin 15 (less depression-dominated, smaller MDS).

3.4.3. Basic vs. Improved HEC-HMS Modeling of Depression-dominated Areas

Figures 3.7a and 3.7b respectively show the hydrographs for the calibration event and the validation event simulated by the basic and improved HEC-HMS models, compared against the observed hydrographs at the final outlet of the Baldhill Creek watershed. Although the basic HEC-HMS model simulated peak discharge and total discharge well for the calibration event (Figure 3.7a), the initiation of direct runoff was delayed due to the lumped Ia for each subbasin. Therefore, the simulation missed the initial increase in discharge shown in the observed hydrograph. In addition to the delayed initiation of direct runoff, the basic HEC-HMS model

simulated two peaks for this event rather than one peak in the observed hydrograph. This occurred because the basic model did not account for the actual ponding storage and the dynamic filling-spilling processes, which delayed the runoff water contribution to the outlet. Instead, all excess rainfall was consistently routed to the outlet of each subbasin in the basic model. In the basic model framework, lag time cannot be changed as a function of surface depression storage. In contrast, the hydrograph simulated by the improved HEC-HMS model matches the timing of direct runoff initiation and the simulated discharge follows the general shape of the observed hydrograph (Figure 3.7a). In the improved HEC-HMS model, the storage-discharge function clearly controlled the volume of water released from each subbasin in the watershed and helped create the smooth stepwise increases reflected in the observed hydrograph. However, the attenuated discharge from the 'reservoir' feature caused a slight overestimation for the falling limb of the hydrograph. Figure 3.7b shows the hydrographs simulated by the basic and improved HEC-HMS models for the validation event. The basic HEC-HMS model underestimated surface runoff because the Ia was too large to allow any excess rainfall. The simulations for these two events prove that using the traditional delineation and modeling for depression-dominated areas tends to overestimate or underestimate the total discharge, depending on the size and temporal distribution of the storm event being simulated. This makes calibration of an event model very difficult especially considering the fact that the size, duration, and distribution of rainfall over the study area vary from storm to storm; whereas the DTCP in the improved model controls the ponded water storage and release, which reflect the real overland flow generation and runoff processes over a depression-dominated surface.

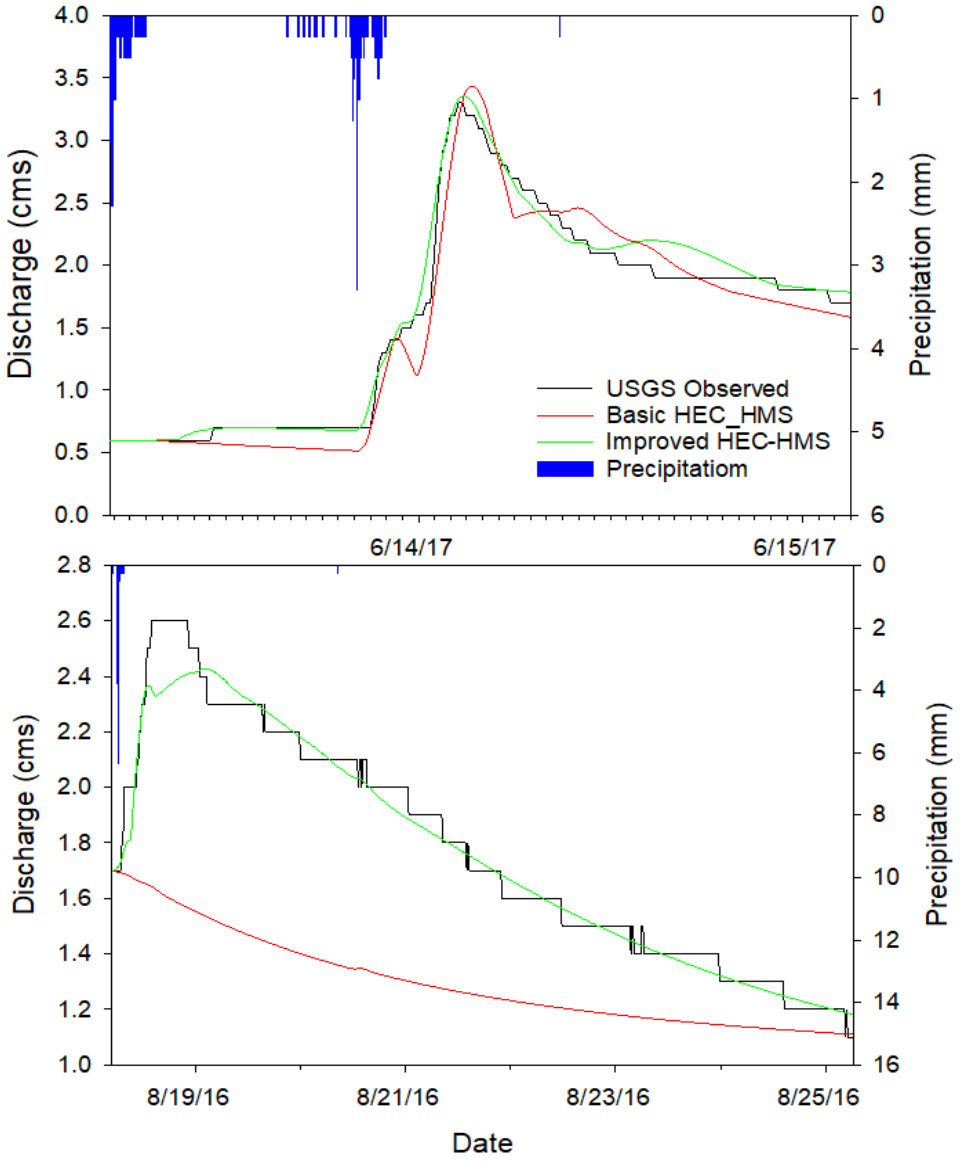

Figure 3.7. Basic HEC-HMS model, improved HEC-HMS model, and observed USGS hydrographs for (a) Calibration event and (b) Validation event.

Table 3.3 shows the statistical summary of the simulation results from the basic and improved HEC-HMS models for the two events. The improved model only slightly overestimated the peak discharge (Q_p) by 0.06 m^3/s, while the basic model overestimated Q_p by 0.14 m^3/s (Table 3.3). The basic model slightly underestimated the total runoff water volume while the improved model slightly overestimated the total runoff water volume for the

calibration event (Table 3.3). This slight overestimation of the improved model occurred on the falling limb of the hydrograph, resulting in a negative PBIAS value (Table 3.3). However, all statistics for the improved model fall well within the recommended satisfactory ranges (Table 3.3). The statistics for the basic model also fall well within the recommended ranges for the calibration event simulation (Table 3.3). However, the statistics for the basic model for the validation event all fall outside the recommended ranges (Table 3.3). In addition, Qp and the total volume of runoff water for the validation event were drastically underestimated because no direct runoff was simulated by the basic model. The improved model also resulted in better NSE and RSR statistics for the validation event.

Table 3.3. Statistical summary of results for the basic and improved HEC-HMS models for events 1 and 2.

	Qp (m^3/s)	**Residual Runoff Water Volume ($x10^3$ m^3)**	**NSE**	**PBIAS (%)**	**RSR**
Calibration Event 6/13/2017 – 6/15/2017					
Observed Hydrograph	3.30	N/A	N/A	N/A	N/A
Basic HEC-HMS	3.44	-9.93	0.95	3.74	0.22
Improved HEC-HMS	3.36	8.07	0.98	-3.04	0.14
Validation Event 8/18/2016 – 8/25/2016					
Observed Hydrograph	2.6	N/A	N/A	N/A	N/A
Basic HEC-HMS	1.7	-288.19	-0.74	26.67	1.32
Improved HEC-HMS	2.43	-8.98	0.97	0.83	0.17

3.4.4. Impact of Dynamic Contributing Area and Depression Storage on Outlet Discharge

In addition to the better simulations of the discharge at the final outlet, the improved model also provided essential details on the dynamic changes in contributing area and depression storage during the rainfall events. Due to the new conceptual framework, which divided a subbasin into NDA and DA, dynamic contributing area across the subbasin can be analyzed. For

instance, Figure 3.8a shows the surface runoff over subbasin 20 generated by the basic model, and the surface runoff over the NDA and DA of subbasin 20 generated by the improved HEC-HMS model. Because the NDA is smaller than the DA for subbasin 20, the lag time is shorter for the NDA, leading to an earlier peak.

The separation of a subbasin into NDA and DA also allowed the DA to be routed through the DTCP (i.e., 'reservoir' feature), which mimicked the dynamic P2P processes. Figure 3.8b shows the water input into the DTCP of subbasin 20 (i.e., runoff generated in the DA of subbasin 20), the storage of the DTCP, and the discharge from the DTCP of subbasin 20. Based on the storage-discharge function for subbasin 20, the discharge from the DTCP is delayed. This is what is to be expected for a depression-dominated subbasin. The storage curve shows the incremental filling of the lumped depression storage in subbasin 20, indicating the percentage of the MDS that is reached during each event (i.e., peak storage/ MDS).

Figure 3.8c compares the runoff generated by the basic and improved models for subbasin 20. Direct runoff generation occurred earlier for the improved model because no surface runoff was generated in the basic model until the large Ia was surpassed. In addition, the impact of dynamic contributing area can be identified by the two peaks. The first peak shows the initial contributing area or the response of the NDA of the subbasin, while the second peak shows the gradual increase in the depressional contributing area. Not only is the dynamic contributing area identifiable, but also Q_p and the total discharge are reduced in this subbasin compared to the discharges simulated by the basic model. Although the basic model considers a lumped depression storage in the Ia, it is still not reflected in the modeling results, whereas the improved model simulates the dynamic changes in depression storage and water release.

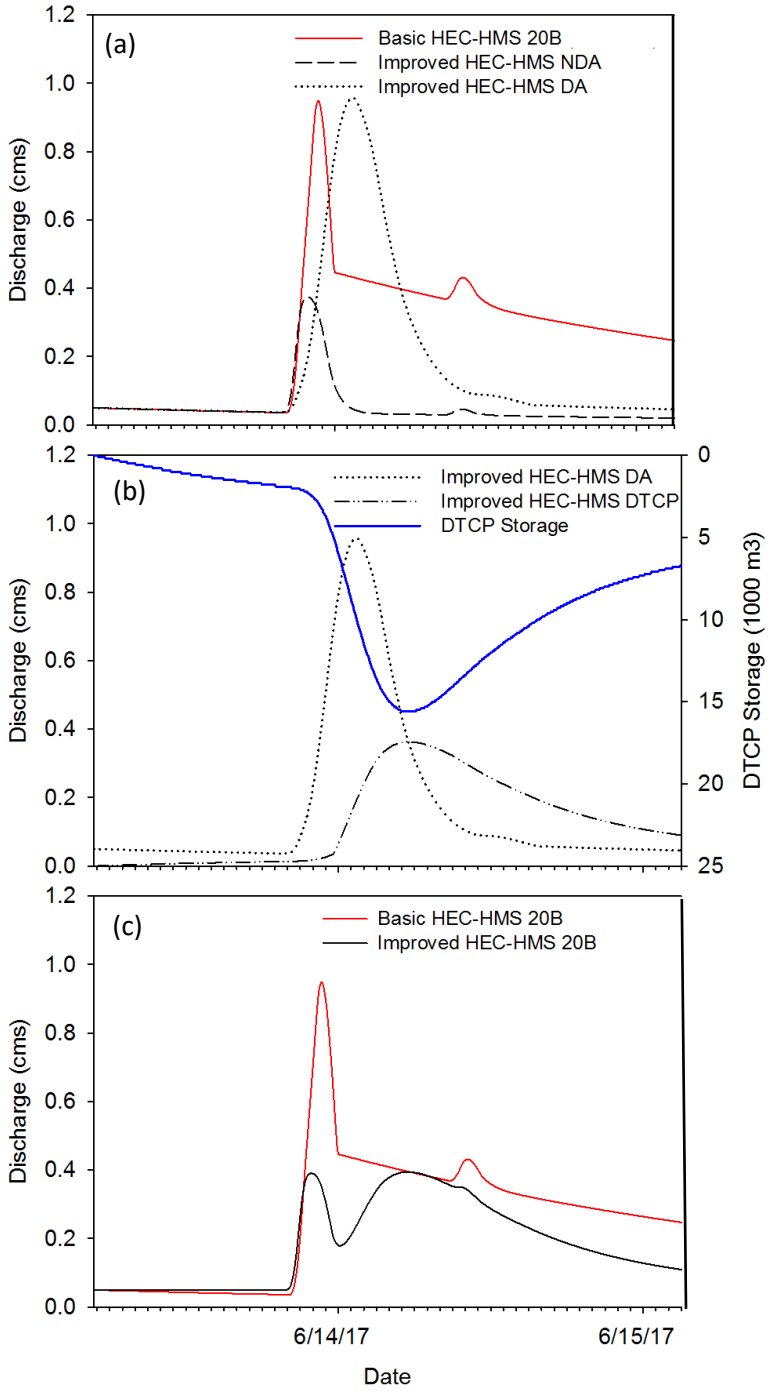

Figure 3.8. (a) hydrograph of subbasin 20 (20B) simulated by basic HEC-HMS and hydrographs of 20B non-depressional area (NDA) and 20B depressional area (DA) simulated by improved HEC-HMS; (b) hydrograph of 20B DA [i.e., inflow to depression threshold control proxy (DTCP)] simulated by improved HEC-HMS, depression storage in the 20B DTCP, and hydrograph of 20B DTCP simulated by improved HEC-HMS; (c) hydrograph of 20B simulated by basic HEC-HMS and hydrograph of 20B (i.e., subbasin 20 NDA discharge + subbasin DTCP discharge) simulated by improved HEC-HMS.

3.5. Conclusions

An improved HEC-HMS model was developed to simulate the effects of the depression threshold behavior on outlet discharge in order to improve the modeling for depression-dominated areas. The concept of DTCP was proposed and incorporated in the HEC-HMS model as a 'reservoir' feature for each subbasin. The topographic characteristics and storage capabilities of each subbasin were incorporated into the storage-discharge function to facilitate the 'reservoir' routing, which mimicked the filling and spilling of depressions. A new conceptual framework was designed to divide a subbasin into NDA and DA that have distinct mechanisms of runoff contribution.

It was demonstrated that the improved HEC-HMS model more accurately simulated discharge at the final outlet than the basic HEC-HMS model. To prevent the overestimation of total discharge, the 'reservoir' feature was introduced to store rainfall excess and release the ponded water through a threshold control. The storage-discharge function then mimicked the dynamic P2P filling-spilling processes. With the storage-discharge function, the DTCP delayed the initiation of surface runoff, which mimicked the dynamic changes in contributing area in a depression-dominated watershed. In this way, the improved model was able to separately simulate (1) NDA direct runoff and (2) DA direct runoff. The 'reservoir' feature in the improved model also allowed the depression storage to be analyzed temporally, rather than as part of the subbasin Ia in the basic model.

This study emphasized the importance of accounting for the key topographic characteristics of a depression-dominated watershed in hydrologic modeling. In practice, however, not all hydrologic models facilitate the simulation of the P2P processes and the

dynamic changes in runoff contributing area. Therefore, the concept of DTCP and the improved HEC-HMS modeling framework, developed in this study, can be used to fill this gap.

3.6. References

Amoah JK, Amataya DM, Nnaji S. 2012. "Quantifying watershed surface depression storage: determination and application in a hydrologic model." *Journal of Hydrological Processes*, 27(17), 2401-2413. DOI: 10.1002/hyp.9364

Antoine M, Javaux M, Bielders C. 2009. "What indicators can capture runoff-relevant connectivity properties of the micro-topography at the plot scale?" *Advances in Water Resources* 32, 1297–1310. DOI: 10.1016/j.advwatres.2009.05.006

Appels WM, Bogaart PW, van der Zee S. 2011. "Influence of spatial variations of microtopography and infiltration on surface runoff and field scale hydrological connectivity." *Advances in Water Resources*, 34(2), 303–313. DOI: 10.1016/j.advwatres.2010. 12.003

Arnold JG, Srinivasan R, Muttiah RS, Williams JR. 1998. "Large Area Hydrologic Modeling and Assessment Part I: Model Development." *Journal of the American Water Resources Association*, 34(1), 73–89. DOI: 10.1111/j.1752-1688.1998.tb05961.x

Chen YD. 2004. "Watershed modeling: Where are we heading?" *Environmental Informatics Archives*, 2, 132–139.

Chu X. 2015. "Delineation of pothole-dominated wetlands and modeling of their threshold behaviors." *Journal of Hydrologic Engineering*, 22, 431–438. DOI: 10.1061/(ASCE)HE.1943-5584.0001224

Chu X, Yang J, Chi Y, Zhang J. 2013. “Dynamic puddle delineation and modeling of puddle-to-puddle filling-spilling-merging-splitting overland flow processes.” *Water Resources Research*, 49(6), 3825–3829. DOI: 10.1002/wrcr.20286

Chu X, Zhang J, Chi Y, Yang J. 2010. “An improved method for watershed delineation and computation of surface depression storage.” *Watershed Management Conference 2010: Innovations in Watershed Management under Land Use and Climate Change*, 1113–1122. DOI: 10.1061/41143(394)100

Darboux F, Davy P, Gascuel-Odoux C, Huang C. 2002. “Evolution of soil surface roughness and flowpath connectivity in overland flow experiments.” *Catena*, 46, 125–139. DOI: 10.1016/S0341-8162(01)00162-X

Darboux F, Huang C. 2005. “Does Soil Surface Roughness Increase or Decrease Water and Particle Transfers?” *Soil Science Society of America Journal*, 69(3), 748-756. DOI: 10.2136/sssaj2003.0311

Flemming M, Doan J. 2009. *Geospatial hydrologic modeling extension HEC-GeoHMS-user’s manual-version 4.2*. US Army Corps of Engineers Hydrologic Engineering Center, Davis, California, USA

Gabrecht J, Martz LW. 1999. *TOPAZ: An Automated Digital Landscape Analysis Tool for Topographic Evaluation, Drainage Identification, Watershed Segmentation and Subcatchment Parameterization: TOPAZ User Manual.* USDA Forest Service: Grazinglands Research Laboratory, USDA Agricultural Research Services, El Reno, OK.

Grimm K, Chu X. 2018. “Modeling of spatiotemporal variations in runoff contribution areas and analysis of hydrologic connectivity.” *Land Degradation & Development*, 29(8), 2629-2643. DOI: 10.1002/ldr.3076

Gyawali R, Watkins D. 2013. “Continuous hydrologic modeling of snow-affected watersheds in the Great Lakes basin using HEC-HMS.” *Journal of Hydrologic Engineering*, 18(1), 29–39. DOI: 10.1061/(ASCE)HE.1943-5584.0000591

Habtezion N, Tahmasebi Nasab M, Chu X. 2016. “How does DEM resolution affect microtopographic characteristics, hydrologic connectivity, and modelling of hydrologic processes?” *Hydrological Processes*, 30, 4870-4892. DOI: 10.1002/hyp.10967

Hawkins RH, Ward T, Woodward DE, Van Mullem J. 2009. *Curve Number Hydrology: State of the Practice.* American Society of Civil Engineers, Reston, Virginia.

Homer C, Dewitz J, Yang L, Jin S, Danielson P, Xian G, Coulston J, Herold N, Wickham J, Megown K. 2011. “Completion of the 2011 National Land Cover Database for the conterminous United States--representing a decade of land cover change information.” *Photogrammetric Engineering & Remote Sensing*, 77(9), 858–864.

Jenson SK, Domingue JO. 1988. “Extracting topographic structure from digital elevation data for geographic information system analysis.” *Photogrammetric Engineering and Remote Sensing*, 54(11), 1593–1600. DOI: 0099-1112/88/5411-1593$02.25/0

Lindsay JB, Creed IF. 2005. “Removal of artifact depressions from digital elevation models: towards a minimum impact approach.” *Hydrological Processes*, 19(16), 3113–3126. DOI: 10.1002/hyp.5835

Marks D, Dozier J, Frew J. 1984. “Automated basin delineation from digital elevation data.” *Geo-Processing*, 2(3), 299–311.

Martz LW, Garbrecht J. 1993. “Automated extraction of drainage network and watershed data from digital elevation models.” *Journal of the American Water Resources Association*, 29(6), 901–908. DOI: 10.1111/j.1752-1688.1993.tb03250.x

Moriasi DN, Arnold JG, Van Liew MW, Binger RL, Harmel RD, Veith TL. 2007. "Model evaluation guidelines for systematic quantification of accuracy in watershed simulations." *Transactions of the ASABE,* 50(3), 885–900. DOI: 10.13031/ 2013.23153

Moriasi DN, Zeckoski RW, Arnold JG, Baffaut C, Malone RW, Daggupati P, Guzman JA, Saraswat D, Yuan Y, Wilson BN, Shirmohammadi A, Douglas-Mankin KR. 2015. "Hydrologic and Water Quality Models: Key Calibration and Validation Topics." *Transactions of the ASABE,* 58(6), 1609–1618. DOI: 10.13031/trans.58.11075

Mushet D M, Goldhaber MB, Mills CT, McLean KI, Aparicio VM, McCleskey RB, Holloway JM, Stockwell CA. 2015. *Chemical and biotic characteristics of prairie lakes and large wetlands in south-central North Dakota—Effects of a changing climate*. Scientific Investigations Report 2015-5126. DOI: 10.3133/sir20155126

Nash JE, Sutcliffe JV. 1970. "River flow forecasting through conceptual models part I - A discussion of principles." *Journal of Hydrology,* 10(3), 282–290. DOI: 10.1016 /00221694(70)90255-6

O'Callaghan JF, Mark DM. 1984. "The extraction of drainage networks from digital elevation data." *Computer Vision, Graphics, and Image Processing,* 28(2), 323–344. DOI: 10.1016/S0734-189X(84)80011-0

Paudel M, Nelson EJ, Scharffenberg W. 2009. "Comparison of lumped and quasi-distributed Clark runoff models using the SCS curve number Equation." *Journal of Hydrologic Engineering*, 14(10). DOI: 10.1061/(ASCE)HE.1943-5584.0000100

Peñuela A, Javaux M, Bielders CL. 2015. "How do slope and surface roughness affect plot-scale overland flow connectivity?" *Journal of Hydrology,* 528, 192–205. DOI: 10.1016/j.jhydrol.2015.06.031

Soil Survey Staff, Natural Resources Conservation Service, United States Department of Agriculture. Web Soil Survey. Available online at http://websoilsurvey.nrcs.usda.gov/. Accessed [10/20/2016].

Tahmasebi Nasab M, Jia X, Chu X. 2016. "Modeling of subsurface drainage under varying microtopographic, soil and rainfall conditions." *Proceedings of the Tenth International Drainage Symposium,* American Society of Agricultural and Biological Engineers, Minneapolis, MN, 1–6. DOI: 10.13031/IDS.20162499952

Tahmasebi Nasab M, Zhang J, Chu X. 2017a. "A new depression-dominated delineation (D-cubed) method for improved watershed modeling." *Hydrological Processes*, 31, 3364-3378. DOI: 10.1002/hyp.11261

Tahmasebi Nasab M, Singh V, Chu X. 2017b. "SWAT modeling for depression-dominated areas: How do depressions manipulate hydrologic modeling?" *Water,* 9(1), 58. DOI: 10.3390/w9010058

Tahmasebi Nasab M, Grimm K, Wang N, Chu X. 2017c. "Scale analysis for depression-dominated areas: How does threshold resolution represent a surface?" *Watershed Management, Irrigation and Drainage, and Water Resources Planning and Management, Proceedings of World Environmental and Water Resources Congress 2017,* American Society of Civil Engineers, Reston, VA, 164–174. DOI: 10.1061/9780784480601.016

Tarboron DG. 1997. "A new method for the determination of flow directions and upslope areas in grid digital elevation models." *Water Resources Research*, 33(2), 309–319. DOI: 10.1029/96WR03137

USACE-HEC. 2000. *Hydrologic modeling system HEC-HMS technical reference manual*. US Army Corps of Engineers, Hydrologic Engineering Center, Davis, CA.

USACE-HEC. 2016. *Hydrologic Modeling System HEC-HMS - User Manual*. US Army Corps of Engineers Institute for Water Resources Hydrologic Engineering Center, Davis, CA.

U.S. Bureau of Reclamation. 1949. "Flood routing." *Flood Hydrology* part 6 *in Water Studies* Vol. 4, Washington, D.C.

USDA. 1986. *Urban Hydrology for Small Watersheds. Technical Release 55 (TR-55)*, Natural Resources Conservation Services, Washington, D.C.

USEPA. 2006. *2006-2011 EPA Strategic Plan: Charting Our Course*. Office of the Chief Financial Officer, Office of Planning, Analysis, and Accountability, U.S. Environmental Protection Agency.

Wałęga, A. 2013. "Application of HEC-HMS programme for the reconstruction of a flood event in an uncontrolled basin." *Journal of Water and Land Development*, 18(9), 13–20. DOI: 10.2478/jwld-2013-0002

Winter TC. 2003. *Hydrological, Chemical, and Biological Characteristics of a Prairie Pothole Wetland Complex Under Highly Variable Climate Conditions- The Cottonwood Lake Area, East-Central North Dakota,* pp109. U.S. Geological Survey Professional Paper 1675. Denver, CO.

WMS. 2015. *WMS User Manual 10.1*. Brigham Young Univ., Environmental Modeling Research Laboratory, Provo, Utah.

Yang J, Chu X. 2012. "Effects of surface microtopography on hydrologic connectivity." In: *Crossing Boundaries, Proceedings of the 2012 ASCE World Environmental and Water Resources Congress,* American Society of Civil Engineers, Reston, VA, 339–348. DOI: 10.1061/9780784412312.037

Yang J, Chu X. 2015. “A new modeling approach for simulating microtopography-dominated, discontinuous overland flow on infiltrating surfaces.” *Advances in Water Resources,* 78, 80–93. DOI: 10.1016/j.advwatres.2015.02.004

Zhang J, Chu X. 2015. “Impact of DEM resolution on puddle characterization: Comparison of different surfaces and methods.” *Water*, 7, 2293–2313. DOI: 10.3390/w7052293

4. EVALUATING THE EFFECTS OF WETLAND CLASSIFICATION ON MODELING HYDROLOGIC PROCESSES IN SWAT

4.1. Abstract

There are many suggested wetland classifications used to describe a wetland's interaction with groundwater, hydrologic connectivity, and the impact of climatic and hydrologic conditions on wetland ecology. Incorporating the hydrologic characteristics of these different wetland classifications into a model is necessary to assess the extent, to which wetlands impact a watershed's hydrologic and ecologic responses. Therefore, the objectives of this study are (1) to evaluate the impact of different wetland classifications on the Soil and Water Assessment Tool (SWAT) modeling and (2) to investigate the hydrologic processes impacted by wetland functions. To accomplish these objectives, an improved SWAT modeling approach is proposed to simulate dynamic contributing area and the hydrologic processes related to different types of wetlands. Results show that the new modeling approach provides accurate representation of discharge from a watershed outlet and subbasin storage in two different types of wetlands. The new modeling approach and the findings from this study help improve the understanding of wetland classifications and the extent of wetlands' impacts on watershed-scale ecohydrologic modeling.

4.2. Introduction

Wetlands of a ecosystem affect hydrologic processes, sediment/nutrient retention, and habitat for numerous species. Human societies may benefit from wetlands such as water impoundment to protect against floods, pollution abatement, and aesthetic appreciation. However, only recently have this appreciation of wetlands and concern for their preservation been recognized (MA Board, 2005). During the last century, land use change has reduced and/or

segmented wetland habitats in many coastal and inland regions. Of the inland wetland regions, the North American Prairie Pothole Region (PPR) has been dramatically impacted by the conversion of grassland to cultivated cropland and/or pastureland.

The PPR encompasses 5 U.S. states (North Dakota, South Dakota, Montana, Minnesota, and Iowa) and 3 Canadian Provinces (Alberta, Saskatchewan, and Manitoba). Millions of pothole lakes and wetlands created during the last glaciation (Winter, 2003) reside in this region. Many of the wetlands in this region have been termed as geographically isolated wetlands (GIWs) because the depressional areas, in which the wetlands reside, are surrounded by uplands (Brinson, 1988; Golden et al., 2014; Tiner, 2003) which restrict their hydrologic connection to regional surface water systems. Hence, upstream GIWs can mitigate downstream flooding, sediment transfer, and nutrient pollution in watersheds where GIWs reside. On the other hand, recent debate regarding GIWs has suggested that the term, "geographic isolation", implies incorrect assumptions about wetland functions and hydrologic connectivity (Mushet et al., 2015). Based on the need, whether regulatory/management, hydrologic, or ecological, wetland classifications may differ, and one term over another may better represent the conceptualization of wetlands in decision-making tools (e.g., models) (Golden et al., 2017).

Hydrologically speaking, many other wetland classifications have been suggested. For example, wetland function has been used to describe a wetland's interaction with groundwater (Kantrud et al., 1989), the hydrogeomorphic (HGM) classes have been used to account for dynamic wetland functions by considering dynamic connectivity across wetland landscapes (Brinson, 1993), and wetland continuum has been used to address the influence of climatic and hydrologic conditions on wetland ecology (Euliss et al., 2004). Incorporating the hydrologic characteristics of these different wetland classifications is necessary to assess the extent, to

which wetlands impact water quality and watershed hydrologic and ecologic responses (Hayashi et al., 2016)

Assessing the extent of the wetlands' impacts on a watershed is difficult for two reasons. First, wetlands have varying hydrologic connectivity (e.g., surface water to groundwater, or wetland to wetland). And second, models and modeling approaches which specifically simulate wetland processes at the watershed scale are limited. Several studies have investigated the effects of depression storage and the puddle-to-puddle (P2P) filling, spilling, merging, splitting processes on the related hydrologic modeling. For instance, Chu et al. (2010) developed a Puddle Delineation (PD) algorithm for identifying depressions and their hierarchical relationships. PD was then incorporated into the physically-based P2P hydrologic modeling system (Chu et al., 2013) to simulate the P2P processes of overland flow, dynamic hydrologic connectivity (Yang and Chu, 2013), and stepwise outlet discharge (Yang and Chu, 2015). However, the cell-to-cell and puddle-to-puddle modeling over a large watershed can be computationally intensive, especially in regions like the PPR where millions of potholes and wetlands reside. The VS2DI model was used to investigate groundwater interactions and groundwater connectivity of wetlands (Neff and Rosenberry, 2018). Other modeling efforts, such as the Soil and Water Assessment Tool (SWAT) (Neitsch et al., 2011), have also been made to improve the ability to characterize wetlands (Golden et al., 2014). Specifically, SWAT has been modified in various ways to account for depression storage (e.g., Mekonnen et al., 2016; Tahmasebi Nasab et al., 2017; Wang et al., 2008; Yang et al., 2010). For example, Wang et al. (2008) and Yang et al. (2010), and Mekonnen et al. (2016) used the wetland and pond impoundment water routing functions, respectively, to account for depression storage. Tahmasebi Nasab et al. (2017) developed a coupled PD-SWAT in which depression storage was lumped at the subbasin scale

using the pothole impoundment water routing function in SWAT. Although these SWAT studies highlighted the importance of representing the physical characteristics of depressions (i.e., size, surface area, storage) and depressions as gate keepers, none addressed dynamic hydrologic connectivity or the impacts of wetland functions (e.g., discharge, flow-through, or recharge) or physical conditions (e.g., disturbed or undisturbed) on hydrologic processes.

To ensure that models will provide the most important information regarding wetland connectivity and functions to decision-makers, various tools must be developed to address different management questions (Golden et al., 2017). Therefore, the objectives of this study are (1) to evaluate the impacts of different wetland classifications on SWAT modeling and (2) to investigate hydrologic processes impacted by wetland functions. In order to accomplish these objectives, an improved SWAT impoundment water routing technique is proposed to simulate dynamic contributing area and the hydrologic processes related to different types of wetlands.

4.3. Methodology

4.3.1. Introduction to SWAT: How SWAT Regards Impounded Water

The SWAT model is a time-continuous, semi-distributed, physically-based hydrologic model designed to help decision makers assess the impacts of land management practices on water quantity, water quality, and sediment transport (Arnold et al., 1998). The ArcSWAT interface, an extension of ArcGIS, allows data to be displayed spatially and provides a user-friendly interface to conduct watershed delineation, data processing, and model setup. The semi-distributed framework of the model encourages the division of a large watershed into many delineated subbasins. These subbasins are further divided into hydrologic response units (HRUs) to account for the variations in land use, soil type, and slope characteristics in each subbasin (Neitsch et al., 2011). Hydrologic processes are simulated for each HRU based on user-specified

methods for surface runoff, evapotranspiration, snowmelt, and baseflow. In order to simulate hydrologic processes associated with landscape depressions, the user can utilize different impoundment features in the SWAT model, including Reservoir, Pond, Wetland, and Pothole features (Neitsch et al., 2011). This study utilizes the available Pothole and Wetland features in SWAT and provides guidelines for utilizing these features to represent real depression characteristics.

Each of the impoundment features lumps spatially-distributed depression characteristics into one feature. The water balance of each impoundment is given by (Neitsch et al., 2011):

$$V = V_{stored} + V_{flowin} - V_{flowout} + V_{pcp} - V_{evap} - V_{seep} \quad (4.1)$$

where V is the volume of water stored in the impoundment at the end of the day (m^3 H_2O), V_{stored} is the volume of water stored in the water body at the beginning of the day (m^3 H_2O), V_{flowin} is the volume of water entering the water body during the day (m^3 H_2O), $V_{flowout}$ is the volume of water leaving the water body during the day (m^3 H_2O), V_{pcp} is the volume of precipitation falling on the water body during the day (m^3 H_2O), and V_{evap} and V_{seep} are the volume of water lost from the water body to evaporation and seepage, respectively, during the day (m^3 H_2O).

These impoundment features differ in how they are conceptually defined within the SWAT model and how different variables within the water balance equation (Equation 4.1) are calculated. Specifically, the Pothole feature is specified to an individual HRU in each subbasin. Therefore, the contributing area to the Pothole is only a fraction of the HRU area in which the Pothole resides. Additionally, potholes are conceptualized as a conical-shaped unit to calculate the water body surface area as a function of impoundment water storage. Conversely, the Pond and Wetland features receive runoff contribution from a fraction of the subbasin area in which

the Pond or Wetland resides. This means that these two features allow water contribution from upland sources. The pond and wetland surface areas are given by (Neitsch et al., 2011):

$$SA = \beta_{sa} \times V^{expsa} \quad (4.2)$$

where β_{sa} and $expsa$ are a function of maximum surface area and maximum depression storage. Except for the outflow, the Pond and Wetland features calculate all variables in Equation (4.1), whereas the Pothole feature calculates all variables with Equation (4.1) differently.

As aforementioned, previous studies have utilized the Pond (Mekonnen et al., 2016), Wetland (Wang et al., 2008; Yang et al., 2010), or Pothole (Tahmasebi Nasab et al., 2017) feature in SWAT to address a variety of hydrologic questions related to water quantity. However, to the best of our knowledge, these SWAT features have not been used in conjunction to address the impacts of varying wetland functions or disturbance on water quantity. Therefore, a new modeling approach is proposed, which utilizes the established Wetland and Pothole features in SWAT to represent different wetland functions within a subbasin. The new modeling approach will hence forth be referred to as the Functional Wetland Approach (FWA).

4.3.2. Modeling Approaches

4.3.2.1. Pothole Only Approach

The Pothole Only Approach, hence forth referred to as A1, uses the Pothole feature in SWAT. Input parameters for this approach are maximum amount of water stored in the Pothole (POT_VOLX) and fraction of the HRU area contributing water to the Pothole (POT_FR). POT_VOLX is calculated as the lumped maximum depression storage (MDS) of each subbasin. MDS is calculated in ArcGIS by filling sinks in a digital elevation model (DEM) using the method developed by Planchon & Darboux (2001), and then removing storage in identified channel reaches from the USGS observed hydrography dataset (USGS, 2013). The MDS is then

specified to the largest HRU within the subbasin. This way, a large range of different contributing areas to the Pothole (i.e., POT_FR) can be selected during calibration. Water may flow out of the Pothole when MDS is surpassed. The excess water then spills and contributes to the main channel of the subbasin following Equation 4.3 (Neitsch et al., 2011).

$$\text{If } V > V_{pot,mx}$$
$$V_{flowout} = V - V_{pot,mx} \tag{4.3}$$

where $V_{pot,mx}$ is the maximum amount of water that can be stored in the pothole (m^3 H_2O) and $V_{flowout}$ is the volume of outflow from the pothole (m^3 H_2O).

4.3.2.2. Wetland Only Approach

The Wetland Only Approach, hence forth referred to as A2, uses the Wetland feature in SWAT. Input parameters for this approach are volume of water held in the Wetland when filled to the maximum water level (i.e., MDS) (WET_MXVOL), volume of water held in the Wetland when filled to the normal water level (WET_NVOL), surface area of the Wetland when filled to the maximum water level (WET_MXSA), surface area of the Wetland when filled to the normal water level (WET_NSA), and fraction of the subbasin area contributing water to the Wetland (WET_FR). The same method is used to calculate WET_MXVOL and POT_VOLX, while the surface area is extracted from ArcGIS processing for WET_MXSA. WET_FR can be selected and modified during the calibration process. Wetland outflow occurs when wetland storage exceeds the normal storage volume as shown in Equations (4.4) and (4.5) (Neitsch et al., 2011).

$$\text{If } V_{nor} \leq V \leq V_{mx}$$
$$V_{flowout} = \frac{V - V_{nor}}{10} \tag{4.4}$$

$$\text{If } V > V_{mx}$$
$$V_{flowout} = V - V_{mx} \tag{4.5}$$

where V_{nor} is the specified WET_NVOL (m^3 H_2O), V_{mx} is the maximum amount of water that can be stored in the Wetland (WET_MXVOL) (m^3 H_2O), and $V_{flowout}$ is the volume of outflow from the Wetland (m^3 H_2O).

4.3.2.3. Functional Wetland Approach (FWA)

The FWA is developed to address different management issues related to wetland functions, such as sedimentation of prairie wetlands (Gleason and Euliss, 1998), water quality in wetlands, and wetland health (Euliss et al., 2004, 2014). The FWA uses both the Wetland and Pothole features in SWAT. Since these two features differ in how contributing area to the water body is defined, dynamic contributing area is simulated in the FWA. Additionally, since different types of contributing area are accounted for, different wetland functions can be represented. To use the FWA, the physical wetland characteristics such as MDS, MPA, normal depression storage (NDS), and normal ponding area (NPA) must be lumped based on two wetland functions for each subbasin. In this study, wetlands were categorized into (1) discharge wetlands and (2) recharge/flow-through wetlands. Hydrologic processes and storage related to discharge wetlands are simulated using the Wetland feature in SWAT, whereas recharge/flow-through wetlands are simulated using the Pothole feature in SWAT. This may seem contradictory because most permanent water bodies or discharge wetlands are identified as potholes, whereas temporary/seasonal waterbodies are identified as wetlands. In fact, discharge wetlands or permanent water bodies often have more areas contributing to them than upland flow-through/recharge wetlands. In order to accurately represent contributing area to these water

bodies, the Wetland function (i.e., contributing area from a percentage of the entire subbasin) must simulate discharge wetland storage.

In using the Wetland feature to simulate hydrologic processes related to discharge wetlands, three assumptions are introduced: (1) discharge wetlands will not contribute any water downstream unless their maximum depression storage is exceeded, (2) the contributing area to discharge wetlands is a portion of the flow from the subbasin, in which the Wetland is specified, and (3) discharge wetlands are typically permanently/semi-permanently filled with water. Discharge wetlands were identified by using the processed remote sensing data from the study conducted by Rover and Mushet (2015). In Rover and Mushet (2015), the wetland function was identified by processing historical Landsat scenes using the decision-tree approach to capture surface water variations over years and a wetland delineation technique described by Rover et al. (2011), which increased the number of classified depressions. The identified wetlands were then classified into 7 different clusters based on the changing patterns in water surface area over years where Clusters 1 and 2 were identified as areas with permanent water during wet years (i.e., after 1990). Clusters 3-7 showed more variability in surface water, indicating that they are likely flow-through or recharge wetlands.

4.3.3. Study Area Characteristics and Model Setup

To test the FWA in SWAT, a study area in the PPR of North Dakota was selected. The selected study area is the upper portion of the Pipestem watershed (hereafter, Pipestem watershed) defined by the area draining to the selected USGS stream gauging station outlet at Pipestem Creek NR Pingree (i.e., USGS 06469400) (Figure 4.1). The Pipestem watershed predominately is an agricultural basin with crop lands covering nearly 43%, hay and rangeland covering about 41%, open water and wetlands covering about 13%, and residential only about

3% (USDA, 2018). Land use/Land cover and Soil Survey Geographic Database (SSURGO) data were obtained from the United States Department of Agriculture (USDA) Natural Resources Conservation Service (NRCS) Geospatial Data Gateway (USDA, 2018). The Pipestem watershed also spans two different geologic regions created during the last glaciation: (1) the drift plain to the east characterized by flat topography, Pipestem Creek, and agricultural land, and (2) the Missouri Coteau to the west characterized by varying topography and larger and more permanent wetlands (Brooks et al., 2018). A 10-m resolution DEM was downloaded from the USGS National Map Viewer (USGS, 2018) and used to delineate the surface. The watershed was divided into 21 subbasins and 202 HRUs with land use, soil, and slope thresholds of 1%, 20%, 20%, respectively. The climate in Central North Dakota is typified by continental conditions with a mean annual temperature and mean annual precipitation of 4ºC and 440 mm, respectively (Winter, 2003). The long, cold, and dry winters paired with the short and variably wet summers mean that evapotranspiration is the major water loss in the system (mean lake evaporation = 810 mm per year) (Winter, 2003). Climate data (including precipitation, temperature, wind speed, relative humidity, and solar radiation) for the selected simulation period, ranging from January 1st, 1994 to December 31st, 2002, were downloaded from the National Centers for Environmental Protection (NCEP) Climate Forecast System Reanalysis (CFSR) dataset at a daily interval (NCEP, 2018). A 4-year model warmup period was selected, while the periods of 1998-2000 and 2001-2002 were respectively selected for model calibration and validation.

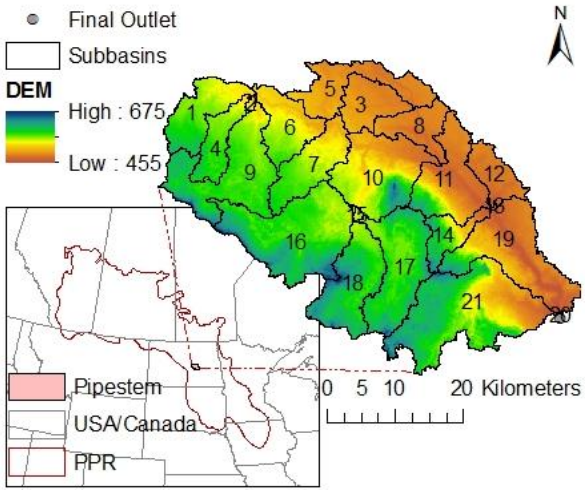

Figure 4.1. Location of the Upper Pipestem watershed and the delineated subbasins in relation to the North American Prairie Pothole Region.

The identified wetlands from the study by Rover and Mushet (2015) in the Pipestem watershed (Figure 4.2) show that the wetland surface areas vary temporally due to differences in hydroperiod and wetland hydrology. Unlike historical datasets which used aerial photography to identify wetlands, the cluster analysis by Rover et al. (2011) and Rover and Mushet (2015) used over 10 years of imageries to classify wetlands based on surface water dynamics, DEM-based delineation, and NDVI vegetation (Figure 4.2).

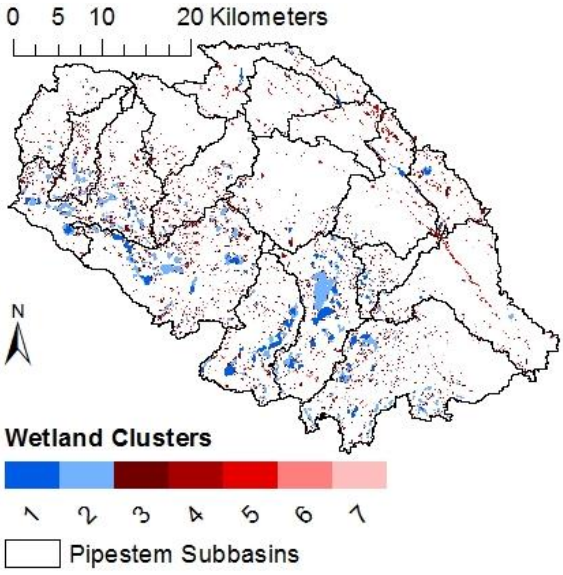

Figure 4.2. Spatial distribution of wetland clusters in the Upper Pipestem watershed.

4.3.4. Model Calibration, Validation, and Evaluation

The pre-calibrated FWA, A1, and A2 models were assessed by analyzing storage and dynamic contributing area capabilities. The FWA SWAT model was calibrated using SWAT-CUP 2012 SUFI2 (Abbaspour, 2013). Daily average streamflow obtained from the USGS gauging station 06469400 were used to calibrate the best parameter ranges for the calibration period, which were then used to validate the model for the validation period. Table 4.1 shows the calibration parameters and their initial ranges.

To evaluate the performance of the FWA SWAT model, 3 statistics recommended for daily, continuous streamflow models were selected: (1) Nash-Sutcliffe efficiency (NSE) coefficient (Equation 4.6), (2) percent bias (PBIAS) (Equation 4.7), and (3) root mean square error- observations standard deviation ratio (RSR) (Equation 4.8) (Moriasi et al., 2007; 2015).

$$NSE = 1 - \sum_{i=1}^{n}\left(Q_i^{obs} - Q_i^{sim}\right)^2 \Big/ \sum_{i=1}^{n}\left(Q_i^{obs} - \bar{Q}^{obs}\right)^2 \tag{4.6}$$

$$PBIAS = \sum_{i=1}^{n}\left(Q_i^{obs} - Q_i^{sim}\right)^2 \times 100 \Big/ \sum_{i=1}^{n} Q_i^{obs} \tag{4.7}$$

$$RSR = \sqrt{\sum_{i=1}^{n}\left(Q_i^{obs} - Q_i^{sim}\right)^2} \Big/ \sqrt{\sum_{i=1}^{n}\left(Q_i^{obs} - \bar{Q}^{obs}\right)^2} \tag{4.8}$$

where Y_i^{obs} is the *i*th observed value; Y_i^{sim} is the *i*th simulated value; $\bar{Y}^{obs}$ is the mean of the observed values; and *n* is the total number of observations. NSE > 0.5, -15 ≤ PBIAS ≥ 15, and RSR ≤ 0.7 reflect a satisfactory performance of the hydrologic model according to Moriasi et al. (2007,2015).

Table 4.1. Model calibration parameters for the Functional Wetland Approach (FWA).

Parameter	Definition	Initial Value	Range	SWAT File
CN2	SCS Curve Number	Varies	[-0.2, 0.2]	.mgt
ALPHA_BF	Baseflow recession constant (1/day)	0.048	[0, 1]	.gw
GW_DELAY	Groundwater delay (day)	31	[0, 500]	.gw
GWQMN	Threshold depth of shallow aquifer for return flow to occur (mm H_20)	1000	[0, 1000]	.gw
SURLAG	Surface runoff lag coefficient (day)	4	[0, 24]	.bsn
SMTMP	Snowmelt temperature (ºC)	0.5	[-5, 5]	.bsn
SMFMX	Maximum snowmelt rate	4.5	[1.4, 6.9]	.bsn
TIMP	Snowpack temperature lag factor	1	[0.01, 1]	.bsn
MSK_CO1	Muskingum translation coefficient for normal flow	0.75	[0, 10]	.bsn
MSK_CO2	Muskingum translation coefficient for low flow	0.25	[0, 10]	.bsn
REVAPMN	Threshold depth in the shallow aquifer for percolation (mm H_20)	750	[0, 500]	.gw
WET_FR	Fraction of sub-basin area draining into wetland	Varies	[0.05, 0.9]	.pnd
CH_N1	Manning's n value for the tributary channels	0.014	[0.025, 0.5]	.sub
CH_N2	Manning's n value for the main channels	0.014	[0.016, 0.15]	.rte
ESCO	Soil evaporation compensation factor	0.95	[0.01. 1]	.hru
WET_NVOL	Volume of water in the wetland when filled to normal level (10^4 m^3 H_20)	Varies	[-0.9, 0.9]	.pnd
WET_K	Effective saturated hydraulic conductivity (wetland bottom) (mm/hr)	0.5	[0, 1]	.pnd
WETEVCOEFF	Wetland evaporation coefficient	1.5	[0, 5]	.pnd

4.4. Results

4.4.1. Classified Wetlands and Geometric Properties

The wetland clusters classified by Rover and Mushet (2015) (Figure 4.2) were reclassified to the Pothole and Wetland functions in SWAT. Because Clusters 1 and 2 represent a more permanent water body regime, similar to discharge wetlands, lumped geometric properties of these wetlands were specified for the Wetland feature, in which the entire subbasin contributes

runoff to the wetlands. Clusters 3-7 represent a mixture of water regimes from temporary to seasonal, indicative of recharge and flow-through wetlands. Because these wetlands typically have a smaller upland area contributing to them, lumped geometric properties of clusters 3-7 were specified for the Pothole feature. Table 4.2 shows the maximum depression storage properties for all subbasins. As specified in the methodology, the maximum depression storage for clusters 1-2 and clusters 3-7 were defined by DEM-based delineation (Planchon and Darboux, 2001). Figure 4.3 shows the spatial distributions of maximum surface areas for clusters 1-2 and clusters 3-7. The total MDS or MPA equals the summation of the MDS or MPA values of clusters 1-2 and clusters 3-7, respectively, for FWA. The summation of contributing areas (CA) for the Pothole function in A1 and the Wetland function in A2 equals the total contributing area to water bodies in the FWA. By utilizing both the Wetland and Pothole functions, more areas can be specified as contributing to depression storage rather than directly contributing to the subbasin outlet. Previous studies show the impact of depression-dominated topography on dynamic contributing area to the outlet and localized connected areas (ACs) to depressions (Grimm and Chu 2018).

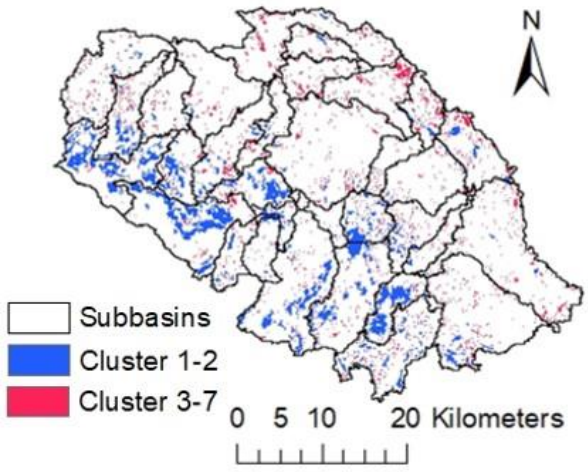

Figure 4.3. Spatial distributions of wetland clusters combined into the Wetland function in SWAT for Clusters 1-2 and the Pothole function in SWAT for Clusters 3-7 for the Functional Wetland Approach.

Table 4.2. Maximum depression storage (MDS) and contributing area (CA) of subbasins for different clusters in the Pothole Only Approach (A1), Wetland Only Approach (A2), and Functional Wetland Approach (FWA).

	Total		**A1**	**A2**	**FWA**			
					Cluster 1-2		Cluster 3-7	
Subbasin	MDS ($x10^5m^3$)	MPA ($x10^5m^2$)	CA ($x10^5m^2$)	CA ($x10^5m^2$)	MDS ($x10^5m^3$)	MPA ($x10^5m^2$)	MDS ($x10^5m^3$)	MPA ($x10^5m^2$)
1	54.0	84.2	292.5	430.3	14.5	14.4	39.5	69.8
2	0.4	0.6	6.4	17.0	0.0	0.0	0.4	0.6
3	18.3	46.3	132.4	333.9	1.5	4.2	16.8	42.2
4	125.7	75.3	104.9	278.0	108.3	47.1	17.5	28.2
5	32.4	62.6	152.9	490.7	2.5	3.2	29.9	59.4
6	18.5	25.8	156.0	407.9	5.0	3.6	13.6	22.1
7	75.4	82.3	319.3	460.0	45.7	34.8	29.7	47.5
8	27.4	55.3	170.0	299.7	0.0	0.0	27.4	55.3
9	742.5	279.9	387.4	848.1	700.8	233.1	41.7	46.8
10	64.4	67.6	412.6	780.3	15.3	12.3	49.1	55.3
11	69.3	88.5	252.7	616.8	39.6	27.0	29.7	61.6
12	36.7	65.9	132.3	264.2	18.2	19.3	18.5	46.6
13	1.1	1.3	1.0	3.8	0.0	0.0	1.1	1.3
14	77.0	48.6	36.3	228.0	51.5	22.1	25.5	26.5
15	0.2	0.5	11.5	13.7	0.0	0.0	0.2	0.5
16	1002.8	375.2	261.0	1079.0	950.3	311.8	52.6	63.4
17	373.9	218.3	143.9	734.0	330.3	165.9	43.6	52.4
18	248.0	133.2	131.3	618.4	224.8	101.7	23.2	31.5
19	74.9	93.1	422.4	859.3	31.7	12.7	43.2	80.3
20	0.0	0.1	1.6	5.2	0.0	0.0	0.0	0.1
21	706.8	312.5	233.7	1270.5	592.7	197.8	114.1	114.7

4.4.2. Pre-calibrated Results: Comparison of Different SWAT Modeling Approaches

4.4.2.1. Pre-calibrated Streamflow Results

Figure 4.4 compares the initial streamflow results simulated by A1, A2, and FWA Although A1 and A2 show certain temporal differences, they are generally close to each other (Figure 4.4a). However, when A1 and A2 results are compared against those from the FWA (Figure 4.4b and Figure 4.4c), a significant decrease in the simulated streamflow can be observed for FWA although the maximum depression storage for A1, A2, and FWA are all the same.

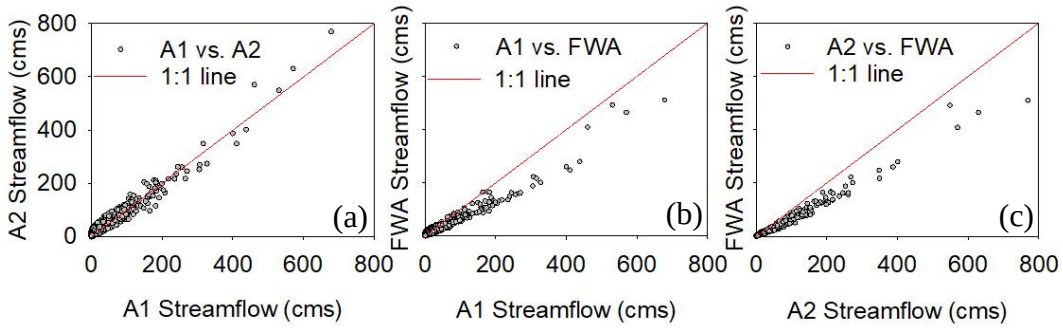

Figure 4.4. Comparisons of the uncalibrated streamflow results at the Pipestem watershed outlet for Approaches A1 and A2, and the Functional Wetland Approach (FWA).

4.4.2.2. Simulated Storage Dynamics

In order to develop the best toolset to answer different management questions relating to wetland habitat and ecology, the FWA must be able to simulate storage dynamics unique to different wetland types. The wetland clusters identified by Rover and Mushet (2015) were also analyzed temporally in their study. Specifically, the water area of each water body identified in their study area was converted to a normalized water area (i.e., water volume/ maximum water volume) and then averaged for each year, creating a mean percent water area based on each cluster for years 1997, 2000, and 2003. Similarly, the FWA analyzes storage dynamics of different wetland types or water body clusters by utilizing the Wetland function for clusters 1 and 2 and the Pothole function for clusters 3-7. Figure 4.5a shows the simulated normalized water volume of discharge wetlands for clusters 1 and 2 and recharge/flow through wetlands for clusters 3-7. The water volume varies greatly year-to-year and throughout the year in the recharge/flow through wetlands, whereas the discharge wetlands maintain a more permanent water volume throughout the year (Figure 4.5a), similar to the findings by Rover and Mushet (2015). The yearly mean normalized water volume results in Figure 4.5b show a similar trend for the same wetland clusters in Rover and Mushet (2015) for mean percent water area. For instance, the normalized water volume in 1997-2003 for clusters 1 and 2 varied between 80% and 100% in

Rover and Mushet (2015) and between 80%-100% in this study (Figure 4.5b). Higher variability was identified in the mean percent water in Rover and Mushet (2015) for clusters 3-7. The mean percent water values for cluster 3-7 were consistently lower than those for clusters 1 and 2. A similar conclusion can be drawn for wetland clusters of Subbasin 1 (Figure 4.5b).

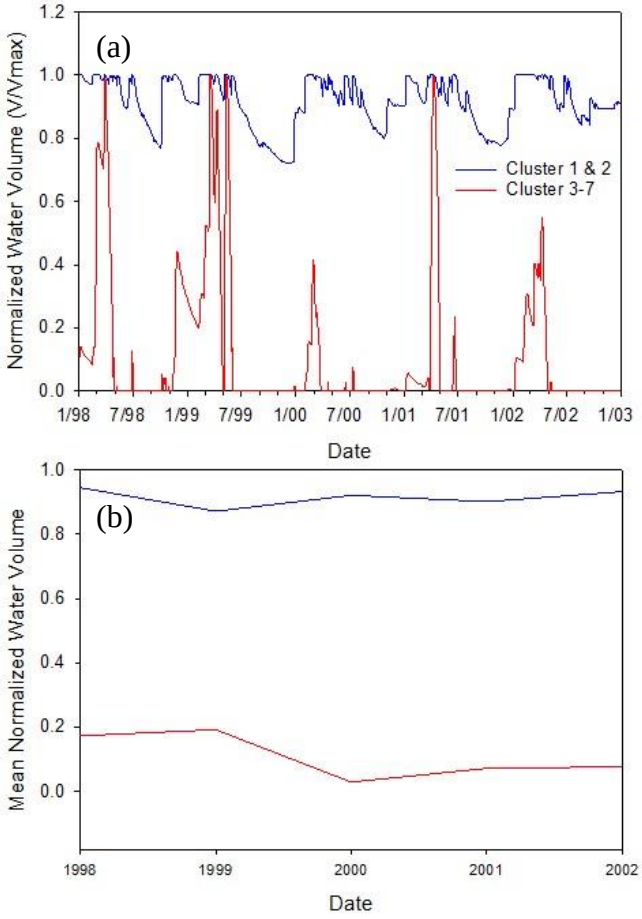

Figure 4.5. Temporal distributions of (a) normalized water volume (water volume/ maximum water volume) results and (b) mean normalized water volume results simulated by the Functional Wetland Approach (FWA) for clusters 1 and 2 and clusters 3-7 in Subbasin 1.

4.4.3. Calibrated Results

To evaluate the performance of the new FWA, the observed USGS discharge data were compared to the discharges simulated by FWA at the outlet of Subbasin 20 for the calibration

and validation periods (Figure 4.6). Generally, underestimation of peak discharges and slight overestimation of dry-period low flows can be observed.

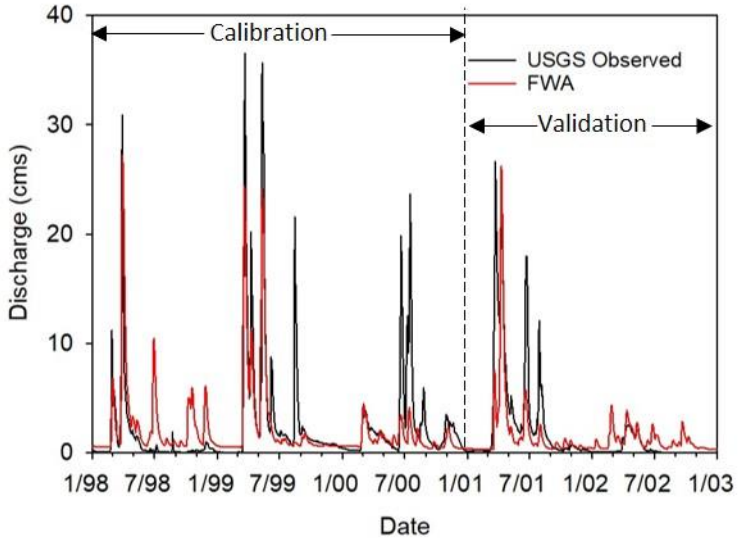

Figure 4.6. Simulated hydrograph of the Functional Wetland Approach (FWA) in SWAT compared to the USGS observed hydrograph for the calibration and validation period.

Overall, the statistics of the simulation results (i.e., NSE, PBIAS, and RSR) for the calibration and validation periods indicate satisfactory model performance (Table 4.3). The NSE and RSR statistics fall within the recommended range for continuous modeling of streamflow as suggested by Moriasi et al. (2007; 2015) for the calibration and validation periods. The PBIAS for the calibration period falls well within the recommended range (i.e., +/- 15%) (Moriasi et al., 2015); however, the PBIAS for the validation period only falls within the recommended range suggested by Moriasi et al. (2007) (i.e., +/- 25%).

Table 4.3. Statistical summary of the calibration and validation results from the Functional Wetland Approach (FWA) in SWAT.

Event	NSE	PBIAS (%)	RSR
Calibration	0.67	9.64	0.57
Validation	0.61	19.49	0.63

The parameters for contributing area in the Wetland function (i.e., WET_FR) and the Pothole function (i.e., POT_FR) were calibrated to be 45-60% for the subbasin and 90-100% for the HRU for clusters 1 and 2 and clusters 3-7, respectively. These contributing area results are consistent with the studies conducted by Kantrud et al. (1989) discussing the interactions of different wetland types with groundwater and by Brinson (1993) introducing hydrogeomorphic (HGM) classes to account for dynamic wetland functions and dynamic connectivity. Therefore, it can logically concluded that the discharge wetlands (clusters 1 and 2) would have a larger contributing area than the recharge/flow-through wetlands. Following Brinson (1993), dynamic contributing area is also introduced into the model by separating water storage into two different entities.

4.5. Conclusions

A new SWAT modeling approach was developed, which utilized the pothole and wetland functions in SWAT. By using these two features, different hydrologic processes associated with the dynamics of surface depressions were simulated. Although many studies have highlighted the impacts of spatial and temporal variability in surface depressions on hydrologic processes, few modeling studies have investigated the impact of wetland type or function on depression storage and subbasin outlet discharge.

The identified wetlands and functions from the study by Rover and Mushet (2015), were separated into two groups: (1) permanent water bodies or discharge wetlands (clusters 1 and 2) and (2) temporal/seasonal water bodies or recharge/flow-through wetlands (clusters 3-7). The Functional Wetland Approach (FWA) developed in this study accounted for the hydrologic processes unique to wetland functions. The FWA was able to significantly reduce streamflow compared to the pothole only approach (A1) and the wetland only approach (A2) due to the

increased contributing area to depression storage from an individual HRU and the entire subbasin. The simulated storage results related to the wetland function complement the observed water-ponded area for specific wetland types identified by Rover and Mushet (2015). Resultantly, the FWA improved the modeling of basin/subbasin discharge. These positive results encourage the use of the FWA to investigate water quality problems and address the wetland-related ecological issues.

Additional applications of the FWA throughout the PPR could highlight the impact depressions play on regional water-balance. By analyzing the spatial distribution of wetland types (i.e., recharge, flow-through, discharge wetlands), local impacts may be assessed as well. By implementing land management practices into the FWA SWAT model pollutant and nutrient retention supplied by depression storage could be quantified. Moreover, the detrimental effect of land use change in the PPR could be quantified by modifying the spatial distribution, size, and storage of different wetland types. The preceding suggestions highlight areas for future work which may be elevated with observed water level data, waterbody bathymetry, known groundwater connections, and additional stream gauges to monitor streamflow and nutrients/pollutants.

4.6. References

Abbaspour KC. 2013. “SWAT-CUP 2012: SWAT Calibration and Uncertainty Program - A Users Manual.” *EAWAG Swiss Fede Inst. Aquatic Science Technology*.

Arnold JG, Srinivasan R, Muttiah RS, Williams JR. 1998. “Large area hydrologic modeling and Assessment Part I: Model development.” *Journal of the American Water Resources Association*, Blackwell Publishing Ltd, 34(1), 73–89.

Millennium Ecosystem Assessment Board (MA Board). 2005. *Ecosystems and human well-being:Wetlands and water synthesis*. Washington, D.C.

Brinson MM. 1988. “Strategies for assessing the cumulative effects of wetland alteration on water quality.” *Environmental Management*, Springer-Verlag, 12(5), 655–662.

Brinson MM. 1993. *A hydrogeomorphic classification for wetlands. Wetlands Research Program Technical Report WRP-DE-4*. Vicksburg, MS.

Brooks JR, Mushet DM, Vanderhoof MK, Leibowitz SG, Christensen JR, Neff BP, Rosenberry DO, Rugh WD, Alexander LC. 2018. “Estimating Wetland Connectivity to Streams in the Prairie Pothole Region: An Isotopic and Remote Sensing Approach.” *AGU Water Resources Research*.

Chu X, Yang J, Chi Y, Zhang J. 2013. “Dynamic puddle delineation and modeling of puddle-to-puddle filling-spilling-merging-splitting overland flow processes.” *Water Resources Research*, 49(6), 3825–3829.

Chu X, Zhang J, Chi Y, Yang J. 2010. “An improved method for watershed delineation and computation of surface depression storage.” *Watershed Management Conference 2010: Innovations in Watershed Management under Land Use and Climate Change*, 1113–1122.

Euliss NH, Labaugh JW, Fredrickson LH, Mushet DM, Laubhan MK, Swanson GA, Winter TC, Rosenberry DO, Nelson RD. 2004. “The Wetland Continuum: A Conceptual Framework For Interpreting Biological Studies.” *Wetlands*, Springer Netherlands, 24(2), 448–458.

Euliss NH, Mushet DM, Newton WE, Otto CRV, Nelson RD, LaBaugh JW, Scherff EJ, Rosenberry DO. 2014. “Placing prairie pothole wetlands along spatial and temporal

continua to improve integration of wetland function in ecological investigations." *Journal of Hydrology*, 513, 490–503.

Gleason RA, Euliss NH. 1998. "Sedimentation of Prairie Wetlands." *Great Plains Research: A Journal of Natural and Social Sciences*, 8(1), 97–112.

Golden HE, Creed IF, Ali G, Basu NB, Neff BP, Rains MC, McLaughlin DL, Alexander LC, Ameli AA, Christensen JR, Evenson GR, Jones CN, Lane CR, Lang M. 2017. "Integrating geographically isolated wetlands into land management decisions." *Frontiers in Ecology and the Environment*, 15(6), 319–327.

Golden HE, Lane CR, Amatya DM, Bandilla KW, Raanan Kiperwas H, Knightes CD, Ssegane H, Kiperwas HR, Knightes CD, Ssegane H. 2014. "Hydrologic connectivity between geographically isolated wetlands and surface water systems: A review of select modeling methods." *Environmental Modelling and Software*, Elsevier Ltd, 53, 190–206.

Grimm K, Chu X. 2018. "Modeling of spatiotemporal variations in runoff contribution areas and analysis of hydrologic connectivity." *Land Degradation & Development*, 29(8), 2629-2643. DOI: 10.1002/ldr.3076

Hayashi M, van der Kamp G, Rosenberry DO. 2016. "Hydrology of prairie wetlands: Understanding the integrated surface-water and groundwater processes." *Wetlands*, 36, 237-234. DOI: 10.1007/s13157-016-0797-9

Kantrud HA, Krapu GL, Swanson GA, Allen JA. 1989. *Prairie basin wetlands of the Dakotas: a community profile*. No. FWS-85 (7.28). U.S. Fish and Wildlife Service, Washington, DC.

Mekonnen BA, Mazurek KA, Putz G. 2016. "Incorporating landscape depression heterogeneity into the Soil and Water Assessment Tool (SWAT) using a probability distribution." *Hydrological Processes*, 30(13), 2373–2389.

Moriasi DN, Arnold JG, Van Liew MW, Binger RL, Harmel RD, Veith TL. 2007. “Model evaluation guidelines for systematic quantification of accuracy in watershed simulations.” *Transactions of the ASABE,* 50(3), 885–900.

Moriasi DN, Gitau MW, Pai N, Daggupati P. 2015. “Hydrologic and Water Quality Models: Performance Measures and Evaluation Criteria.” *Transactions of the ASABE,* 58(6), 1763–1785.

Mushet DM, Calhoun AJK, Alexander LC, Cohen MJ, DeKeyser ES, Fowler L, Lane CR, Lang MW, Rains MC, Walls SC. 2015. “Geographically Isolated Wetlands: Rethinking a Misnomer.” *Wetlands,* 35(3), 423–431.

National Centers for Environmental Prediction (NCEP). “Global Weather Data for SWAT.” <https://globalweather.tamu.edu/> (accesed 8, 2018).

Neff BP, Rosenberry DO. 2018. “Groundwater connectivity of upland-embedded wetlands in the prairie pothole region.” *Wetlands* 38, 51-63. DOI: 10.1007/s13157-017-0956-7

Neitsch S, Arnold J, Kiniry J, Williams J. 2011. “Soil & Water Assessment Tool Theoretical Documentation Version 2009.” *Texas Water Resources Institute,* 1–647.

Planchon O, Darboux F. 2001. “A fast, simple and versatile algorithm to fill the depressions of digital elevation models.” *Catena,* 46, 159–176.

Rover J, Mushet DM. 2015. “Mapping Wetlands and Surface Water in the Prairie Pothole Region.” *R. Tiner, M. Lang and V. Klemas (eds) Remote Sensing of Wetlands: Applications and Advances,* CRC Press, Boca Raton, FL, 347–367.

Rover J, Wright CK, Euliss NH, Mushet DM, Wylie BK. 2011. “Classifying the hydrologic function of prairie potholes with remote sensing and GIS.” *Wetlands,* Springer Netherlands, 31(2), 319–327.

Tahmasebi Nasab M, Singh V, Chu X. 2017. “SWAT Modeling for Depression-Dominated Areas: How Do Depressions Manipulate Hydrologic Modeling?” *Water*, Multidisciplinary Digital Publishing Institute, 9(1), 58.

Tiner RW. 2003. “Geographically isolated wetlands of the United States.” *Wetlands*, Springer Netherlands, 23(3), 494–516.

United States Department of Agriculture (USDA) NRCS: Geospatial Data Gateway:Home. <https://datagateway.nrcs.usda.gov/> (accessed on March 8th, 2018).

United States Geological Survey (USGS) (2013) National Hydrography Dataset available online: https://nhd.usgs.gov (accessed March 15th, 2018)

United States Geological Survey (USGS) National Map Viewer available online: https://viewer.nationalmap.gov/basic/ (accessed on March 8th, 2018)

Wang X, Yang W, Melesse AM. 2008. “Using hydrologic equivament weltand concept with in SWAT to estimate streamflow in watersheds with numerous wetlands.” *Transactions of the ASABE*, 51(1), 55–72.

Winter TC. 2003. *Hydrological, Chemical, and Biological Characteristics of a Prairie Pothole Wetland Complex Under Highly Variable Climate Conditions- The Cottonwood Lake Area, East-Central North Dakota*. *Professional Paper*, U.S. Dept. of the Interior, U.S. Geological Survey, 109.

Yang J, Chu X. 2013. “Quantification of the spatio-temporal variations in hydrologic connectivity of small-scale topographic surfaces under various rainfall conditions.” *Journal of Hydrology*, 505, 65–77.

Yang J, Chu X. 2015. “A new modeling approach for simulating microtopography-dominated, discontinuous overland flow on infiltrating surfaces.” *Advances in Water Resources,* 78, 80–93.

Yang W, Wang X, Liu Y, Gabor S, Boychuk L, Badiou P. 2010. “Simulated environmental effects of wetland restoration scenarios in a typical Canadian prairie watershed.” *Wetlands Ecology and Management,* Springer Netherlands, 18(3), 269–279.

5. OVERALL CONCLUSIONS

The close proximity of the PPR to North Dakota State University inspired this research. The goal was to provide valuable research relating to hydrologic processes of the PPR, specifically hydrologic connectivity. Research regarding hydrologic connectivity is relatively new and encompasses many fields of study such as hydrology, ecology, wetland studies, and climate studies, and therefore, lacks a preferred foundation. Hydrologically speaking, connectivity is difficult to simulate in depression-dominated regions like the PPR because hydrologic connectivity is a dynamic process impacted by the topographic characteristics of depressions. The thousands of permanent and semi-permanent potholes and associated wetlands within the PPR create a complex topographic surface in which dynamic hydrologic connectivity, storage, or the timing and quantification of overland flow are difficult to simulate. Thus, this dissertation highlights three studies which involve:

- Developing a new procedure to analyze functional hydrologic connectivity related to topography, specifically in depression-dominated areas;
- Evaluating the impacts of the P2P processes and dynamic hydrologic connectivity on watershed outlet discharge; and
- Addressing the combined effect of topographic depressions and wetland functions on hydrologic connectivity and watershed outlet discharge.

Chapter 2 assessed the topographic similarities and differences of various land surfaces (i.e., depression-dominated surfaces and dendritic surfaces). These different surfaces were used to further define, quantify, and locate hydrologic connectivity and contributing area. A new procedure was developed for identifying and analyzing hydrologic connectivity. The normalized connected area function (NACf) was proposed in this study to analyze hydrologic connectivity of

areas not necessarily connected to an outlet and the established relative surface connection function (RSCf) (Antoine *et al.*, 2009) and simplified hydrographs were created to examine the intrinsic relationships and interactions between structural topographic characteristics and dynamic hydrologic processes. Results from this study show the unrealistic representation of contreibuting area (CA), especially for depression-dominated surfaces, simulated by tradition delineation and modeling methods. Using the new modeling procedure, it was found that NACf and RSCf were interrelated and they both identified stepwise trends unique to depression-dominated areas due to the threshold behaviors observed during the P2P process. For dendritic surfaces, a smoother increasing pattern of NACf and RSCf was observed. The simplified hydrographs highlighted the impacts of surface topography, mainly depression storage, on the timing and available water for runoff. Lastly, the established TauDEM method did not provide all the topographic parameters calculated in the new procedure. Thus, it was difficult to determine the initial structural connectivity by using TauDEM, in which all depressions on a surface were already filled.

Chapter 3 applied conclusions drawn from Chapter 2 to an event-based case study of the Baldhill Creek watershed in North Dakota. Since traditional hydrologic models cannot simulate the dynamic hydrologic processes indicative of depression-dominated areas, the HEC-HMS model was improved upon. Specifically, the approach for identifying and quantifying hydrologic connectivity and depression storage was applied and used to create an improved HEC-HMS model. In doing so, the impacts of the P2P processes and dynamic contributing area on outlet discharge are highlighted and accurately simulated compared to the basic HEC-HMS model. The improved modeling methodology introduced a depression threshold control proxy and an initial subdivision of contributing and non-contributing area [i.e., depressional area (DA) and non-

depressional area (NDA)]. The depression threshold control proxy specified unique storage-discharge functions for each subbasin which reflected dynamic contributing area to the outlet. The improved model was compared to the basic HEC-HMS model to highlight the improved model accuracy and supplementary storage data provided by the improved model. The additional storage data can provide details relating to varying water availability and water levels within a subbasin which may help predict water shortages and ecological stresses on wetland habitats.

Lastly, chapter 4 analyzed the impact of wetland type/function on hydrologic connectivity. This study developed a new methodology which utilized the Pothole and Wetland water routing functions in SWAT. An improved SWAT modeling approach, the functional wetland approach (FWA), was developed to simulate two different wetland functions and their impact on hydrologic connectivity. Classified wetlands from the cluster analysis in Rover et al. (2011) and Rover and Mushet (2015) were used to divide contributing areas and depression storage. The new modeling approach introduced a new hydrologic categorization of wetlands to be used in watershed-scale hydrologic modeling and created a more realistic representation of hydrologic processes within a depression-dominated region. More detailed water storage results based on wetland function were reported in this new FWA which may help identify hydrologic and ecologic changes in different types of wetland habitats over time. Further, these storage results have the ability to indicate how land use change or climate may impact wetland areas.

Opportunity for future work lies within some of the current research limitations. Such limitations include the limited observed data and model framework limitations. In chapters 3 and 4 only one observed USGS gaging station was available to calibrate and validate the improved HEC-HMS model with DTCP and FWA in SWAT, respectively. Additional validation points at the outlets of depression-dominated subbasins would help calibrate the models further leading to

more accurate results. Further calibration and validation of depression-dominated subbasins rather than only the final watershed outlet may also help identify sensitive model parameters unique to depression-dominated subbasins. Although modeling framework limitations were superseded by the proposed DTCP and FWA, no changes were made to the modeling code. In future work, improving the modeling code in HEC-HMS and SWAT may present new opportunities for simulating depression storage and hydrologic processes unique to different wetland types. Specifically, validating groundwater connections and the impact of wetland hydrological position on factors like water-balance or salinity may support current literature in hydrologic and wetland sciences.

Overall, results and conclusions from this research identify the importance of modeling purpose. The data and details useful to modelers depends on the overall purpose and use of the model. In order for decision-makers to solve water crises or establish legislature impacting the quantity and quality of water in a region, it is necessary to have a thorough understanding of the hydrologic processes within that region. Therefore, the connectivity analysis and modeling advancements made with this research have the opportunity to enhance future studies related to land use change, climate change, and ecosystem impacts in depression-dominated areas.